NTNU

Norwegian University of
Science and Technology

Finite Element Simulations of Unconsolidated Keel Actions from First-Year Ice Ridges.

A Comparison of a Numerical Model and
Analytical Equations from ISO 19906:2010

Sjur Moe Grevsgård

Civil and Environmental Engineering
Submission date: December 2015
Supervisor: Knut Vilhelm Høyland, BAT

Norwegian University of Science and Technology
Department of Civil and Transport Engineering

Preface

The following master's thesis is written during the autumn semester of 2015 at Norwegian University of Science and Technology (NTNU), Department of Civil and Transport Engineering. The submission of this work means the completion of my 5 years Master's Degree in Civil and Environmental Engineering at NTNU with a specialization in Marine Civil Engineering.

I wish to thank my supervisor, Professor Knut Vilhelm Høyland at NTNU, who fortunately lead me into the field of Arctic Technology. Thanks to you, my last year has been an incredible journey filled with Arctic experiences. First during the spring semester of 2015 at the University Centre in Svalbard (UNIS), and now during the work with my thesis. My fieldwork in Svalbard and the topic for my final thesis are not related, yet it feels like that they complement each other. UNIS gave me the practical approach of Arctic research, and Trondheim the theoretical side of it. Thank you, Knut, for all valuable discussions during this period.

The objective for the thesis was to examine and compare how the structural width affects the horizontal rubble keel actions. ISO 19906:2010 gives analytical equations for determination of the described forces. It was performed as a comparison of these values with a finite element model. Related to the modelling, special thanks go to Sergey A. Kulyakhthin, who works as a researcher in Sustainable Arctic Marine and Coastal Technology (SAMCoT) at NTNU in Trondheim. Thank you for great discussions and guidance when I struggled with my finite element model, and for providing me with the user-defined subroutine for the material model. It was certainly valuable for the work.

The challenges have been many. One of the lesser known is that the servers continually ran out of capacity due to the time consuming model. On Svalbard, however, the main challenge was polar bears who ate snowmobiles and scientific equipment. I am more than grateful for the variation this work has given me!

Trondheim 17/12/2015
Sjur Moe Grevsgård

Abstract

The thesis aimed for an assessment of the current standard for determination of the keel rubble actions from a first-year ice ridge. ISO 19906:2010 (2010) gives regulations for determination of these loads, based on the work of Dolgopolov et al. (1975). The assessment involved a comparison of the ISO recommendations with the results from a numerical finite element (FE) model. Particularly the effect of the width of the structure was a target of investigation.

The FE model used the theory of a Continuum Breakage Mechanism (CBM) to describe the rubble keel's material behaviour. The material model was implemented as a user-defined subroutine (developed by Sergey A. Kulyakhtin), and the FE analyses were performed in the ABAQUS software. It was modelled as a coupled Eulerian-Lagrangian (CEL) analysis. This type of analyses are advantageous for large deformations and fluid flows etc., in accordance with the behaviour of an ice ridge. In comparison, the analytical model rests on a Mohr-Coulomb yielding criterion.

It was mainly focused on the direct comparison of the two models (the analytical and the numerical) by the predicted keel actions. This parameter compared easily, regardless of the material model in use. In other words, the comparison of the material models came indirectly through the comparison of the keel actions.

The reaction forces from the numerical model are highly dependent on the prescribed keel velocities. An increased keel velocity yielded reaction forces that approached the analytical results from Dolgopolov et al. (1975), but it also seemed to spoil the accuracy of the energy balance.

The FE model proved to give a linear fit just as the ISO standards, but it was a gentle slope compared to the analytical suggestions. For every unit length increase in structural width, the ISO predicted more than twice (approximately 2.5 times) the keel actions from the FE model. This comparison applies for the FE model with a predefined keel velocity of 2000 mm/s. In addition, the order of magnitude of the maximum forces were significantly lower than the ISO predictions. It means that the FE model and the corresponding keel actions showed a two-way effect compared to the ISO suggestions. It implied that the ISO standard suggests too high keel actions from the unconsolidated part, and the width had less to say for the total force than stated in the standards.

Sammendrag

Retningslinjer for bestemmelse av kjølkreftene fra en første-års skrugard er styrt av ISO 19906:2010 (2010), og baserer seg på arbeidet til Dolgopolov et al. (1975). Denne masteroppgaven har gjort en vurdering av ISO-regelverket, ved å sammenligne det med en numerisk modell basert på elementanalyser. Med kjølkreftene menes i dette tilfellet den ikke-konsoliderte delen av kjølen. Det har vært av spesiell interesse å se på hvordan kjølkreftene endrer seg når konstruksjonsbreddene endres.

For å beskrive kjølens oppførsel er det blitt brukt en ulik materialmodell for den numeriske modellen sammenlignet med ISO-standarden. Det analytiske regelverket i ISO 19906:2010 (2010) baserer seg på et Mohr-Coulomb bruddkriterium, mens i elementmodellen benyttes det en kontinuumsmodell (CBM) (Einav, 2007a). Denne modellen tar høyde for både elastisk og plastisk knusning som vil frigjøre energi. Materialmodellen er blitt implementert som en egendefinert subrutine. Subrutinen er utviklet av Sergey A. Kulyakhtin ved Norges teknisk-naturvitenskapelig universitet. ABAQUS, som er moduleringsprogrammet som er benyttet for å kjøre elementanalysene, har ikke en innebygd funksjon for denne type materialmodell. Selve analysen i ABAQUS ble kjørt som en såkalt CEL-analyse, der det benyttes en kombinasjon av Euleriske- og Langrangeelementer. Denne typen analyser er særs effektiv i tilfeller der det forventes store deformasjoner eller det er væske som flyter. Dette er overførbart til hvordan den ikke-konsoliderte kjølen ville oppføre seg.

Hovedfokuset har vært på å sammenligne de to modellene direkte, gjennom å se nærmere på kjølkreftene. I denne sammenhengen tenkes det på den maksimal reaksjonskraften som oppstår i interaksjonen mellom konstruksjonen og skrugarden. Dette er en parameter som lett lot seg måle, uavhengig av valg av materialmodell. Det innebefatter en indirekte sammenligning av materialmodellene gjennom at kjølkreftene har blitt sammenlignet.

Reaksjonskraften fra den ikke-konsoliderte kjølen viste seg i stor grad å være avhengig av starthastigheten til kjølen (i den numeriske modellen). Reaksjonskraften nærmet seg gradvis anbefalingene fra ISO 19906:2010 (2010) da kjølhastighetene økte, men det virket også til å påvirke energibalansen på en negativ måte. Det ble sett større energitap for det siste tilfellet, sammenlignet med de lavere hastighetsfeltene.

Fra elementanalysene ble det funnet en lineær sammenheng mellom kjølkreftene og konstruksjonsbredden. Dette samsvarer med ISO-standarden, men helningen på den lineære grafen var betydelig slakere for den numeriske modellen sammenlignet med de analytiske verdiene. Følgende konklusjon kunne derfor bli dratt: For en enhets økning i konstruksjonsbredde økte kjølkreftene omtrent to og en halv gang mer enn den numeriske modellen. I tillegg var startverdiene og ekstremalverdiene betraktelig lavere for den numeriske modellen. Dette gir en dobbelteffekt i form av at kreftene er lavere og helningen er slakere. Sammenlignet med den numeriske modellen gir derfor ISO-standarden et for høyt anslag, og effekten av konstruksjonsbredden er betydelig mindre (2.5 ganger mindre).

Contents

List of figures

List of tables

1 Introduction

1.1 Background

There is a growing interest for exploration of oil and gas and design of fixed or floating structures in cold climates and in the Arctic. It is not surprising that the oil industry is one of the key stakeholders: The Arctic holds among the largest oil and gas deposits in the world that is still not developed. Technical challenges, partly because of ice, deep waters and remoteness, has made projects less profitable. Especially with a relatively low oil price, the high-cost projects put on hold. That said, these dynamic factors could quickly turn around and lead to a renewed faith in projects high north.

Another major commercial interest group is the shipping industry. Climate change and its consequences for the ice melting may open up new sea-lanes for regular traffic. For instance, the Northwest Passage connects the Atlantic and the Pacific Ocean in waters where it usually occurred pack ice. The route follows the northern coast of North America through the Arctic Ocean. In the next decades, this route may provide a shortcut for ship transport between Europe and Asia. The same applies to the Northeast Passage that goes along the northern coast of Russia and connects Europe and Asia through Artic waters. Figure 1 illustrates how the Northeastern Passage may shave off significant distances compared to today's conventional southern route.

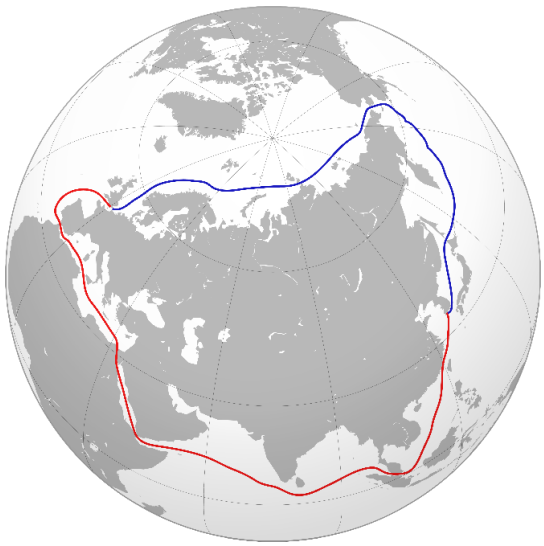

Figure 1 A graphical comparison of the Northeastern Passage (blue line) and the alternative, more common southern route (red line). (Knopp-Schwyn and Flame, 2009)

The examples above intend to show the importance of extensive research on Arctic and cold climate technology. Whether the ice melts faster or later than expected over the next decades, the risk of ice will always be present. It sets requirements for reliable predictions of the ice actions. The ice ridge loads may be the critical design load for structures in such

environments. The actions are in general more complex compared to the ice loads from a level ice cover. Especially, “the determination of the forces caused by keels of first-year ridges is one of the problems in ice engineering.” (Kärna and Nykänen, 2004, p. 42)

1.2 Problem formulation and investigations

The following thesis aims for an assessment of the current standard for determination of the keel rubble actions from a first-year ice ridge. ISO 19906:2010 (2010) gives regulations for determination of these loads, based on the work of Dolgopolov et al. (1975). The assessment involves a comparison of the standard with a numerical model. In that relation, it has primarily arisen two questions for further investigation: Firstly, are the forces from the current standard in a reasonable order of magnitude? Secondly, does the width of the structure have any other effects than the current suggestions?

In order to address these questions, it is necessary with a review of the assumptions behind the material models. The model of Dolgopolov et al. (1975) assumes a Mohr-Coulomb yielding criterion where the ice ridge behaves as an elastic-perfect plastic material. The numerical finite element model applies a Continuum Breakage Mechanism (CBM) by Einav (2007a). For this model, “as the breakage proceeds, the breakage energy increases, and the yielding criterion increases” (Einav, 2007a, p. 1294).

1.3 Limitations

The two material models from Dolgopolov et al. (1975) and Einav (2007a) base on highly different assumptions. It is advantageous in terms of a comparison of the ISO standard with a more advanced model. Since the Mohr-Coulomb model is quite simple and behaves perfectly plastic, the CBM is likely to describe the ice-structure interactions in a more credible manner. Especially when the majority of the volumetric strains expects to be plastic. The downside is of course that it also makes it more complicated with a direct comparison of the numerical and analytical results. For instance, in a case where the finite element model based on a Mohr-Coulomb criterion. The ISO standard could then be used as a calibration tool to optimize the accuracy of the numerical model. They should then ideally give equal results. In this thesis, one have to rely on the numerical model itself. It leaves the energy balance as the only tool to check the model for potential errors.

It is necessary to introduce the reader to both the CBM model and the Mohr-Coulomb criterion. These models base on soil mechanics and geotechnical engineering, and requires knowledge about these fields for a full understanding. The main purpose here is to state the most important parameters, and to make measurable results for further, similar research. From a material model point of view, there is little focus on why the two models give similar (or different) results. The focus is rather on the direct comparison of the two models by the predicted keel actions. This parameter easily compares, regardless of the material model. In other words, the comparison of the material models comes indirectly through the comparison of the keel actions.

The extent of the work is a limiting factor itself. It means that the fewer simulations performed, the more increases the weight on each result. When only three different structural widths submits for analyses, there could be a significant spread in between. As mentioned, there is also a lack of "calibration tools" for the numerical model (to check the credibility of the results). One suggestion is to include empirical data from structures where this has been measured, for instance fixed structures such as lighthouses, or the floating oilrig of Moliqpak. These data are valuable reference points for a qualitative comparison. Still, this comparison is not included. Mainly because it is regarded outside the scope of work for this thesis. The main scope is to compare the keel actions from the numerical model and the ISO standards. For the same reason, the investigations do not attempt to fit the FE model to the corresponding values from the ISO standards.

1.4 Structure of the thesis

The report starts with a theory chapter divided into three sections. The first section includes the most relevant theory for ice ridges with descriptions of geometry, morphology and mechanical properties. The next section shows the theory behind the keel rubble actions from Dolgopolov et al. (1975), which leads to the ISO 19906:2010 (2010) formulations. Related to the keel actions is also a description of the Mohr-Coulomb failure criterion. The last section addresses ABAQUS (the FE software) and relevant theory for the modelling part of the thesis. It includes further descriptions of the Coupled Eulerian-Lagriangian (CEL) analyses, explicit dynamic analyses and the energy balance. Additionally, it includes a description of the CBM model. CBM is completely independent of ABAQUS, but there is a close link between the two (from a modeling perspective).

The model chapter includes two sections, where the first one states the most important assumptions for the keel and for the structure. These assumptions are important for all the further work in this thesis. The second section gives a detailed description how the equivalent model implements into ABAQUS.

The results chapter mainly distinguishes between the energy balances and the reaction forces, and presents these data systematically. Then follows the "discussion and analysis" chapter, where the most prominent trends from the results chapter is processed and further analysed.

The conclusions chapter summarize the most important findings from the work, while the "further work" proposes a natural continuation from where this thesis ends. After the references comes the appendix as a support to the report.

2 Theory

2.1 Ice ridges

2.1.1 Introduction

Ice ridges form when an ice cover is subjected to stresses from shear or compression, where the driving forces comes from currents and winds. The ice floes collide and rubbles of ice forms above and below the original ice cover. A common description of ice ridges bases on the ice ridge' age. A first-year ice ridge has formed during the cold season, and will not survive during the melt season. A multi-year ice ridge is likely to survive over two or more seasons.

In this paper, the focus is on first-year ridges. Figure 2 shows s typical model for a first-year ice ridge. The keel is defined as the volume of the ridge below the water surface, with a depth H_K. The keel is usually made up of a consolidated and an unconsolidated part with a depth h_c and h_k respectively ($H_K=h_c+h_k$). After the ice ridge has initially formed, the upper part of the keel will continue to grow. "It is not clear how the consolidated layer should be defined, nor does a standardized method for examining the thickness of this layer" (Høyland, 2002, p. 15-2). Also ISO 19906:2010 points out that "existing field data suggest that the parameters h_c and H_k is not correlated with each other" (ISO 19906:2010, 2010, p. 181). Thus, it may be hard to determine exact values without use of specific field data.

The unconsolidated layer is the rubble below the consolidated part, as seen in figure 2. In addition, the sail is the rubble that forms above the waterline, where h_s is the sail's height. The other parameters are:

W_S, the width of the sail.

Θ_k, the keel angle.

W_k, the width of the keel.

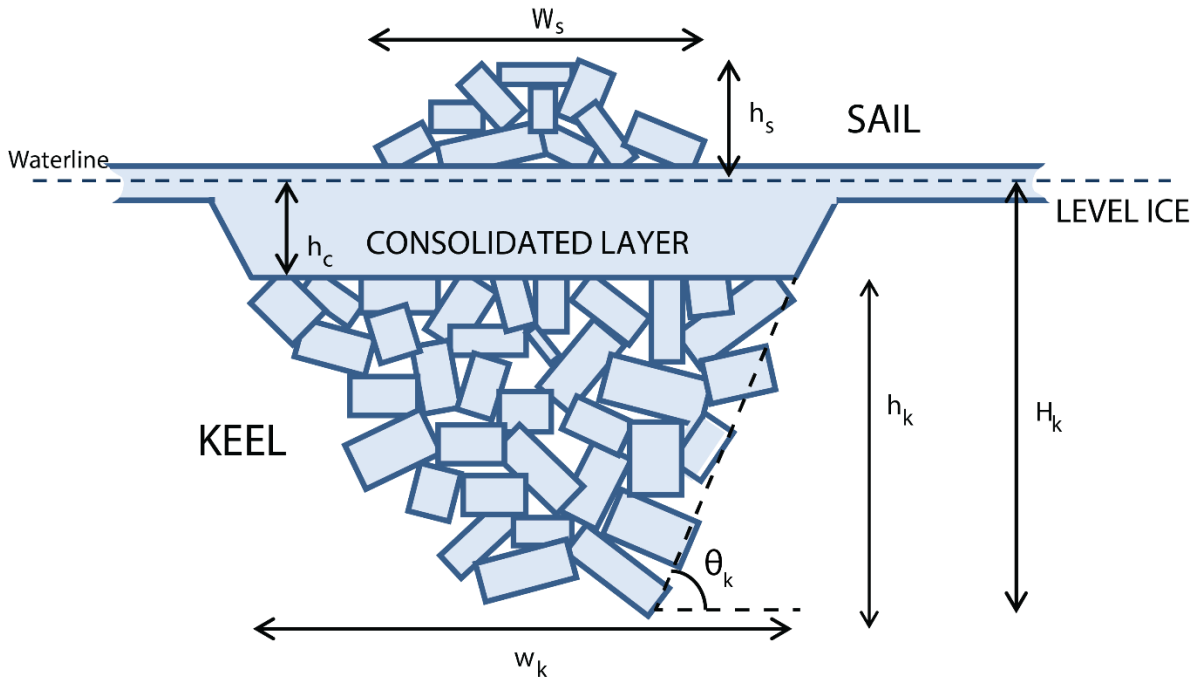

Figure 2 Typical model of a first-year ice ridge (Strub-Klein and Sudom, 2012, p. 95) with some modifications. h_k corresponds to the ISO notations.

2.1.2 Morphology

The geometry and the shape of first-year ice ridges varies considerably, and is highly dependent on the local metrological conditions where the ridge forms. In order to characterize the ridges' geometry and to describe the shape relations, it is beneficial to use shape ratios. These rations typically bases on the variables showed in figure 2.

Timco and Burden (1997) investigated 112 first-year ice ridges, based on discrete measurements. In general, there are two techniques available for investigation and measurements of ridges: Discrete measurements or continuous scanning. The continuous scanning approach makes us of a sonar or laser to scan the ice ridge. A continuous scanning may give detailed data about the given ridge relatively fast. The scanning is conducted from a fixed point, and may not cover the whole ridge both above and below the waterline. Thus, the results from a continuous scan may be insufficient regarding the different shape ratios.

As mentioned, it is often a desire to determine these ratios. In section 2.2.2, one will see that similar ratios are of importance for the keel action formulations found in the ISO 19906:2010 (2010).

In the discrete technique, holes are drilled through the ridge and the relevant dimensions are measured, for instance by a probe or a tape measure. The method gives precise information regarding the sail height and the keel depth, as described by Timco and Burden (1997). As a main drawback of the discrete technique, it is time consuming, and requires a lot of manual work for each investigation.

Forty-six of the first-year ice ridges investigated by Timco and Burden (1997) came from the Beufort Sea region. The remaining sixty-six from "the temperate regions, including the Labrador Sea, Baltic Sea, Northumberland Strait, and the south Bering Sea."(Timco and Burden, 1997, p. 67). Timco and Burden propose the following results from the investigations of the first-year ridges: The keel-depth (H_k) to sail-height (h_s) ratio equal to 4.4, the ratio of the keel-area (A_k) to the sail-area (A_s) equal to 8, keel-width (W_k) to sail-height (h_s) ratio equal to approximately 15, and the keel-width (W_k) to keel-depth (H_k) ratio equal to 3.9. (Timco and Burden, 1997, p. 65).

In addition, Timco and Burden's (1997) investigations showed the following trends:

- The keel depth increases with increasing sail height.
- The keel width increases with increasing keel depth and increasing sail height respectively.
- A linear relationship between the keel and the sail area.
  (Timco and Burden, 1997, pp. 69-70)

Strub-Klein and Sudom (2012) did similar comparisons of over 300 first-year ice ridges. The investigations and analyses originate from a range of different seas, including Bering and Chukchi Sea, Beufort Sea, Svalbard waters, Barents Sea, East Coast Canada, Baltic Sea and Offshore Sakhalin. For all the ridges, it was found a mean value of $H_k/ h_s = 5.2$. The value is considerably higher than Timco and Burden's 4.4, and the ISO-standard recommends a value of 4.5. (ISO 19906:2010, 2010, A.8.2.4.5). In all cases, the scatter is quite significant.

For the ratio of the keel width (W_k) to the sail width (W_s), Strub-Klein and Sudom (2012) propose an average value of 6.75, but there is found a relatively large variation, especially compared to other parameters.

It is also worth to mention that "a number of other properties were investigated for first year ridges, but they did not show any pronounced trend." (Timco and Burden, 1997, p. 72). Dolgopolov et al. 1975 assumed for instance the keel rubble depth to sail width ratio (h_k /W_s) to be approximately 4 to 5, and a trapezoidal cross-section for first-year ridges. (Dolgopolov et al., 1975, p. 470). Compared to figure 3 it may be raised doubts regarding the validity for this assumption - but it is not a topic for this thesis. These relations are more thoroughly described in section 2.2.2, but either Timco or Burden (1997) or Strub-Klein and Sudom (2012) have proposed any relationships for the keel depth to sail width ratio. Timco and Burden did not find any more correlations, except for the ones described earlier in this section.

For design of a structure, it is also of interest to know the extremal values or typical dimensions for a first-year ice ridge. Strub-Klein and Sudom (2012) proposed mean and extremal values for all the ridges they investigated. Table 1 shows a summary of the key data.

Table 1 Key parameters and corresponding values for first-year ice geometries. (Strub-Klein and Sudom, 2012, p. 99)

Parameter [m]	**Mean value [m]**	**Max value [m]**	**Min value [m]**
Maximum sail height, h_s^{max}	2.0	8.0	0.0
Average sail height, $\bar{h}_s$	0.7	3.7	0.1
Sail width, W_s	12.1	73.2	1.8
Maximum keel depth, H_k^{max}	8.0	28.0	0.9
Average keel depth, $\bar{H}_k$	4.5	12.5	1.3
Keel width, W_K	36.0	201.9	3.1

From these data, it was drawn an illustration of a typical first-year ice ridge. Figure 3 shows the dimensions:

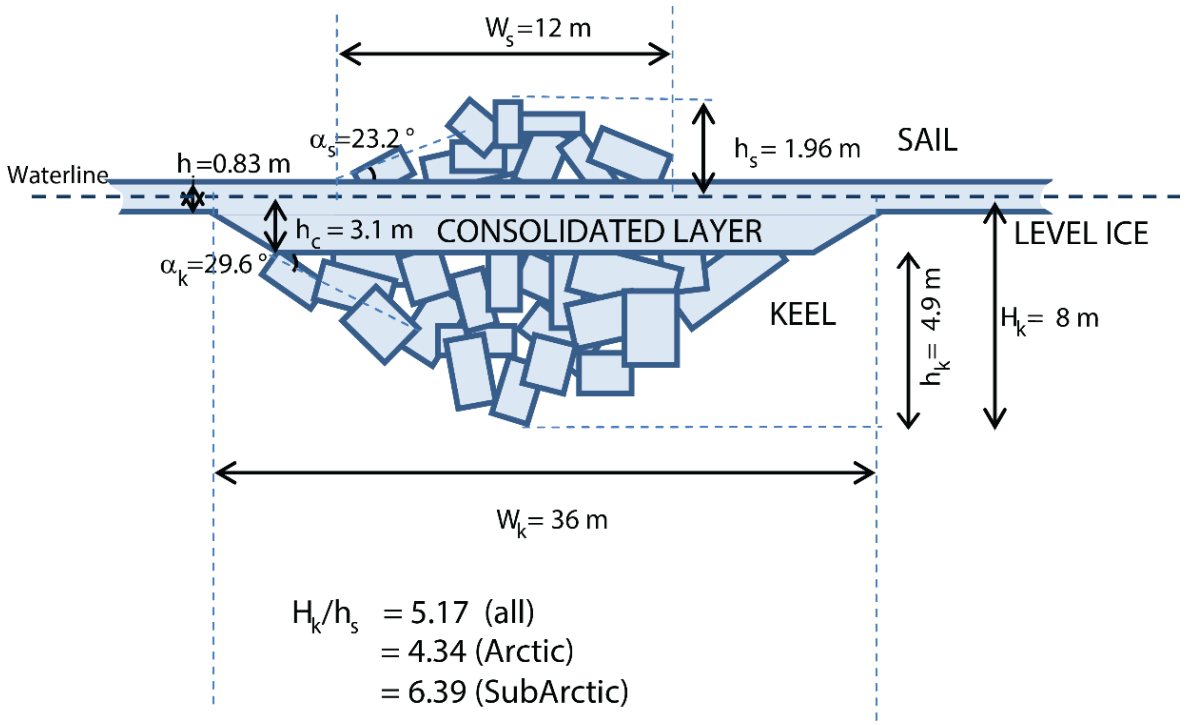

Figure 3 Typical dimensions of a first-year ice ridge (Strub-Klein and Sudom, 2012, p 103) with some modifications.

2.1.3 Mechanical properties

The action effects from a level ice cover is well investigated and understood compared to the actions from first-year ice ridges. As Høyland points out, "the current knowledge about ice ridges and forces from ridges is not exhaustive, and both ridge characteristics and physico-mechanical properties are so far insufficiently investigated" (Høyland, 2007, p. 170)

The mechanical properties of sea ice depends on the following four parameters. (Høyland, 2014 p. 10)

- Temperature, T
- Loading rate, $\dot{\varepsilon}$
- The porosity, η
- The grain size, d and orientation

The temperature is important by itself, but also in relation with the porosity of the ice. Low temperatures usually gives a more brittle behaviour of the ice, and expected higher uniaxial strength.

In addition, during the consolidation phase, the temperature plays an important role for the degree of salt that expels or traps inside the ice. Low temperatures may speed up the consolidation phase, and more salt traps inside the structure. These brine pockets, together with the air porosity affects the uniaxial strength in a negative way. Moslet (2008) conducted experiments that showed the effect of porosity on the uniaxial strength on columnar sea ice, as seen in figure 4.

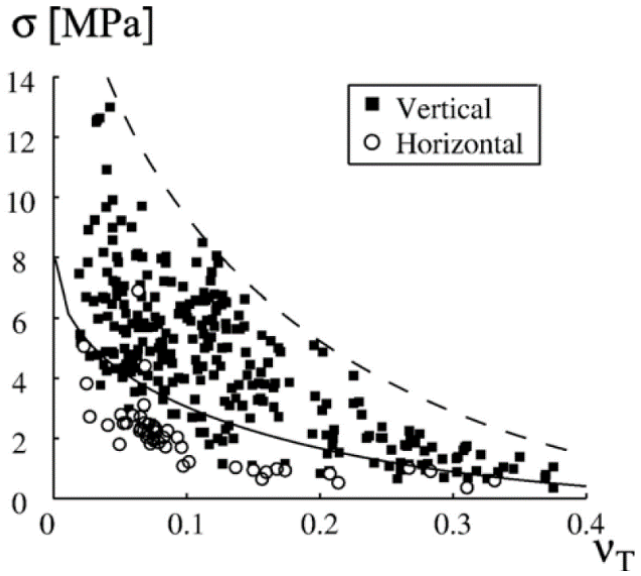

Figure 4 Maximum strength vs total porosity for columnar sea ice (Moslet, 2006 p. 8)

Høyland (2007) finds the same effect for the uniaxial compressive strength of first-year ice ridges. Figure 5 shows these results. The porosity is calculated as a function of the salinity, the density and the temperature. It seems reasonable that the conclusion of a decrease in strength with increasing porosity also holds for first-year ridges. (Høyland, 2007, pp. 181-182)

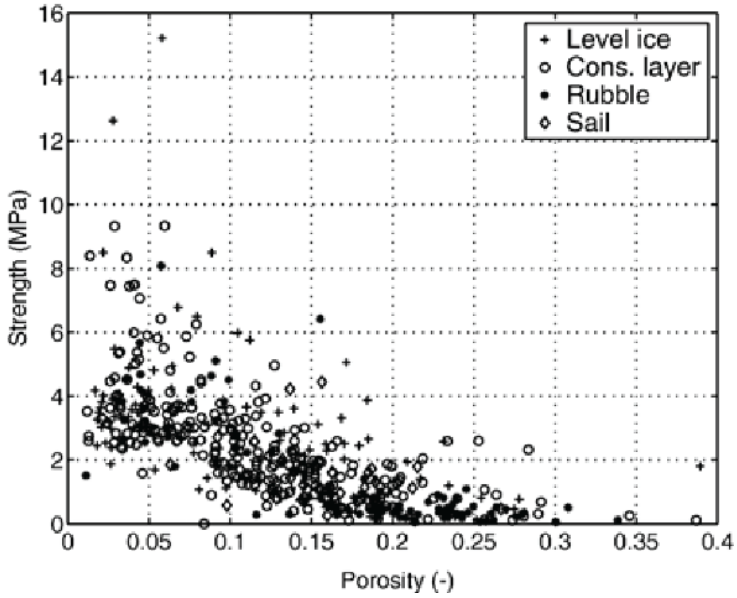

Figure 5 The uniaxial compression strength vs the porosity (Høyland, 2007, p. 177)

The strength of the different parts (see figure 2 for descriptions) is also of great interest for ice ridge characterization. Figure 6 clearly shows that the lower parts of a first-year ridge has a lower strength. There is a drop in the strength for the unconsolidated part, also known as the rubble. From these findings, it is likely to believe that the consolidated ice should stand for the design load in case of an ice-structure interaction. However, it is pointed out that "a higher or lower uniaxial strength does not necessarily tell whether the level ice or the consolidated layer fails first when being crushed against a structure" (Høyland, 2007, p. 183).

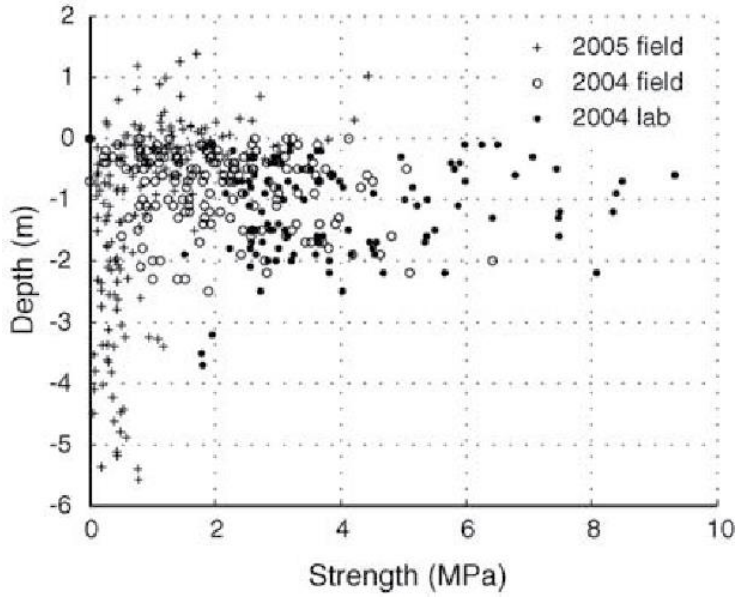

Figure 6 The depth vs the uniaxial strength for first-year ice ridges (Høyland, 2007, p. 179)

This thesis opts to focus on the ice ridge actions from the unconsolidated part of the first-year ice ridge. The general mechanical properties has been mentioned. More specific, "a

combination of three factors determines the mechanical properties in the unconsolidated part:" (Høyland, 2007, p. 170)

- The age of the ridge
- The temperature, the salinity and the velocity of the surrounding waters.
- The initial ice conditions at ridge formation.
  (Høyland, 2007, p. 170)

2.2 Actions from first-year ice ridges

To describe the keel forces is not a straightforward procedure and it involves a number of uncertainties. These challenges mainly relates to find applicable material models to describe the loosely bond, rubble keel. The general approach is described in ISO 19906:2010 (ISO 19906:2010, 2010, A.8.2.4.5), which is based on the work of Dolgopolov et al. (1975), and later upgraded by Kärna and Nykänen (2004). The theory assumes a Mohr Coulomb material as a base for the derivations. A further description of the Mohr Coulomb yielding criterion follows in the next section.

2.2.1 The Mohr Coulomb failure criterion

The Mohr Coulomb criterion describes how the yielding shear stress on a plane varies for a given normal stress. Equation 1 shows the given relationship:

$$\tau_f = \left(\sigma'_f + a\right)\tan(\varphi) \tag{1}$$

, where

τ_f is the shear stress on the plane

σ_f' is the plane's effective normal stress

a is the attraction

φ is the material's angle of friction.

Figure 7 shows the Mohr Coulomb criterion drawn as a failure criterion. As seen, the Mohr Coulomb failure criterion has a linear dependency between the shear stresses and the normal stresses. An increase in normal stresses allows for higher shear stresses before failure occurs. A material with a high angle of friction is more capable of withstand shear stresses when the normal stresses are increased, compared to a material with a small angle of friction.

(Emdal, 2012, pp. 167-169)

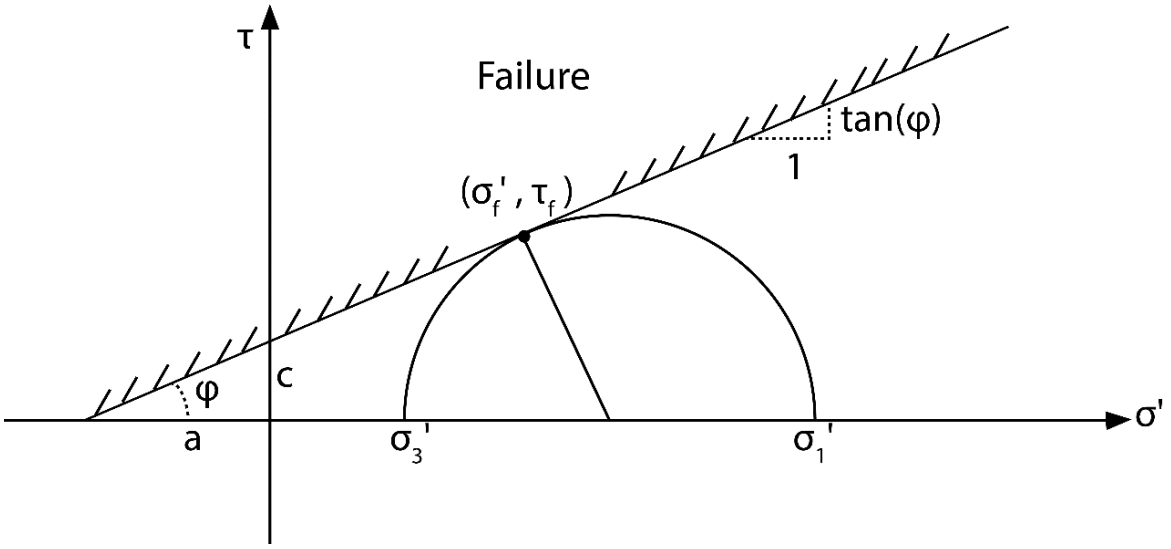

Figure 7 The Coulomb Mohr failure criterion. The cohesion, c, is given by a tan (φ) = c. σ_1' and σ_3' are the main principle stresses.

Instead of a plot in the σ'-τ domain, it is often practical to plot the mean stresses versus the deviator stresses, given by equation 2 and 3 respectively:

$$p' = \frac{1}{3}(\sigma_1' + \sigma_2' + \sigma_3') \tag{2}$$

$$q = \sigma_1' - \sigma_2' \tag{3}$$

"The reason why this plot is so advantageous relates to the fact that it keeps volumetric and distortional stress-strain effects apart in a theoretically sound and well defined manner" (Nordal, 2014, Ch 3. Page 6). However, the failure surface is not uniquely defined in a p'-q plot for a Mohr Coulomb criterion. In a case where the failure stresses are of importance, the investigation of the major and minor principle stresses are more suitable, as shown in figure 8. The inclination N is a factor that relates to the degree of mobilization, given by,

$$N = \frac{1 + \sin(\rho)}{1 - \sin(\rho)} \tag{4}$$

In case of the unconsolidated keel, tan(ρ) is assumed equal to tan(φ). It is not introduced a factor of safety against failure in the model for the ridge keel action, and will not be discussed any further in this paper.

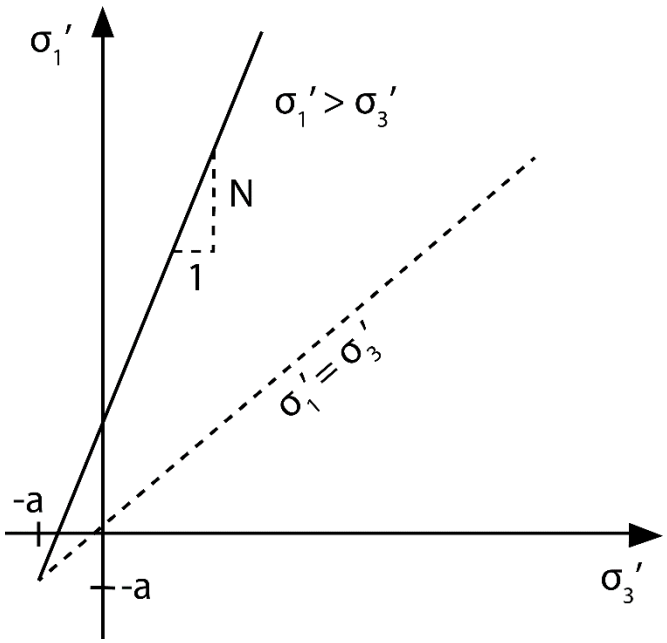

Figure 8 The Coulomb Mohr criterion in a σ_1' - σ_3' stress space (Nordal, 2014, Ch 3, Page 4)

2.2.2 First-year ice ridge actions from the unconsolidated keel

Dolgopolov et al. (1975) proposed to use a Mohr Coulomb failure criterion to describe the unconsolidated rubble in a first-year ridge. The assumption bases on field, experimental and analytical data. In addition, the rubble assumes to have an elastic-perfect plastic material behaviour, analogous to figure 9. After the material yields, an increase in strain, ϵ, will not develop any higher stresses, σ. The yielding stress corresponds to the peak stress.

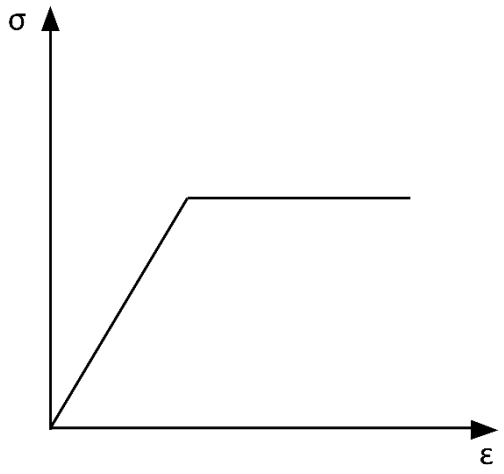

Figure 9 an elastic-perfect plastic material model.

The total force, F_R from a first-year ice ridge is usually assumed to be the sum of the forces from the consolidated part, F_C, the keel actions, F_K, and the actions from the sail, F_S.

Equation 5 gives the formula. The sail action component, F_S, is usually negligible because the sail volume and corresponding forces are assumed small compared to the actions from the consolidated part and the rubble.

$$F_R = F_c + F_K + F_S \tag{5}$$

In this thesis, the focus is on the unconsolidated keel action, F_K. The consolidated force component, F_C, bases on estimates similar to the ones for a level ice cover, where the global pressure for sea ice is considered.

The rubble contains of blocks of ice that are loosely bond together, and it may refreeze and make new bonds. As later discussed both the cohesion and the material's internal angel of friction is then taken into account. "The magnitude of ridge pressure against the structure is primarily governed by the dimensions and structural integrity of the ridge, viz. by the degree of bonding between ice blocks"(Dolgopolov et al., 1975, p. 470) Thus, the keel actions needs a different approach than the consolidated layer.

Equation 6 shows the formula Dolgopolov et al. (1975) proposed for the unconsolidated keel action from a first-year ice ridge. The notations are according to Kärna and Nykänen (2004),

$$F_K = \mu\, h_e D\left(\frac{\mu\, h_e\, \gamma_e}{2} + 2c\right)\left(1 + \frac{2}{3}\frac{W_s}{D}\right) \tag{6}$$

where,

μ is the passive pressure coefficient given by:

$$\mu = \tan\left(45° + \frac{\varphi}{2}\right) \tag{7}$$

φ is the material's angle of internal friction.

c is the keel cohesion.

W_s is the sail width of the ridge.

h_e is an effective keel depth governed by:

$$h_e \leq h_k + D/2 \tag{8}$$

D is the width of the structure

γ_e is the effective buoyancy as shown in equation 9.

$$\gamma_e = (1 - e)(\rho_w - \rho_{ice})\, g \tag{9}$$

where,

e is the keel porosity

ρ_w is the water density

ρ_{ice} is the ice density

g is the gravity.

The theory assumes a local failure mode for the keel. Timco et al. (1999) did a thorough comparison of ice load calculations algorithms for first-year ice ridges. They point out that Dologpolov's model includes many of the essential variables affecting the keel action, as listed:

- The structure width
- The keel depth
- The keel buoyancy with porosity
- Keel properties of friction and cohesion
- The passive pressure coefficient.

The drawback is that the keel width is not taken into consideration. As previously explained, the main assumption is a keel depth to sail width ratio (h_k /W_s) of approximately 4 to 5.

Kärna and Nykänen (2004) performed a parametric study of equation 6 to derive small modifications to the model. The study showed that the effective keel depth h_e results in an excessively high estimate of the keel action for wide structures. They found $h_e = h_k$ to be a better estimation for the actual keel depth.

In addition, several other parameters were varied in order to find a best fit between Dolgopolov's model and the advanced model. The sail width was initially set equal to the keel depth, and later set to 1/4 and 1/5. The cohesion, c, was varied between 1-20 kPa, the structure width, D, between 2 – 60 m, the keel depth, h_k, between 2-40 m and the angle of internal friction between 10-50°**.** (Kärna and Nykänen, 2004, p. 47). The study showed that Dologopolov's original sail width to keel depth ratio of 1/4 is also applicable for the modified formula. Substituted for the effective keel depth and the given sail width to keel depth ratio gives equation 10, which is identical with the ISO formulation. (ISO 19906:2010, 2010, p 182 (A.8-49)). The notations are according to Kärna and Nykänen (2004).

$$F_K = \mu\, h_k D\left(\frac{\mu\, h_k\, \gamma_e}{2} + 2c\right)\left(1 + \frac{h_k}{6D}\right) \tag{10}$$

2.3 ABAQUS

2.3.1 Introduction

ABAQUS is a finite element software, which provides computer aided engineering (CAE) for different types of engineering problems. An Abaqus/CAE model is built up by the following components, as listed below: (Dassault Systèmes, 2012b, 9.2.1)

- Parts
- Materials and sections
- Assembly
- Sets and surfaces
- Steps
- Loads, boundary conditions, and fields
- Interactions and their properties
- Meshes

In section 3.2 is a thorough description of the listed component in connection with the FE model. In the next sections follows descriptions of the most important theory for the finite element model in this thesis. The reader expects to be familiar with the general concepts behind the finite element method. The focus is mainly on the theory for the material model, and the implementation of it as a user defined subroutine. It also feels necessary with a brief introduction to the combined Eulerian-Lagrangian analyses, which is particularly efficient when dealing with large deformations, material damage and fluid flows. In the last section follows a description of the energy balance in ABAQUS, and how it can be used to assess the accuracy of the model.

Some few words on ABAQUS and units; ABAQUS has no built-in units specified, which means the user has to be particularly careful. It is up to the user, always to check that the units are consistent. Figure 10 shows the corresponding consistent units in ABAQUS for a given choice of length unit.

Consistent units				
Quantity	**SI**	**SI (mm)**	**US Unit (ft)**	**US Unit (inch)**
Length	m	mm	ft	in
Force	N	N	lbf	lbf
Mass	kg	tonne (10^3 kg)	slug	lbf s^2/in
Time	s	s	s	s
Stress	Pa (N/m^2)	MPa (N/mm^2)	lbf/ft^2	psi (lbf/in^2)
Energy	J (N × m)	mJ (10^{-3} J)	ft lbf	in lbf
Density	kg/m^3	tonne/mm^3	slug/ft^3	lbf s^2/in^4

Figure 10 the corresponding consistent units in ABAQUS. The choice of [mm] as the length unit has implications for the other quantities' units. (Dassault Systèmes, 2012c)

2.3.2 Continuum Breakage Mechanism (CBM) for elastic-plastic-breakage models.

As mentioned before, the ISO formulations for the rubble keel actions bases on a Mohr Coulomb failure criterion. For the numerical modelling, it was used a more advanced model

based on continuum theory by Einav (2007a). The continuum model is not included as a subroutine in ABAQUS; hence, it was used a user defined FORTRAN subroutine developed by SAMCoT researcher Sergey A. Kulyakhtin. In this section, it follows a brief description of the Continuum Breakage Mechanism (CBM) and the most important parameters:

Ice is a granular material, and the grain size, d, is one of the main parameters that affects the mechanical behaviour. Thus, it is important to state a material model that is able to express how the grain size is distributed and changes during crushing. Einav (2007a) proposed a model termed continuum breakage mechanism (CBM). The aim was to "establish a soundly based continuum theory that incorporates the concept of breakage" (Einav, 2007a, p. 1276).

One of the main assumptions is that larger grain particles stores more energy than small particles. Larger particles have a larger contact area, and the risk of contact with adjacent particles increases. It is found to be a link between the rate of energy dissipation and the total energy that is stored in the system. "As the breakage proceeds, the breakage energy increases, and the yielding criterion increases" (Einav, 2007a, p. 1294).

When a granular material is subjected to an initial reference pressure, p_r, the appurtenant elastic, volumetric strain, e_v^e may be found from equation 11 (Einav and Puzrin, 2004)

$$e_v^e - e_{v0} = \frac{\left(\frac{p}{p_r}\right)^{1-m} - 1}{\bar{K}(1-m)} \tag{11}$$

, where

e_{v0}	is the initial volumetric strain.
p	is the mean effective stress (effective pressure)
p_r	is the reference pressure.
$\bar{K}$ and m	are material constants

From equation 11, the elastic bulk modulus and the mean effective pressure can be derived, as shown in equation 12 and 13 respectively: (Einav, 2007b, p. 1319)

$$\frac{dp}{de_v^e} = \bar{K}\left(\frac{p}{p_r}\right)^m \tag{12}$$

$$p = p_r \sqrt[1-m]{\bar{K}(1-m)(e_v^e - e_{v0}) + 1}\ , \qquad 0 \leq m < 1 \tag{13}$$

When m = 1 equation 13 boils down to the expression shown in equation 14: (Einav, 2007b, p. 1319)

$$p = p_r e^{\frac{e_v^e - e_{v0}}{\kappa^*}} \tag{14}$$

, where $\kappa^* = \frac{1}{\bar{K}}$, and when m=0, equation 13 becomes as shown below in equation 15: (Einav, 2007b, p. 1319)

$$p - p_r = K(e_v^e - e_{v0}) \tag{15}$$

For the latter case, $K = p_r\bar{K}$, also known as the conventional bulk modulus. (Einav, 2007b, p. 1319)

Einav (2007a) also introduced the parameter ϑ, shown in equation (16), which "measures the proximity of the initial to ultimate grain size distribution (Einav, 2007a, p. 1301).

$$\vartheta = 1 - \frac{J_{2U}}{J_{20}} \tag{16}$$

J_{2U} and J_{20} are the second order moments of the ultimate and the initial grain size distributions. The general form of the n^{th} order moments of the grain size distribution, p(d), is given in equation (17). (Einav, 2007a, p.1285)

$$J_n \equiv \langle d^n \rangle = \int_{d_m}^{d_M} d^n p(d) \mathrm{d}d \tag{17}$$

An increase in the ultimate grain size distribution leads to a decrease in ϑ. A smaller ϑ means crushing has progressed, and the crushing potential has decreased, because larger grain particles stores more energy than small particles. Figure 11 shows the effect for a pure elastic-breakage model, where the stress, p is plotted against the volumetric strain, e_v.

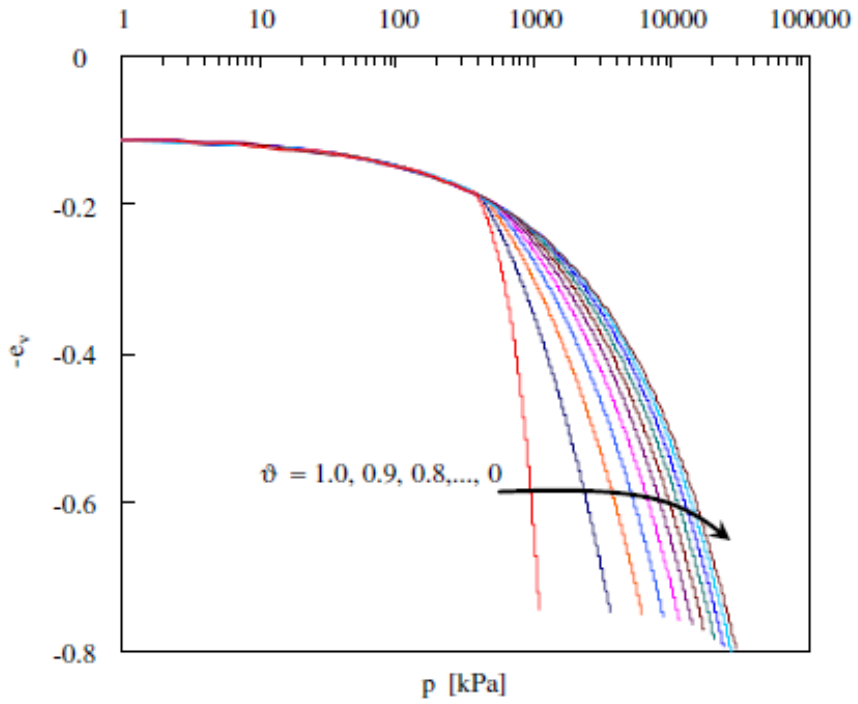

Figure 11 "Effect of grain size distribution on compression curves in pure elastic-breakage model" (Einav, 2007b, p. 1304)

Einav (2007b) points out that a pure elastic-breakage model represents the process of isotropic hardening in a good manner. When the soil is unloaded in the model, "the yield

strength increases because the grain size distribution is shifting gradually towards smaller particles" (Einav, 2007b, p 1305), but the effect of frictional dissipation are not well conserved. The volumetric strains will go back to its initial state, where there should have been a different state with plastic strains after unloading. It shows the need for an elastic-plastic breakage compression model. Figure 11 showed the pure elastic breakage line for varying ϑ. The main concept for both models is that the breakage growth criterion in equation 18 is satisfied: (Einav, 2007b)

$$\widetilde{\Phi}_B = E_B \delta B = \delta E_B^* \tag{18}$$

, where

$\widetilde{\Phi}_B$ is the breakage dissipation potential, E_B is the breakage energy, δB is an incremental breakage variable and δE_B^* is the change in residual breakage energy. If one assume the total dissipation potential, $\widetilde{\Phi}$, to be a sum of a plastic potential, $\widetilde{\Phi}_P$, and the breakage potential, $\widetilde{\Phi}_B$, the total dissipation potential is given in equation 19: (Einav, 2007b, p.1306)

$$\widetilde{\Phi} = \widetilde{\Phi}_B + \widetilde{\Phi}_P \geq 0 \tag{19}$$

In equation 19, the two dissipation terms are uncoupled and regarded as a pure plastic and a pure breakage component respectively. For an elastic-plastic breakage compression model, there needs to be a coupling between the two terms. Equation 20 and 21 shows the coupled forms for plastic and breakage dissipation: (Einav, 2007b, p.1311)

$$\Phi_P^* = \sin^{-1}(\omega)\Phi_P \tag{20}$$

$$\Phi_B^* = \sin^{-1}(\omega)\Phi_B \tag{21}$$

, where Φ_P^* and Φ_B^* are functions of the same order as Φ_B and Φ_P, and ω is the plastic-breakage coupling angle. "The shift from a pure elastic-breakage line to the pure elastic-plastic line is spanned via the coupling angle ω"(Einav, 2007b, p 1311), as shown in figure 12. When ω is zero, equation 20 and 21 go to zero, and the material exhibits an elastic breakage mechanism. A linear elastic-plastic behaviour holds for all ω > 60-70°. Non-linearity occurs for the smaller ω, as seen from figure 12. See table 2 for the applied value for parameter ω in this thesis.

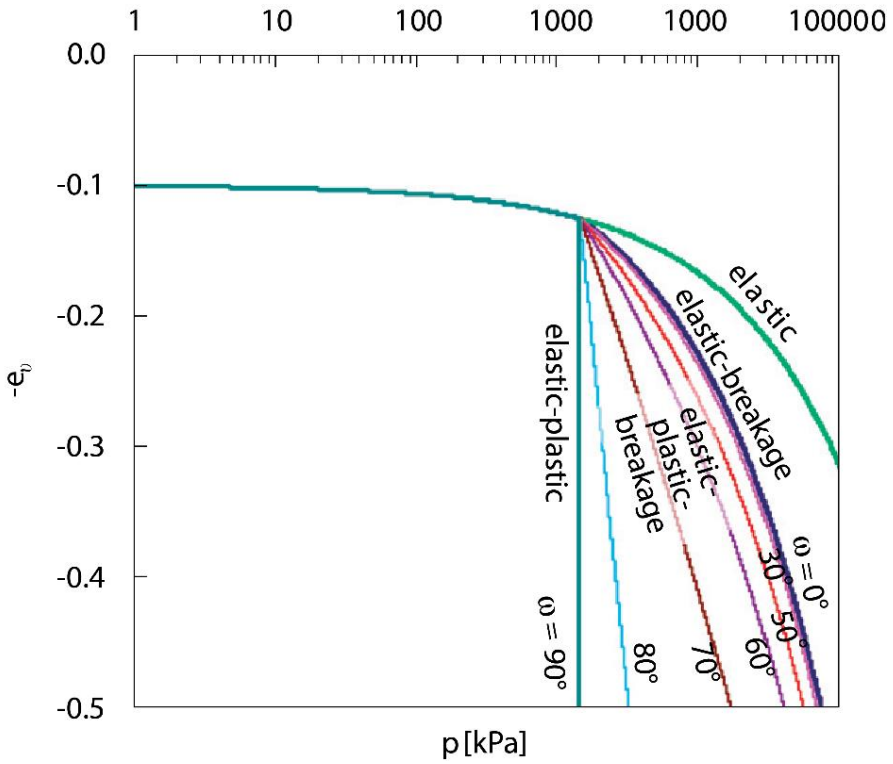

Figure 12 "The coupling effect on the stress–strain curve in semi-logarithmic scale." (Einav, 2007b, p.1312)

Equation 22 shows the parameter "M that relates between the failure shear stress q_u and the failure pressure p_u."(Einav, 2007b, p. 1318).

$$M = \frac{q_u}{p_u} \tag{22}$$

The critical pressure, p_{cr} is analogous to the yield stress of a material, here the yield stress for the rubble keel. It is set to 2300 Pa (see table 2) suggested by Kulyakhtin for the given model. The value is an estimate from model scale experiments at The Hamburg Ship Model Basin (HSVA).

Equation 23 shows the shear modulus, G that per definition describes the ratio between shear stresses, q_{xy}, and shear strains, γ_{xy}. The shear modulus is assumed negligible in our model compared to the stresses and strains from normal forces, and thereby set equal to zero, as seen in table 2

$$G = \frac{q_{xy}}{\gamma_{xy}} \tag{23}$$

The two last parameters in table 2 relates to the number of iterations and the accuracy of the numerical model. The model has to fulfil the two requirements in order to converge to a solution.

Table 2 shows a summary of the most important parameters described in this section. The same set of parameters and corresponding values are included in the ABAQUS model.

Table 2 the material parameters for the CBM model.

#	Parameter	Value	Unit
1	Bulk Modulus, K	0.0048	-
2	Ref. pressure, p_r	1E-06	MPa
3	Shear modulus, G	0	-
4	ϑ	0.8	-
5	Critical pressure, p_{cr}	2.3E-03	MPa
6	M	1.9	-
7	Plastic-breakage coupling angle, ω	80	°
8	Maximum iterations	200	-
9	Accuracy of the convergence	1E-005	-

2.3.3 Coupled Eulerian-Lagrangian (CEL) analyses

For a finite element analyses with pure Lagrangian elements, there is a close link between the assigned material properties and the mapping of elements. It means that when the material deforms in the model, the nodes will deform together with the material, and allows for distortions of the elements. For a nonlinear analyses dealing with large deformations that may ruin the accuracy of the model.

An Eulerian analysis handles the mapping of elements conceptually different to pure Lagrangian analyses. In an Eulerian analysis, the elements are fixed within the domain. Instead of nodes that deforms together with the assigned material, it allows the material to pass through the fixed elements within the domain. Figure 13 and 14 illustrates the two concepts of Lagrangian and Eulerian analyses respectively.

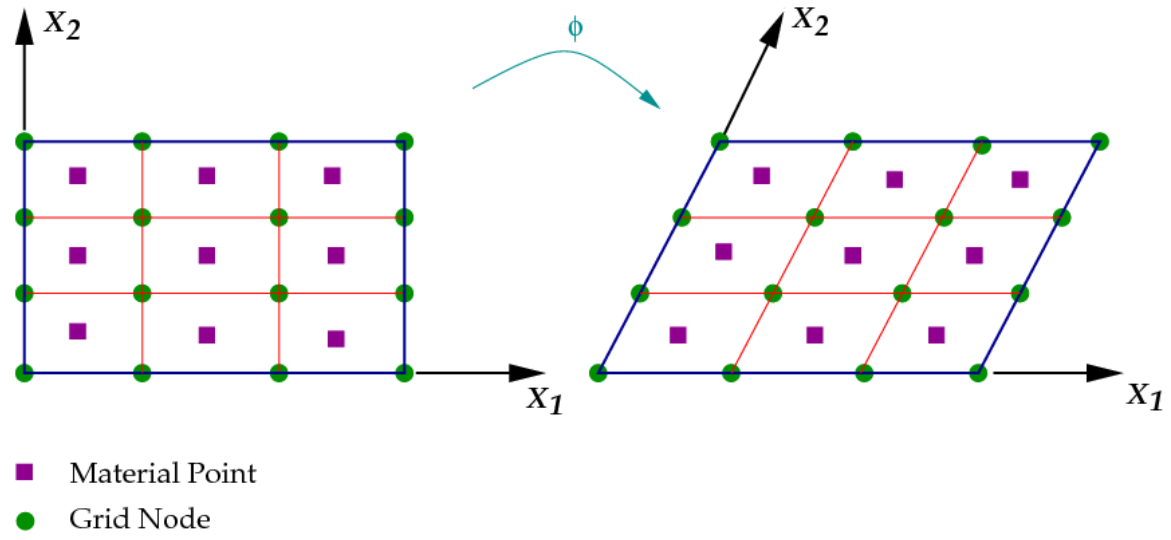

Figure 13 the concept of a pure Lagrangian analysis. The elements and corresponding nodes deforms together with the material, and leads to element distortions. It may cause low accuracy, especially in cases of large deformations. (Wikiversity, 2010)

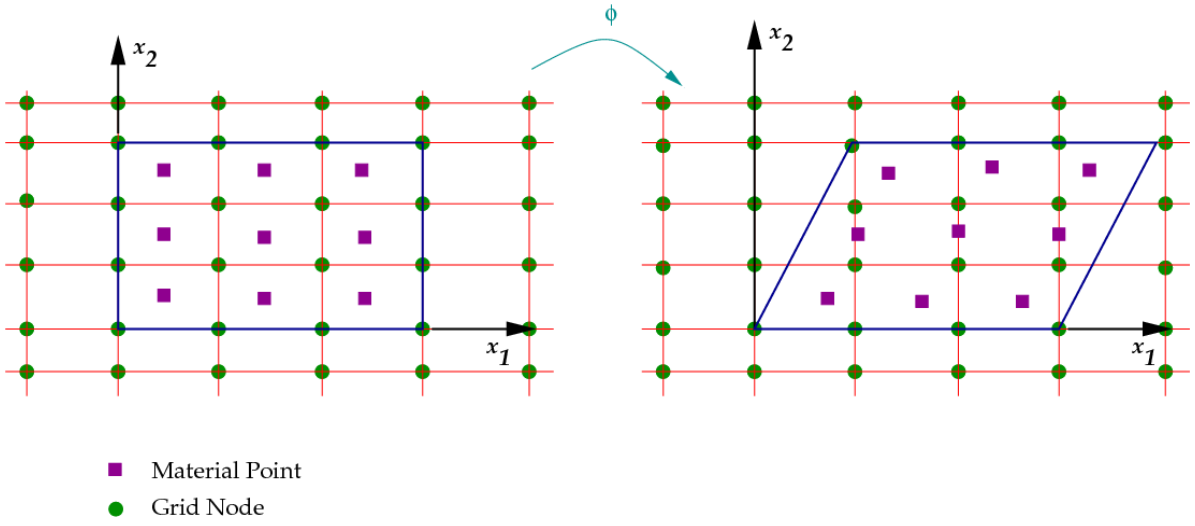

Figure 14 the concept of a pure Eulerian analysis. The material flows and passes the fixed elements within the domain. For extremely high deformation, fluid flows or large material damage, it is advantageous with an Eulerian analysis compared to the pure Lagrangian. (Wikiversity, 2010)

Roughly said, for Eulerian analyses the material flows and passes by the element nodes, while for Lagrangian analyses the nodes deforms together with the material. In addition, for a Lagrangian model, the entire mesh is assigned material properties. This is not necessary for Eulerian analyses: It accepts that there are regions of voids within the domain. That way, the material properties can be assigned to just portions of the domain. The volume fraction tool in ABAQUS calculates percentage voids compared to material within the Eulerian domain.

Eulerian and Lagrangian analyses both have their pros and cons, and they can be combined in a so-called coupled Eulerian-Lagrangian (CEL) model. The advantage of this is that a "CEL analyses typically offer better interpretation of contact conditions than pure Eulerian analyses, particularly for interactions between fluid and solid materials." (Dassault Systèmes,

2012b, 28.2). A CEL analysis is performed by including the Lagrangian element parts inside the Eulerian domain.

For the ice ridge-structure interaction in this thesis, a rigid body beam in contact with a first-year ice ridge makes it very favourable with the CEL technique. The rigid body is modelled with the Lagrangian technique, surrounded by an Eulerian domain where the ice ridge can freely pass by the structure.

In any analysis where the Eulerian technique is included, the analysis must be carried out in dynamic explicit steps. A brief description of explicit dynamic analysis follows in the next section.

2.3.4 Explicit dynamic analyses

Numerical solutions of differential equations are solved by either an implicit or an explicit solution scheme. In time-dependent analysis, an explicit method uses the initial or current time step to predict a solution for a future time. Hence, explicit methods are only dependent on the current time t, and t+Δt, where Δt is a small time step.

On the other hand, an implicit scheme make use of both the current time, t and the next time step t+Δt to obtain a solution. The solution is not explicitly given, and it is more time consuming to solve. For the CEL analyses in ABAQUS, the explicit scheme is the only available option. Dynamic explicit schemes prove to give good results for large models, and especially for short dynamic response times. (Dassault Systèmes, 2012a, 6.3.3)

The dynamic model uses an explicit central-difference integration rule to calculate the velocity and displacement components. At time, t, the dynamic equilibrium fulfils for the acceleration term. Thereafter, it is found a solution for the velocity term at time t+Δt/2 and the displacement component at time t+Δt. Equation 24 and 25 shows the calculation routine for the velocity term and the displacement term, according to Dassault Systèmes (2012a)

$$\dot{u}^N_{i+\frac{1}{2}} = \dot{u}^N_{i-\frac{1}{2}} + \frac{\Delta t_{i+1} + \Delta t_i}{2}\ddot{u}^N_i \tag{24}$$

$$u^N_{i+1} = u^N_i + \Delta t_{i+1}\dot{u}^N_{i+\frac{1}{2}} \tag{25}$$

, where

u is the displacement

$\dot{u}$ is the velocity term

$\ddot{u}$ is the acceleration term

i is the increment number.

N relates to the position in space, which means the algorithm gives an explicit solution (forward in time and central in space).

(Dassault Systèmes, 2012a, 6.3.3)

Equation 24 and 25 are given explicit as long as the terms with increment (i-1/2) and (i) on the right hand side of the equations are assumed known from the last calculated increment.

When it comes to the cost of running a dynamic explicit analysis, one have to look into the stable time increment size. "An approximation to the stability limit is often written as the smallest transit time of a dilatational wave across any of the elements in the mesh" (Dassault Systèmes, 2012a, 6.3.3). Equation 26 shows the approximation:

$$\Delta t \approx \frac{L_{min}}{c_d} \tag{26}$$

, where L_{min} is the length of the smallest element dimension in the model, and c_d is dilatational wave speed. Equation 26 is only an approximation, but it clearly shows the effect of a denser mesh, and thereby increased computational time.

2.3.5 Energy Balance in ABAQUS

"Energy output is particularly important in checking the accuracy of the solution in an explicit dynamic analysis. In general, the total energy (E_{Tot}) should be a constant or close to a constant; the "artificial" energies, such as the artificial strain energy (E_{AE}), the damping (viscous) dissipation (E_{VD}), and the mass scaling work (E_{MW}) should be negligible compared to "real" energies such as the strain energy (E_{SE}) and the kinetic energy (E_{KE})." (Dassault Systèmes, 2012b, 6.3.3)

Equation 27 shows the energy balance for an explicit analysis in ABAQUS: (Dassault Systèmes, 2012b, 4.2.2)

$$E_{Tot} = E_{KE} + E_{IE} + E_{VD} + E_{FD} + E_{IHE} - E_{WK} - E_{PW} - E_{CW} - E_{MW} - E_{HF} \approx Constant \tag{27}$$

For a detailed description of the different terms in equation 27, see appendix A

For our model, the following energy contributions are not relevant or negligible: E_{IHE}, E_{HF}, E_{PD}, E_{CD}, E_{DMD}, E_{DC}, E_{MW}, E_{CW}, E_{FD} and E_{FC}. Equation 27 then becomes as shown in equation 28

$$E_{Tot} = E_{KE} + E_{IE} + E_{VD} - E_{WK} - E_{PW} \approx Constant \tag{28}$$

$$E_{IE} = E_{SE} + E_{AE} \tag{29}$$

As seen in equation 29, the internal energy contains of two terms: Real energies, given as $E_{SE,}$ and artificial strains, E_{AE}. In general, and stated in the ABAQUS documentation, the artificial term should be small or close to zero. E_{AE} comes from the bulk viscosity, which is used to damp element oscillations. It relates to numerical errors in the model, and it has a destructive effect on the accuracy. This is the general case, but because of the user-defined material subroutine, the energy balance is slightly modified. Sergey A. Kulyakhtin points out that ABAQUS cannot distinguish between elastic and plastic volumetric strains when the particular subroutine is in use. Thus, the whole internal energy contribution is stored in the artificial strain variable, E_{AE}, and the real strain energy variable, $E_{SE,}$ shows up as zero.

The main drawback of this (per December 2015): It makes it harder to control which parts of the internal energy that are real energies, and which parts lead to numerical error in form of artificial strains. For the reader's information: From now on, the internal energy, E_{IE} is treated as equal to E_{AE}. In most plots, the artificial strain, E_{AE} will occur instead of E_{IE}.

One of the challenges of assessing the energy balance in an Eulerian analysis relates to the fact that the material flows freely in a rigid mesh. If the material reaches to any of the boundary surfaces or edges, material can disappear and give misleading results for the total energy balance. The domain should be sufficiently large to avoid this, at the sacrifice of the computational time. It requires more elements to conserve the same accuracy of the model, hence, it is a compromise between a sufficiently large domain and a dense enough mesh.

For a quasi-static analysis, the total energy is usually zero or close to zero, but for a dynamic analysis included impact, the initial total energy is equal to the initial kinetic energy and should be constant thereafter. Thus, it can be different from zero but still holds the principle of a constant total energy.

3 Model

3.1 Idealized structures

3.1.1 Structure width and geometry

The main objective for this thesis is to compare the ISO 19906:2010 formulations for the keel rubble actions to the described finite element model. In order to make comparable assumptions for the analytical calculations and the FE model, the choices of structure and keel geometry play an important role. The investigation includes three ideal cases:

- A wide structure
- An intermediate structure
- A narrow structure

Mainly the geometry of the structure is varied. The other parameters are held constant. Table 3 shows suggested values for the ridge keel parameters in equation 10.

Table 3 Material parameters for ridge keels (ISO 19906:2010, 2010, A 8.2.8.8)

Parameter	Value
φ [°]	20-40°
c [kPa]	5-7 kPa
e [%]	10-50 %
ρ_{ice} [kg/m^3]	900-920 kg/m^3

A study of the width effect according to the ISO 19906:2010 formula (equation 10), made it possible to draw some rough conclusion for choice of structures. Figure 15 shows how the keel rubble action according to ISO19906:2010 varies for structural width and keel rubble depth. The following set of parameters were used in equation 10 and figure 15: $\varphi = 30°$**,** c = 5 kPa, e = 0.35 (35%), $\rho_{ice} = 920$ kg/m^3, $\rho_w = 1025$ kg/m^3 and g = 9.81 m/s^2.

The force, F_K varies as a linear function for varying structural width, while the keel rubble depth comes into account as a third order polynomial, seen from equation 10. An increase in the rubble depth should according to this stand for a greater increase in the rubble keel actions compared to the width effect. From figure 15 one can clearly see that the derivative of the keel action with respect to the structure width is greater for the larger keel depths compared to the smaller depths.

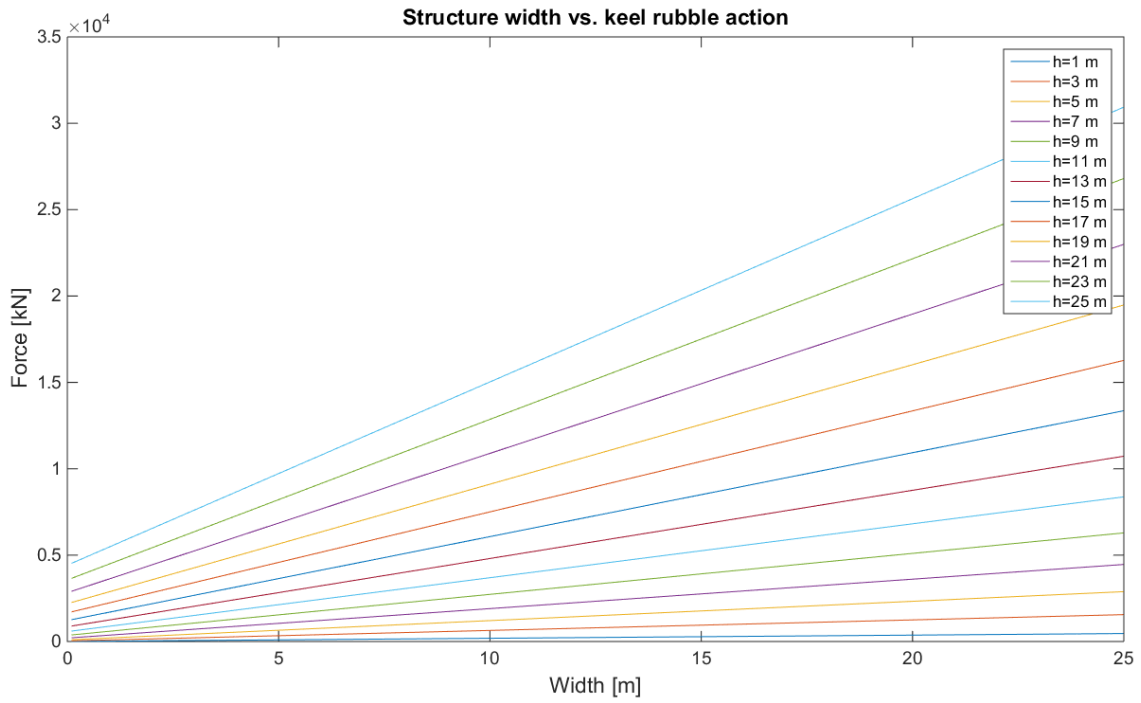

Figure 15 the keel rubble action according to ISO 19906:2010, plotted for varying structural width and keel rubble depth. The force varies as a linear function for varying width, while the keel depth comes into account as a third order polynomial.

On the other hand, an investigation of the global pressure shows a different trend. Figure 16 shows that the effect of the keel rubble depth gradually decreases when the structure width increases. For large widths, the corresponding global pressure seems to approach a finite value, where the effect of the keel depth is small or negligible. It should be noted that figure 16 bases on the assumption that maximum keel force occurs when the full rubble is in contact with the structure. The global pressure, P_G can then be found from equation 30:

$$P_G = \frac{F_K}{h_k D} \tag{30}$$

Given that, equation 30 is a reasonable approximation for the global pressure, equation 31 yields a criterion for the choice of structure width:

$$\frac{dP_G}{dD} \geq A \tag{31}$$

, where A is a coefficient of safety corresponding to the incremental change in global pressure per change in structure width. Figure 16 showed us that the global pressure

decreased for increasing width, but also the keel depth, h_k seems to stabilize. This effect is more clearly seen in figure 17.

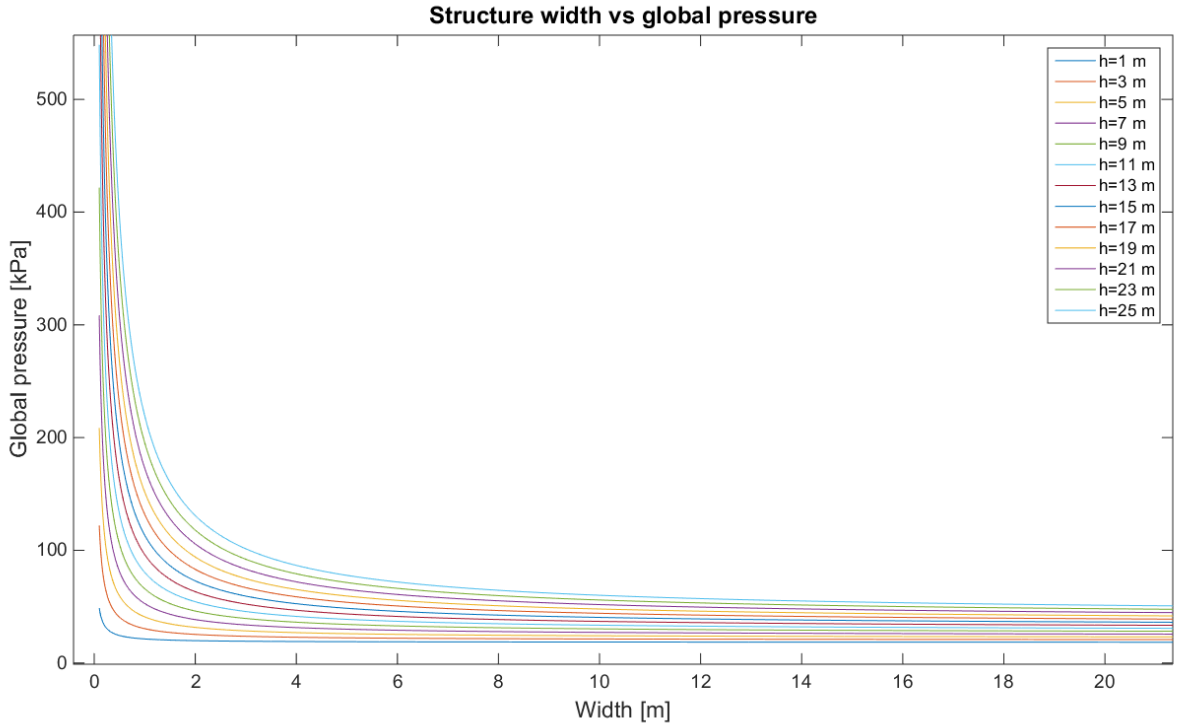

Figure 16 Global pressure as a function of keel rubble depth and structure width.

Figure 17 shows the criterion in equation 31 plotted for varying keel depth, h_k and structure width, D. Equation 31 is given analytically, while figure 17 gives numerical values for $\Delta D = 1/64$ m. See appendix B for descriptions and thorough calculations. Irrespective of analytical or numerical calculations, the conclusion is that the change in global pressure per change in structure width approaches zero when the structure width increases. This conclusion holds for all values of h_k

For instance, a factor $A \geq -200$ is valid for all structures wider than approximately 1 meter, read out from figure 17. Again, it must be stressed that the given factor is a function of the global pressure, where the uncertainty related to the contact area is out of our control. It is still a qualitative method to describe the singularities that occurs for very narrow structures. For the numerical analyses, it seems reasonable to stay away from structures narrower than 1 meter. The reason is simply to avoid or at least minimize the effect of the rubble keel depth on the model.

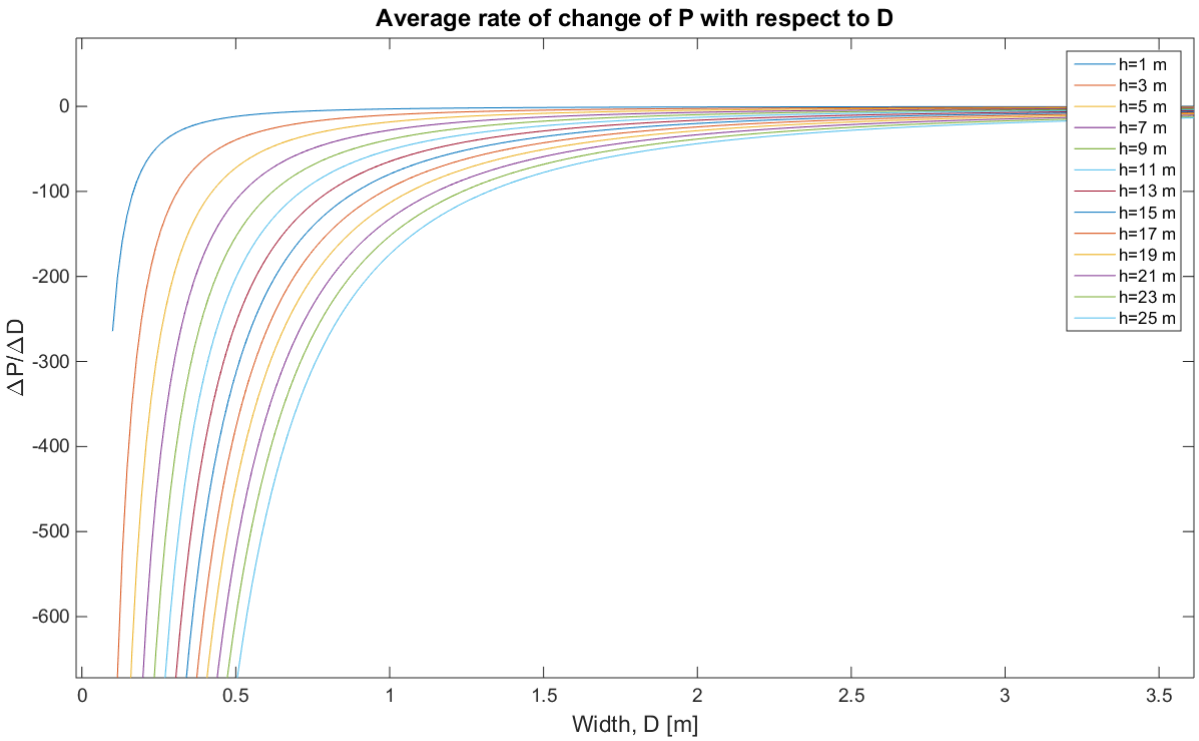

Figure 17 Equation 31 plotted for varying keel depth and structure width.

3.1.2 Rubble keel geometry

For this thesis', the following three main assumptions yields for the rubble geometry:

1. $h_k/W_s = 4$ is assumed to be valid, and should also govern for the rubble in the FE model. This is the fundamental assumption behind Dolgopolov et al. (1975). To make the results comparable, it is important to model the problem as close to the theory as possible. In addition, this is the only relation that directly links the sail width, W_s, to the keel rubble depth, h_k. The ratio seems to contradict Strub-Klein and Sudom (2012) (see figure 3) quite significantly, but Kärna and Nykänen (2004) found the ratio to hold for their parameter study.

2. $H_k/h_s = 4.5$ is used, the same value as ISO recommends. Again, the challenge is to find a reasonable estimate for the rubble keel depth, h_k. One have to rely on the ratio described above.
3. $W_k/W_s=6.75$ as proposed by Strub-Klein and Sudom (2012). This ratio is found important in order to find a keel width. For the FE model, it is more convenient to relate to the keel width than the sail width. Only the keel rubble was in focus for the analysis.

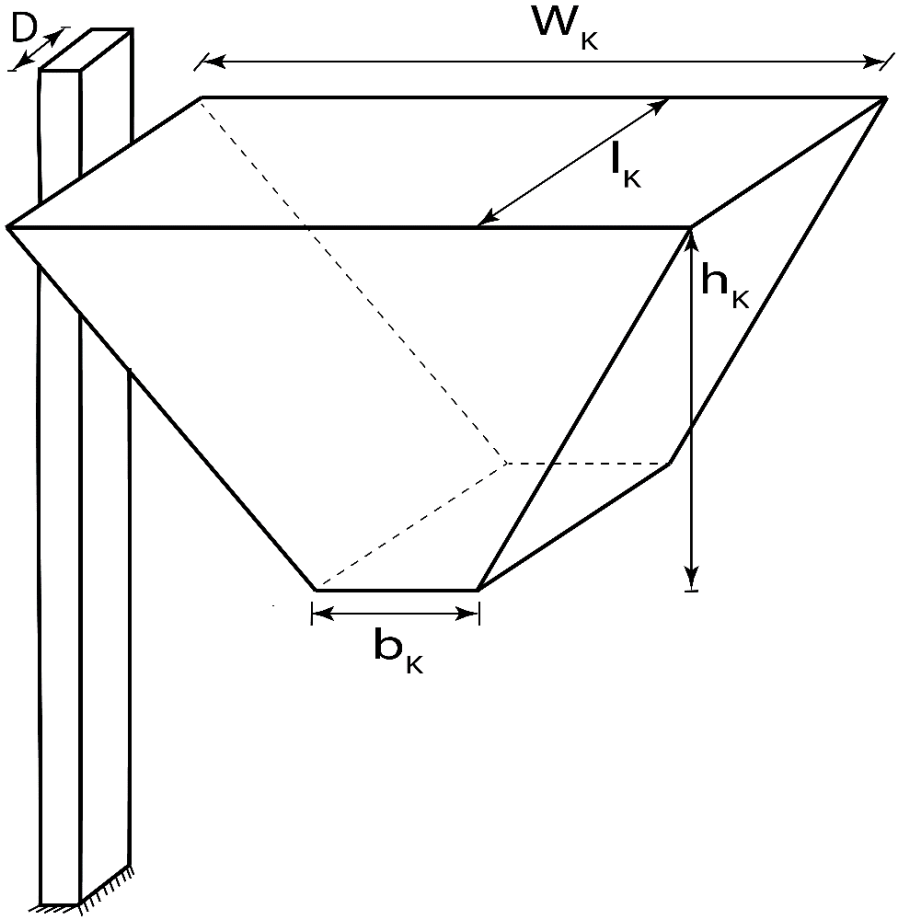

Figure 18 the keel geometry.

Figure 18 shows the main dimensions to be determined. From Strub-Klein and Sudom (2012) (see table 1) it was decided to use the maximum value of the average keel depth, denoted $\bar{H}_k^{max}$ = 12.5 m.

As previously explained, $H_K = h_c + h_k$, and given $h_c \approx 3$ meters (see figure 3), one get a design keel rubble depth, $h_K \approx 10$ meters. Dolgopolov et al. (1975) then yields a sail width, W_S = 2.5 meters. From assumption number 3, the keel depth, W_K = 17 meters, is finally found.

Parameter b_K, which is the width of the lower part of the keel, is given in ISO 19906:2010 (2010) as zero to five times the sail height, H_S. This, together with assumption number 2, yields a value of 0-15 meters for b_K. Below follows a summary of the calculations:

$$\bar{H}_k^{max} = \ 12.5\ m$$

$$H_K = h_c + h_k \quad \underset{h_c=3\ m}{\Longrightarrow} \quad h_k \approx 10$$

$$\frac{W_S}{h_k} = \frac{1}{4} \quad \underset{h_k=10}{\Longrightarrow} \quad W_S = 2.5$$

$$\frac{W_k}{W_S} = 6.75 \quad \underset{W_S=2.5}{\Longrightarrow} \quad W_k = 17\ m$$

$$\frac{H_k}{H_S} = 4.5 \quad \underset{H_k=12.5}{\Longrightarrow} \quad H_S \approx 3\ \text{m}$$

$$b_K = 0 \text{ to } 5H_S \quad \overset{yields}{\longrightarrow} \quad b_K = 0 \text{ to } 15\ \text{m}$$

The length of the keel, l_k has so far not been mentioned. Dolgopolov et al. (1975) assumed a definite ratio for the width parameters, but not the length effect. A more thoroughly description how the length effect is treated in the model, follows in section 3.2.1. Table 4 shows a summary of the relevant dimensional values.

Table 4 Keel dimensions

Parameter	Value
D	Varied
h_k	10 m
W_K	17 m
b_K	4 m
l_k	Varied as a function of D

3.2 ABAQUS model

3.2.1 Introduction

The goal is to guide the reader through the ABAQUS model and describe all the steps listed in section 2.3.1. Figure 18 gives a rough concept of the model: The impact of a first-year ice ridge on a rigid structure fixed at the seabed (or regarded as an anchor point). One of the first questions that arises is the sea depth in relation with the structure depth. In practice, grounding of ice-ridges occurs in shallow water, and may give tremendous force

contributions to the structure. For a harbour or a lighthouse in shallow waters, this effect might play and important role, and should not be forgotten.

From a modelling point of view, grounding introduces an extra set of boundary conditions close to the seabed, which makes the model more complex. In this case, the goal is to model the depth sufficiently deep to avoid such effects. The ice-ridge should ideally pass the structure in a way such that the crushing effect and the rubble build-up is smaller than the sea depth (structure depth).

The second question that arises, and as previously mentioned, what is a sufficiently long keel length, l_k? In the initial phase, these two parameters where carefully monitored and checked. The discussion above leads to the following requirements:

1. The keel should not ground, but pass the structure in free water. It is checked simply by animation of the keel structure interaction to see how the keel deforms.
2. The length, l_k, must be sufficiently long such that the stress distribution on the edges of the keel is negligible and close to zero.

Figure 19 and 20 illustrates the requirements shown above.

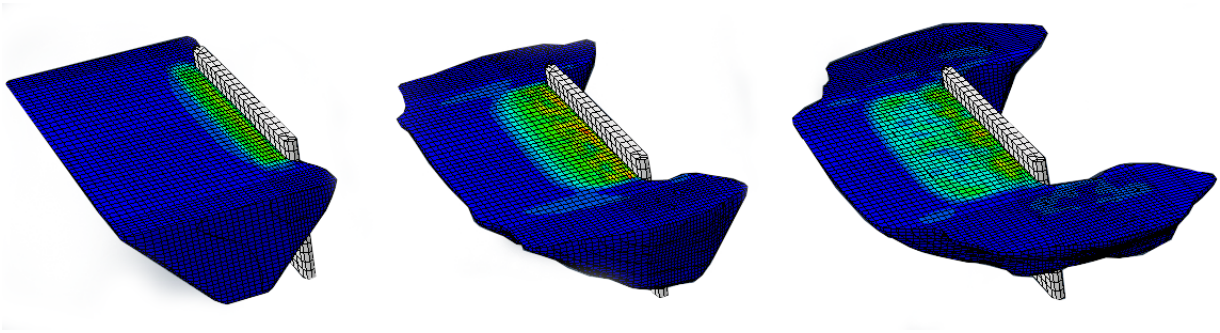

Figure 19 shows the keel's stress distribution at three different time steps during interaction for an arbitrary chosen model. Blue colour means stresses approaching zero. The figure illustrates the requirement of low stress distributions close to the keel's boundaries.

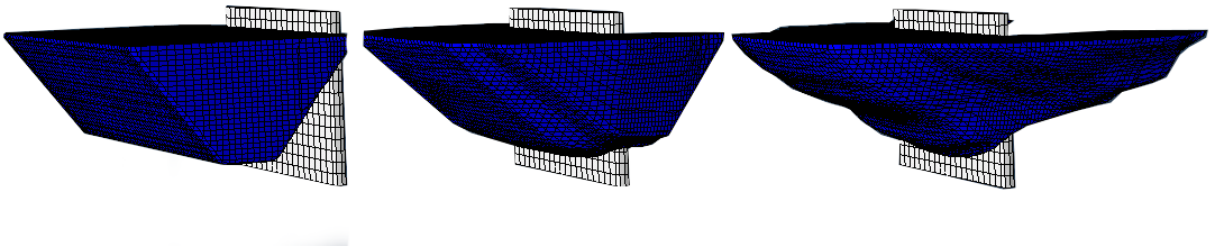

Figure 20 shows the grounding effect during interaction at three different time steps. The keel may ground if the crushing interaction leads the keel to approach the seabed. The seabed and the point where the structure is fixed coincides in the model. As long as the keel do not ground, there are no need for extra boundary conditions here.

3.2.2 Parts

In theory, there are three main parts in the model: The keel, the rigid body structure and the Eulerian domain, which encloses the two others. An Eulerian analysis allows the material to freely flow inside the rigid mesh. The keel part comes into account as a helper to define the initial material assignment, but it is supressed from the final simulation. Related to this, there is a further discussion of the volume fraction tool in section 3.2.7.

First, the structure was drawn with the following specifications: 3D Lagrangian model, type: Discrete Rigid. The concept of rigidity treats the structure as much stiffer than the rest of the model, such that structural deformations are negligible. The ice ridge will yield before the structure. In this case, where the maximum ice ridge forces are of interest, this is a suitable technique to model the structure.

A structure depth of 15 000 [mm] was chosen, based on the following knowledge: The rubble depth was earlier on set to 10 meters. From figure 3, in a real situation there are layers of consolidated ice and level ice on top of the rubble keel. It seems more realistic to lower the contact area a couple of meters down on the structure. It might not play a big role, since the structure is modelled as a rigid body, and it is mainly the reaction force at the fixed point which is monitored. On the other hand, it would play an important role for the reaction moments. Given that the keel hits the structure a couple of meters lowered down, there are roughly three meters left for the keel of free movement without hitting the ground (seabed).

The narrow structure was assigned a width, D = 1250 mm (1.25 m), the intermediate structure D = 10 000 mm, and the wide structure D = 20 000 mm (20m). In addition, all sharp edges expected to be in contact with the ridge keel were assigned with rounded corners. The reason for that, as Nilsen (2015) showed in her thesis, is that sharp edges in contact with the ridge material may cause singularities, and potentially harm the energy balance of the system. In order to keep the parameter steady, the edges was rounded off with a radius, r = 500 mm for all the models. Figure 21 shows the fillets with a 500 mm radius. The picture is for one of the wide models, with a structure width, D = 20 m.

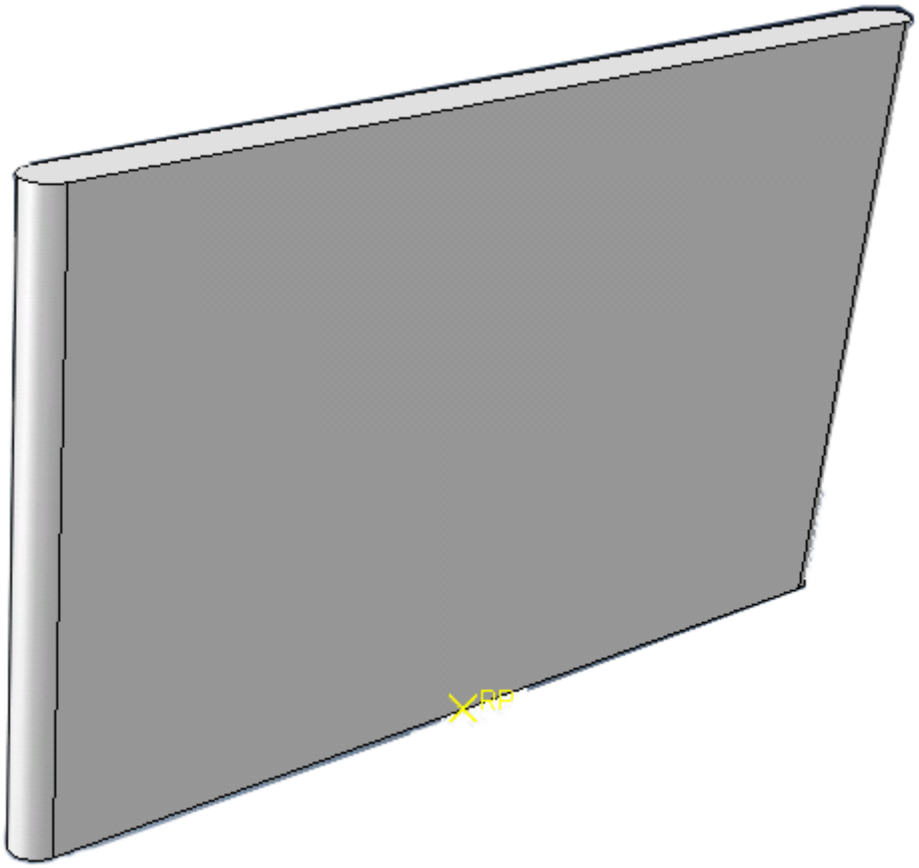

Figure 21 the edges where the keel material most likely will pass the structure is rounded to avoid singularities around sharp corners. It was used a radius equal 500 mm.

The structure length has not been discussed; in all cases, it was set constant to 1 m. As later seen, the tangential contact is neglected and defined as frictionless. For a large length of the structure, this assumption might not be a good approximation. In this thesis, it has not been performed any further investigation of this relation. As a note, the structure length is not in the same plane as the keel length, l_k. The structural length is parallel with the keel's width.

The keel geometry in ABAQUS is similar to the rough sketch showed in figure 18 and the assumptions by Dolgopolov et al. (1975). Except for the keel length, l_k, which was varied to suit the different structural widths, all parameters were constant (see table 4).

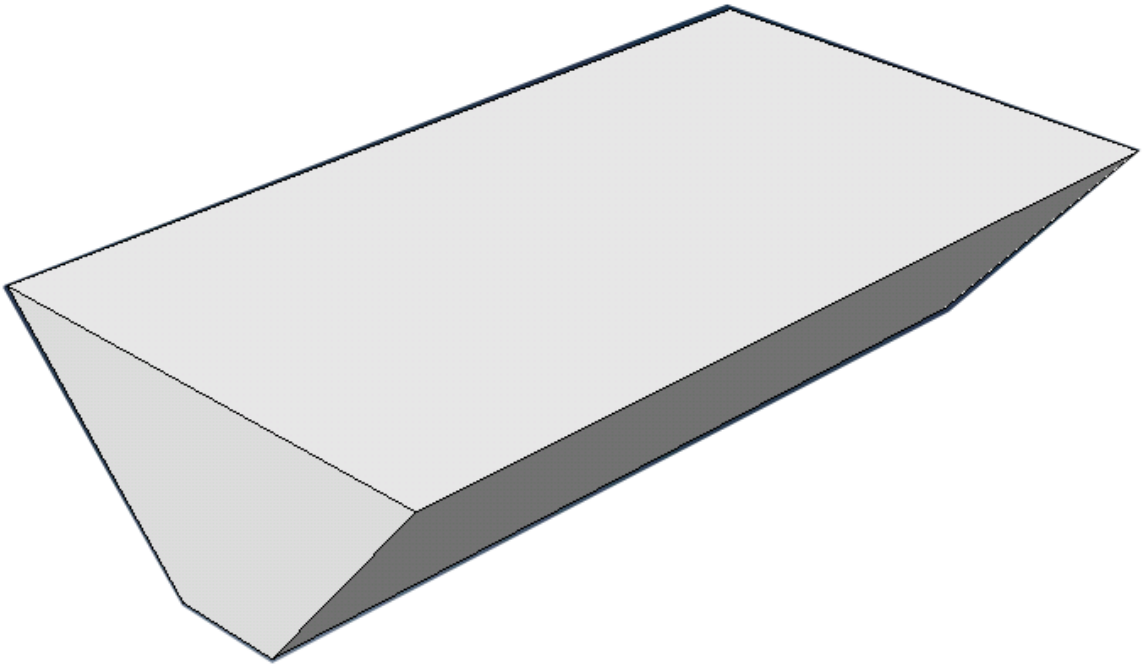

Figure 22 shows the keel geometry for one of the wide models (print screen from ABAQUS).

Finally yet importantly, comes the Eulerian domain. It is fit to adjust the keel and the rigid body structure, but still kept small enough to hold the computational time on an acceptable level. In theory, the Eulerian domain could have an arbitrary shape and size, but; with mesh distortions and irregularities in mind, it seems reasonable to keep the domain of a rectangular shape. Table 5 gives a summary of the most important geometrical dimensions for the four different ABAQUS models, where l_e, w_e and h_e is the length, width and depth of the Eulerian domain. h_s and l_s is the depth and the length of the rigid body structure. Narrow model II, the intermediate model and the wide model have identical geometrical properties, except for the structure width that varies. The reason that there are two narrow models is because of a mesh refinement for narrow model I compared to model II. The keel length is also different, but in theory, it should not play a big role, other than for the magnitude of the kinetic energy. The stress distributions were monitored for both the models. It was done to make sure the stress distributions along the edges and boundary surfaces approached negligible values.

Table 5 shows the most important geometrical dimensions for the keel, the Eulerian domain and the structure. All lengths given in meters [m].

Model	The Keel				Eulerian domain			The structure		
	h_k	W_K	b_K	l_k	l_e	w_e	h_e	D	h_s	l_s
Narrow model I	10	17	4	6	30	50	15	1.25	15	1
Narrow model II	10	17	4	10	50	50	15	1.25	15	1
Intermediate model	10	17	4	20	50	50	15	10	15	1
Wide model	10	17	4	30	50	50	15	20	15	1

3.2.3 Materials and sections

In section 2.3.2, it is included the most relevant theory behind the Continuum Breakage Mechanism (CBM). Table 2 showed the material model parameters equal to the ones that are used for the ABAQUS model. In the "materials section" in the ABAQUS model tree, the nine parameters are included under the general tab as a "user material".

In addition, "Depvar" and "Density" are defined, also from the "General" tab. "Depvar" mainly relates to the number of solution-dependent state variables, which is set equal to one in this model.

Table 3 gives values for the density for sea ice, and here it is set equal to 920E-12 tonnes/mm^3 (920 kg/m^3).

3.2.4 Assembly

The assembly governs the initial setup, and the different parts' position relatively to each other. In order to include the discrete rigid structure into the overall assembly, it needs to be given properties of a rigid shell; with corresponding shell elements (see the mesh section for further descriptions)

The most beneficial set-up proved to be with the top section of the discrete rigid body structure out of the Eulerian domain. The reason relates to the fact that a buoyancy force and a corresponding constraint against vertical velocities at the top surface is easier to change by the given set-up. The alternative is to make a surface section inside the Eulerian domain, which is a more comprehensive process, especially to avoid mesh irregularities. Figure 23 illustrates the general approach used for the assembly. The keel expects to hit the structure and crush; in addition, some of the material will pass by on the sides.

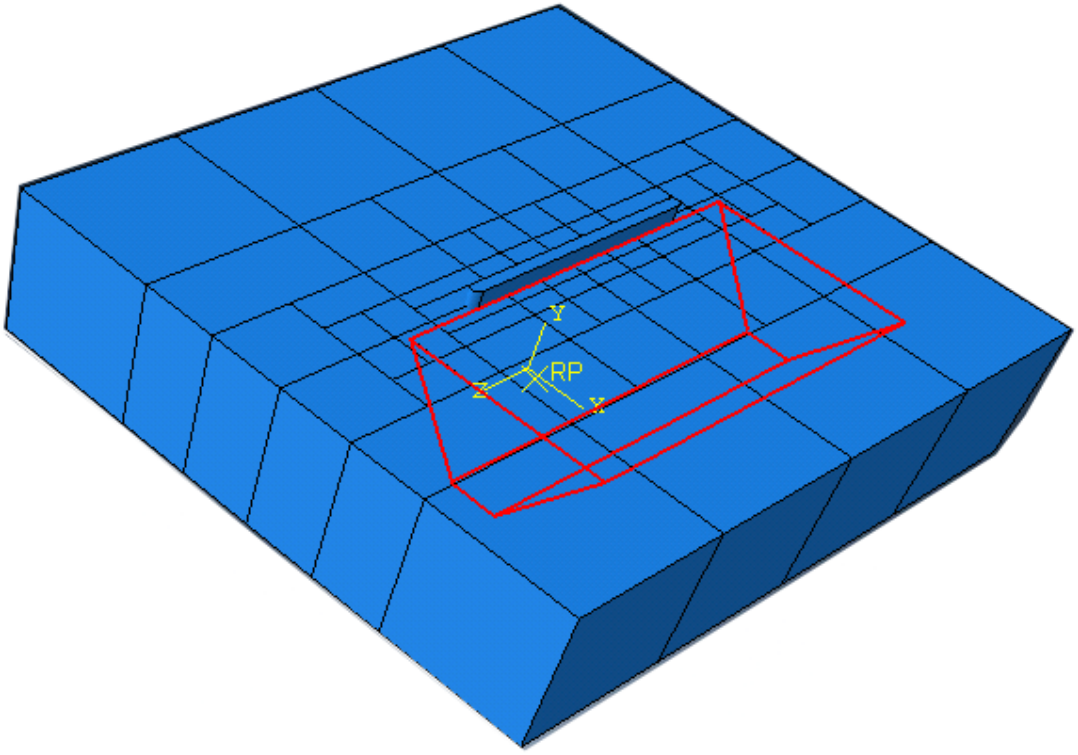

Figure 23 the assembly of the model. The red lines highlight the keel's initial position relatively to the structure. As seen, the top section of the structure (roughly the top 2 meters) is left outside of the Eulerian domain. The black lines indicates partitions where the only function is to assign local seeds to different parts of the domain.

After the rigid structure and the keel geometry are set to theirs desired positions within the Eulerian domain, the keel is suppressed from the final simulation. As previously mentioned, the keel geometry only works as a helper for the volume fraction tool to calculate the initial void ratio for the model. It is the Eulerian domain that governs the keel's behaviour during simulation, not the keel part itself. For that reason, the keel does not get an individual mesh and seeds, as later seen.

3.2.5 Sets and surfaces

The need for a reference point has mainly two practical reasons: To define the contact definition between the structure and the keel and because one needs a point to monitor the loads during interaction. A natural place to go for the reference point was at the middle edge of the lower, fixed end of the structure, as seen in figure 24.

Under the branch for the "History Output Request", it was toggled on for reaction force output for the reference point particularly. The reference point also become the point to constraint the structure from movement, as seen in section 3.2.7.

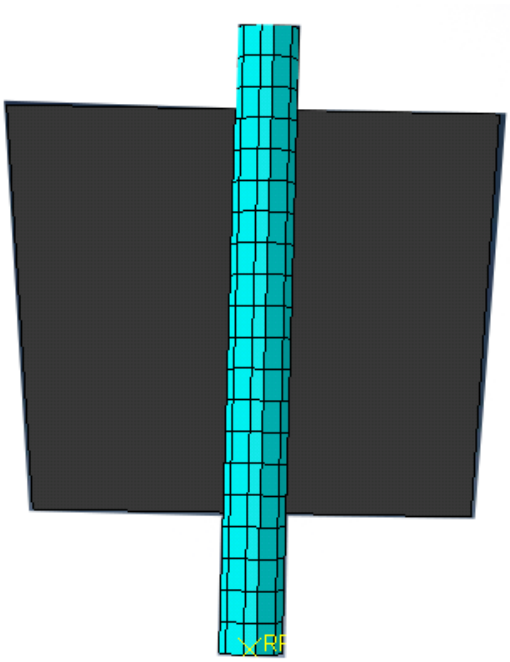

Figure 24 the yellow cross, named "RP" marks the reference point, in this case, for the narrow model. The point works obviously as a reference point but also: Point of structural constraint and point to monitor the reaction force.

For later use, it was made sets for the top surface, the three different parts and for different regions within the domain. The latter to have the opportunity to make local seeds and refinements of the mesh in certain regions.

3.2.6 Steps

The load steps for an Eulerian analysis in ABAQUS is dynamic, explicit, as the only available option. The load step creates after the default initial step. The contact definitions (see section 3.2.8) create in the initial step, and then propagate for the dynamic, explicit load step. The same yields for the material properties and for the structural constraints. The velocity field for the keel adds to either the initial step or the dynamic step; depending on which approach one decides for. An explanation of the two approaches is in section 3.2.7.

The buoyancy force comes into account in the dynamic load step. There were tried two different approaches for the buoyancy:

1. Instantaneously added with full magnitude from the initial start of the step.
2. Gradually ramped up to its full magnitude over the duration of the step. An initial percentage value of the full amplitude comes instantaneously, before it linearly increases.

The field output requests and the history output request obviously adds to the dynamic load step, where the main interaction is. The next section goes more in detail on the loads, definitions for the boundary conditions and the predefined fields.

3.2.7 Loads, boundary conditions, and predefined fields

Loads, boundary conditions and predefined fields closely link together and sometimes even overlap. For instance, the two approaches for modelling of the keel drift:

The first approach applies a keel velocity as a predefined field to the initial step. Based on the initially created velocity, ABAQUS computes a velocity field for the dynamic, explicit load step. This method makes use of the volume fraction tool to assign the load to the right portion of the model. The volume fraction tool (VFT) is available as a discrete field in ABAQUS. It defines the keel instance inside the Eulerian domain, and calculates the keel's volume as a fraction of the whole domain. The VFT is mesh dependent, since the calculated fraction is per element. A denser mesh gives a better approximation according to the initially drawn geometry.

From the VFT, both the velocity field and the material properties may be assigned for the initial keel position. The material assignment follows this procedure independent of how the load applies. The model has been tested for different magnitudes of the keel velocity, in the range 1000 – 3000 mm/s.

The second approach builds on the assumption that the driving forces for the ice ridge are currents and winds. It seems more realistic to apply the ridge drift as a uniform boundary condition over the whole domain. In difference to the first load approach, a drift of 1000-3000 mm/s is quite a high load to apply, since the boundary force assigns to the global mesh. The keel pushes forward by a constant velocity field during the dynamic load step, and not as an initial load. The two methods are conceptually different. For the first method, the keel expects a decrease in velocity during interaction due to the resistance from the structure. One of the risks is that the impact force by the initial contact is dominant compared to later crushing. In that case, the model fails to reproduce the behaviour of a realistic ice ridge.

For the second approach, this is not the case. A constant velocity field applied as a boundary force coincides with the concept where one looks at the driving forces from wind and currents as constant and spread over an infinite area. Different attempts were made in the range 50-100 mm/s, which is significant smaller values than for the initial keel load. The risk here, of course, is that the constant field leads to unrealistically high loads. The keel has nowhere to "escape" from the velocity field, a process that could lead to a much more complex form of crushing. The two different effects will be presented, in the results section.

As seen, either of the two approaches applies the keel velocity as a proper load in ABAQUS; the first approach uses a predefined field, and the second approach applies the velocity as a boundary condition. In addition to the given translational velocity in the horizontal direction, the buoyancy forces must be considered.

The buoyancy force applies as a body force over the keel volume. Equation 9 gave an expression for the effective buoyancy γ_e, as a function of the keel porosity (e), the water density (ρ_w), the ice density (ρ_w) and the gravity (g). The same formula is used to apply the buoyancy force in ABAQUS, with the same set of parameters as in the MATLAB script, see appendix **B**. It yields:

$$\gamma_e = (1 - e)(\rho_w - \rho_{ice})\, g$$

$$\gamma_e = (1 - 0.35)(1025 - 920)9.81 = 669.5 \left[\frac{N}{m^3}\right]$$

$$= 669.5 * 10^{-9} \left[\frac{N}{mm^3}\right]$$

669.5E-09 [N/mm^3] prescribes the loading per unit volume as a body force for the Eulerian mesh. By defining a vertical body force, it presents the risk of the keel to leave the domain and spoil the energy balance. Thus, it is important to fix the top surface against vertical velocities. A boundary condition is introduced where all vertical velocities normal to the plane is set equal to zero.

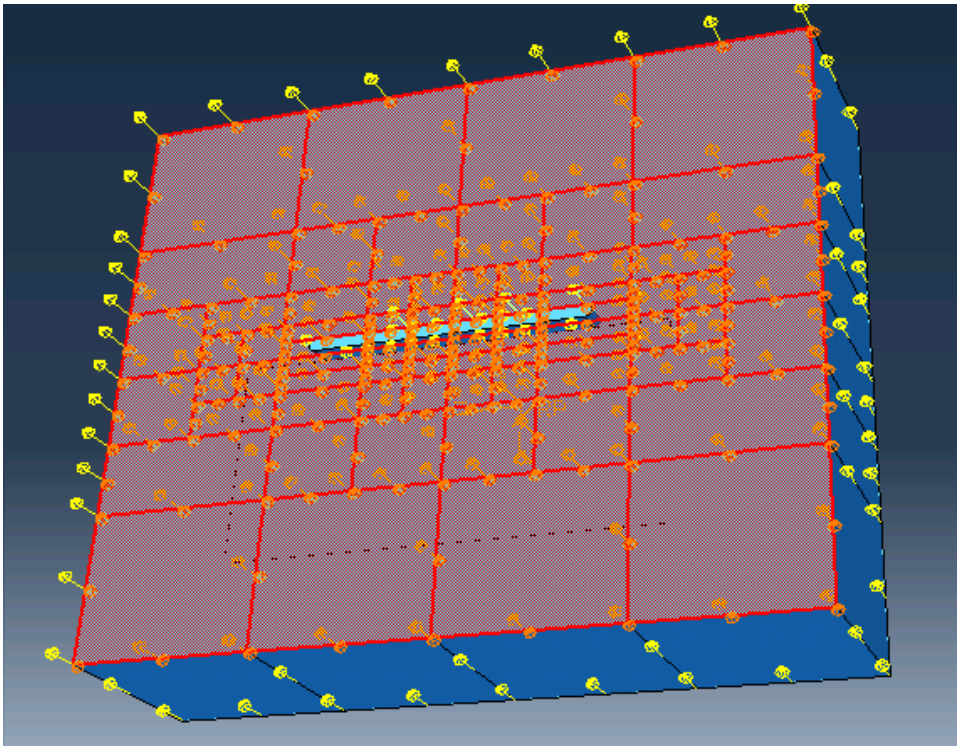

Figure 25 the top surface of the Eulerian domain. Yellow arrows indicate the prescribed buoyancy force, while orange marks/arrows illustrate the constraint against vertical velocities.

3.2.8 Interactions and their properties

The most important interaction property for this model relates to the contact problem between the rigid body structure and the keel material. For a dynamic, explicit analysis in a coupled Eulerian-Lagrangian model, the contact defines as "general contact (Explicit)". From the "general contact" tab, one choose the so called "All* with self" as a contact domain. This function enforces all the Eulerian material to interact with Lagrangian surfaces.

In addition, it was specified properties for the tangential and the normal contact behaviour. For the tangential behaviour, it was used a stiffness penalty method for the friction formulation. The penalty method "permits some relative motion of the surfaces (an "elastic slip") when they should be sticking" (Dassault Systèmes, 2012a, 36.1.5). The penalty stiffness follows the elastic slip, and changes continuously to the required value. When such type of stiffness methods are used, it is also necessary to monitor the energy balance. Primarily, to look out for numerical errors and artificial penalty energies.

In relation to the tangential behaviour, it was defined a friction coefficient of 0.03. It corresponds to an approximate value for a steel-ice friction coefficient. (The Engineering Toolbox, 2015).

The normal contact behaviour is selected as "Hard Contact" and with a default constraint enforcement method.

3.2.9 Seeds and meshes

Figure 23 shows how the Eulerian domain is split into partitions, suitable for local seed refinements. Especially the area around the structure is of greater interest. It seems reasonable to have a finer mesh close to the structure, since the expected largest stress distributions are in this area. At the same time, the whole area where the keel material flows must have a sufficiently dense mesh. The challenge is how time consuming the model becomes. With a keel width equal to 17 m, and keel velocities ranging from 1000-3000 mm/s, the material will cover quite a large area, depending on the length of the dynamic load step. It was attempted with a time step of 5 seconds, with the hope that the reaction forces have come to a steady state. This fact had to be checked from the result files, and thereafter adjusted if necessary.

The following technique applies for the seeding of the Eulerian domain, as illustrated in figure 26: First, it was defined a local seed of approximate size 2000 mm for the rear end of the model. By rear, means the region behind the structure, where the keel eventually will approach. The keel expects not to interact with this part of the domain, which explains the choice of a rather coarse seeding. With the local seeds assigned, the rest of the model was given global seeds equal to approximate 250 mm. ABAQUS calculates the optimal seed distribution for the given input values. Because of the combination of two seeds, the element size is dynamic and not necessarily 250 mm for the "front" region. 250 mm is just a guideline for the approximate size of the elements within this region. It was mainly looked out for element irregularities and initial distortions, which is known as a factor to disturb the accuracy.

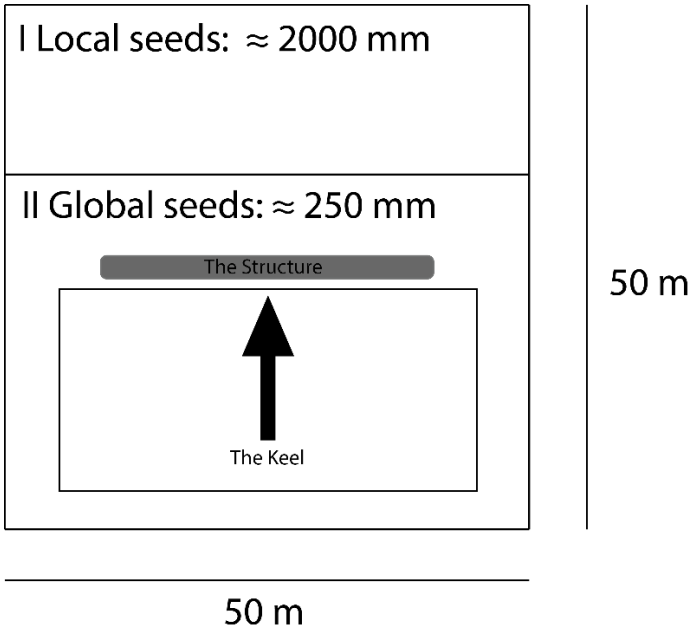

Figure 26 Tactic used to seed the Eulerian domain (bird's view).

Figure 26 relates to the following models (see table 5): Narrow model II, the intermediate model and the wide model. Figure 27 shows the final mesh with elements assigned. The element type for an Eulerian domain is of the type "EC3D8R", which means an 8-node linear Eulerian brick, reduced integration, hourglass control. This is the only available element option for an Eulerian, explicit analysis. The hourglass effect arises in a consequence of reduced integration, where spurious energy modes (zero energy modes) gives highly distorted elements. The problem is simply assessed by a look on the deformed model, where the affected elements get a typical hourglass-shaped deformation. The hourglass control in ABAQUS also addresses this problem. Here, it was used default settings for the hourglass control, with a scaling factor equal one for both the linear and the quadratic bulk viscosity.

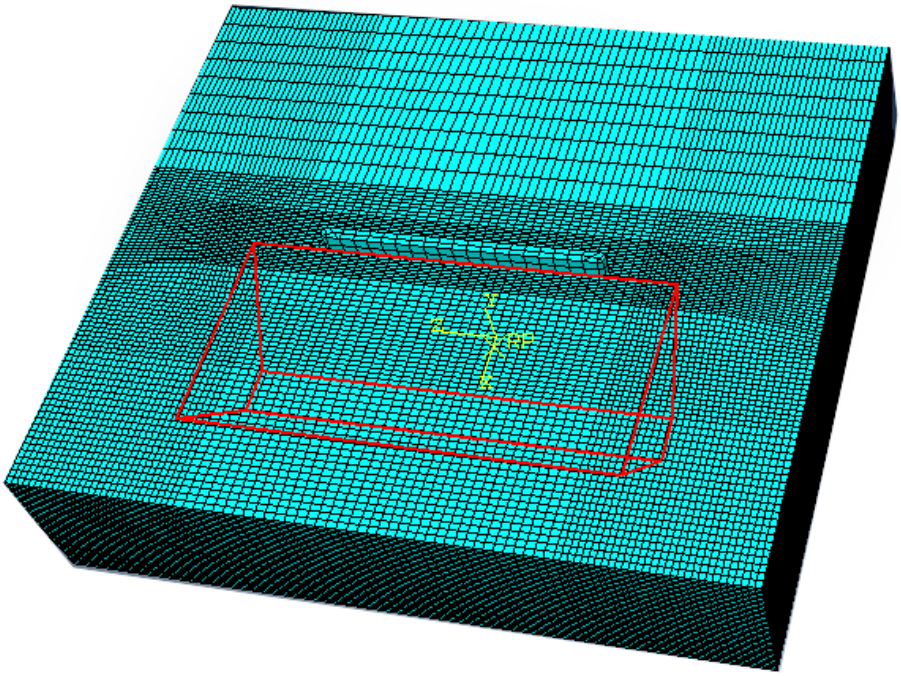

Figure 27 The wide model seeded and meshed. It resulted in 286 344 elements, and the refinements near the structure is clearly seen. The red lines highlights the keel's initial position.

The structure has properties of a rigid body shell, and it has seeds with an approximate global size of 1000 mm per element (see figure 28). For a discrete rigid part of this type, the "R3D4" element type is available. R3D4 is a 4-node 3-D bilinear rigid quadrilateral element, specially developed for this type of constraint. There are no particular element controls available for this type, and as a Lagrangian type element, it makes the coupling to the Eulerian domain and the CEL model.

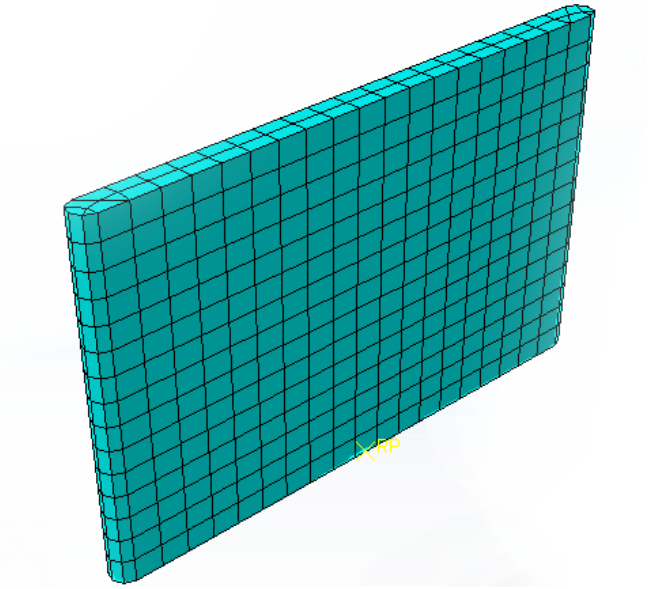

Figure 28 the rigid body structure meshed with R3D4 elements with an approximate global seed size of 1000 mm

Table 5 showed that two different models exists for the narrow structure. The “narrow model II” has identical mesh to the ones described above, while the “narrow model I” has a significant refinement of the mesh. One of the reasons for an additional assessment of the narrow model lies in the effect illustrated in figure 16. The global pressure has according to this an asymptotic effect when the structural diameter, D approaches zero. A higher stress distribution (global pressure) for a narrower structural width, might say that the mesh should be extra dense. If this hypothesis holds or not, as well for the numerical model, is one of the more important questions.

It was used a similar seeding approach for the “narrow model I” to the one described above, but with a slightly modified geometry of the Eulerian domain. A denser mesh for the same domain would mean an inexpedient computational time. In addition, both the structure width and the keel length is smaller.

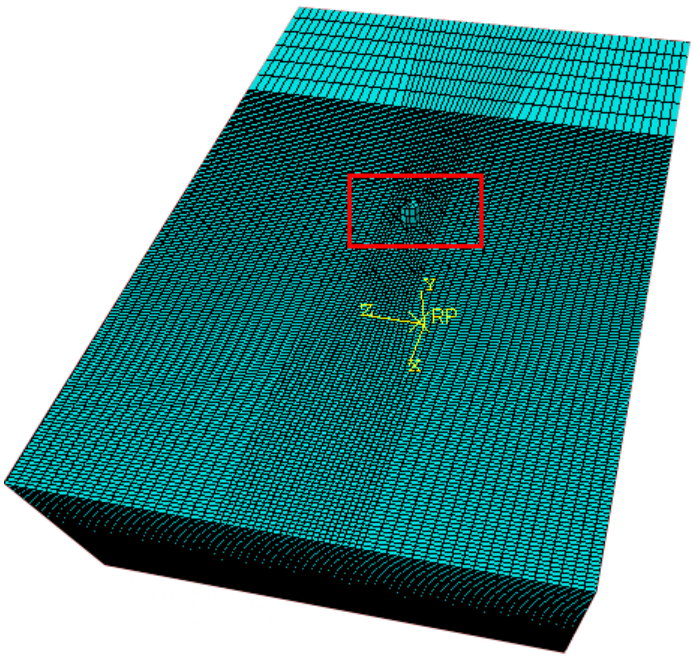

Figure 29 the meshed Eulerian domain for the "narrow model I". The result is a model of 390 156 elements. Given the decrease in the length of the Eulerian domain from 50 to 30 meters, this is a considerable denser mesh than for the “narrow model II”.

4 Results

4.1 Introduction

The result chapter of this thesis divides into mainly two topics: The first section shows the most important energy contributions plotted for the different models. The other section focuses primarily on the reaction forces from the ice ridge action. The link between the two is of course important. A bad energy balance for the system, leads to less trustworthy results for the reaction forces. If inaccurate energy results are caused by numerical errors or other causes will be partly discussed here, and more in the "Discussion and Analysis" chapter.

Before one heads for the general result presentation, some few words is said about the two different approaches for interpretation of the keel velocity. It feels necessary to treat the results from the keel velocity as a boundary velocity by itself. The keel velocity applied as a boundary velocity proved to show misleading results, both for the total energy and the reaction forces. It does not make much sense to present and go in detail on every simulation run with this setup. The focus is rather on the general concepts and common challenges that occurred. There were a clear trend independent of the mesh or structural widths.

On the other hand, the approach of an initial load as a predefined field proves better and more reliable results, and is discussed more in detail and presented systematically. In the end follows some general reflections regarding the use of rounded edges, and some comments about the use of a gradually increased buoyancy force contra a constant force.

4.2 Keel velocity applied as a boundary condition

This section shows some of the general reflections regarding the energy balance and the reaction force for the keel velocity applied as a boundary condition. Figure 30 illustrates the problems explained in this chapter's introduction. The keel material is prevented from freely pass the structure. Instead, it occurs a gradual increase in transversal deformations, perpendicular to the direction of the velocity. It is obvious that the structure interaction provokes the effect. The deformation pattern itself is not a problem, and an enlargement of the width of the Eulerian domain (to avoid material to disappear or leave the domain) could prevent potential odd energy results.

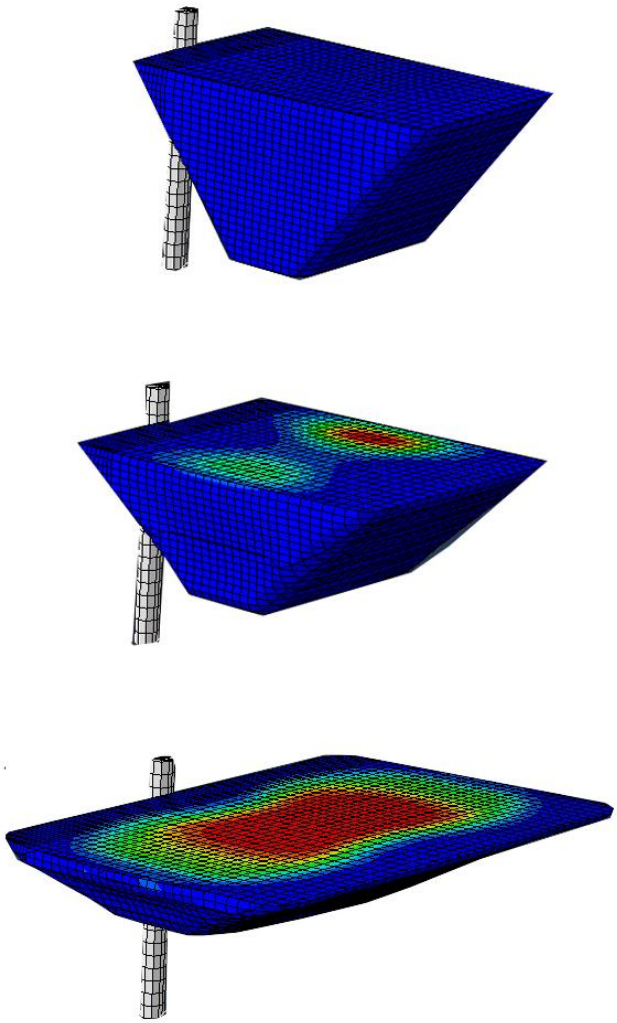

Figure 30 shows deformed shape of the keel during interaction. The sides expect to freely pass the structure, but it does not occur. Instead, the keel deforms more and more in the transversal direction, perpendicular to the applied load. It yields unrealistic results, both for the energy balance and the reaction force.

Figure 31 shows the effect of the deformation pattern in figure 30 for the energy balance of the system. The applied keel drift is here equal to 100 mm/s, which means a lower initial total energy and kinetic energy compared to the other load approach, is reasonable. The problem is the artificial energies that during interaction increases dramatically. The energies from penalty work and the viscous damping are unacceptable high, and gives a pronounced drop in the energy (seen especially after three seconds of simulation).

Different approaches, for instance lowering the keel drift to 50 mm/s did not prove any more realistic results. The resultant force was still unrealistically high and the energy balance showed the same trends seen in figure 31 and 32. In addition, when the keel drift becomes lower, a new challenge arises; it is necessary to increase the time step quite a lot, to get the same amount of interaction between the structure and the keel. It makes the model significantly more costly in terms of computational time.

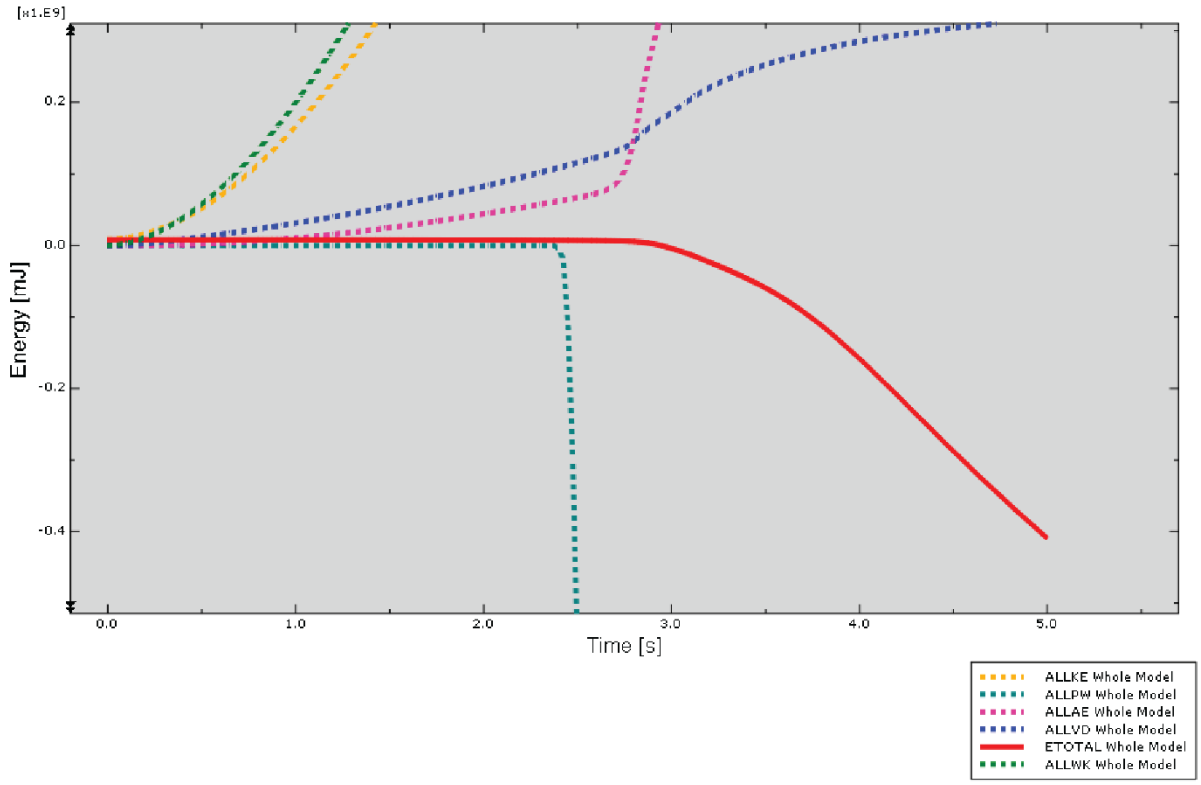

Figure 31 shows plots of the total energy together with the different energy components. The given model has a keel drift applied as a boundary velocity equal 100 mm/s.

To shed light on these challenges, figure 32 includes the graph for the reaction force. It shows a maximum force near 4.0E06 kN, compared to a value of roughly 800 kN suggested by Dolgopolov et al. (1975) (see figure 15). Based on these findings, it was decided to reject the model for further investigations, and rather try to optimize the model with a predefined velocity field. In order to assess and compare the resultant forces, it is also beneficial to have a consistent model and mesh for all the structure widths.

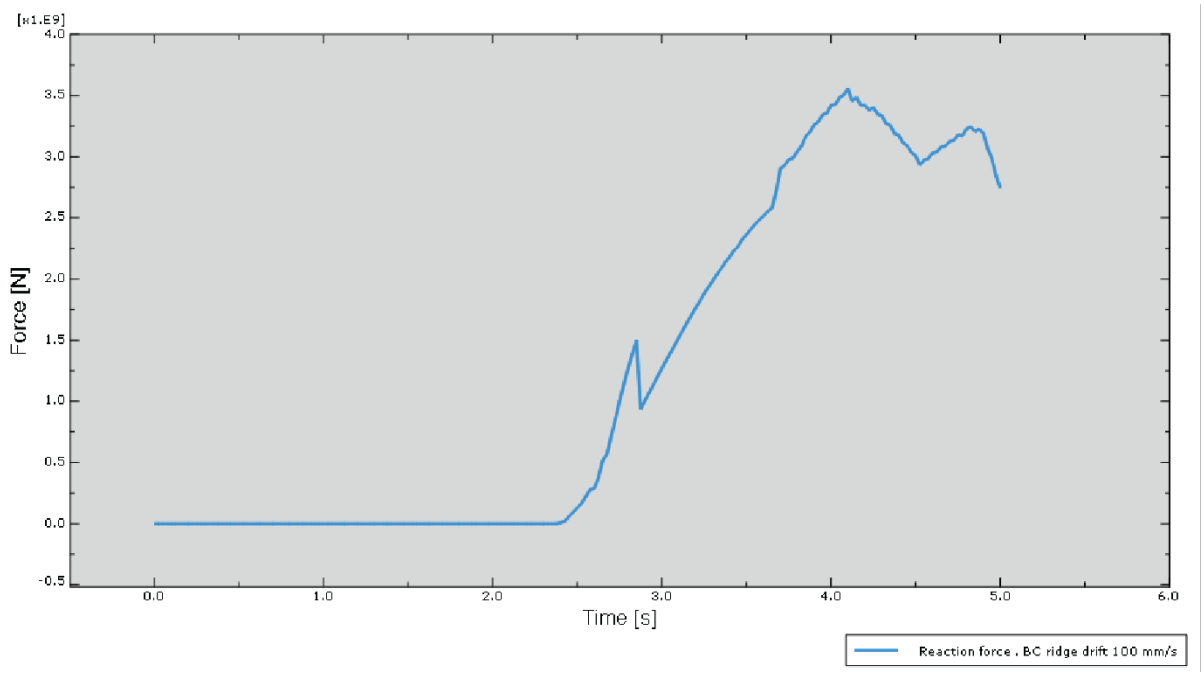

Figure 32 the reaction force for a model where the keel drift applies as a boundary velocity.

4.3 Energy balance

The results presented from here on out relates only to the model with the keel velocity applied as a predefined field. First, it follows a presentation of the energy balance for the three different models. In section 4.4 comes the results for the reaction forces.

4.3.1 Wide model

Figure 33 gives the total energy balance for the wide model (see table 5 for geometrical descriptions) for three different sets of the velocity field: 1000, 2000 and 3000 mm/s. The other parameters, such as seeds, meshes, interaction properties, material parameters etc. were constant.

At first sight, the model seems to yield a stable energy balance, but there is a larger drop in the total energy for an increased velocity. Somehow, the drop is not consistent, and the 3000 mm/s model manages to recover some of the energy during interaction.

Keel velocities of 1000 and 2000 mm/s have a smaller spread in the energy loss, compared to the 3000 mm/s model.

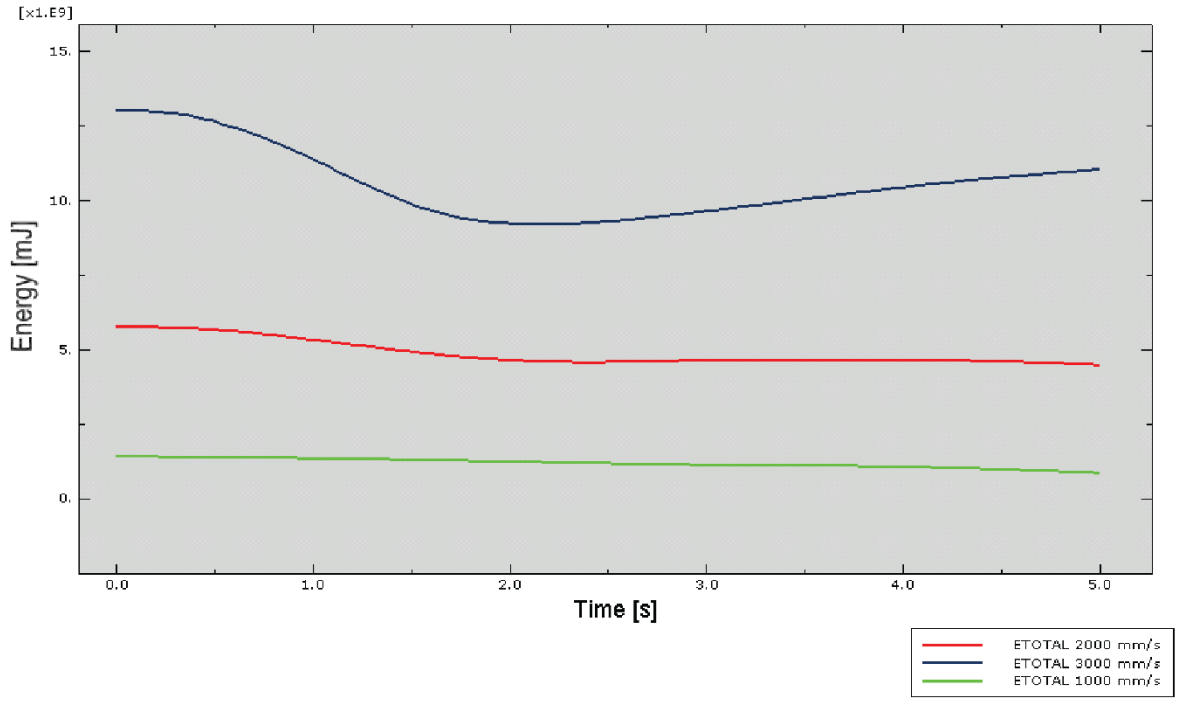

Figure 33 shows the development in the total energy for the wide model (see table 5), for three different predefined velocity fields. As later seen, the initial, total energy corresponds to the initial, kinetic energy. It is reasonable that an increase in velocity, gives a higher initial value for the total energy.

A stable total energy for the whole model is a good sign for the accuracy, but it is important to check which of the energy components that contribute to the total balance. Figure 34, 35 and 36 show the energy components together with the total energy for the wide model. Again, the predefined velocity field is the only variable. Equation 28 gave the energy balance in ABAQUS, and as seen in the figures, the artificial components are negligible and excluded from the plots. It leave us with the following contributors:

ALLVD: Energy from Viscous dissipation

ETOTAL: The total energy for the whole model.

ALLKE: Kinetic energy

ALLWK: Energy from external work.

ALLAE: Artificial strain energy / internal energy (see section 2.3.5 for description)

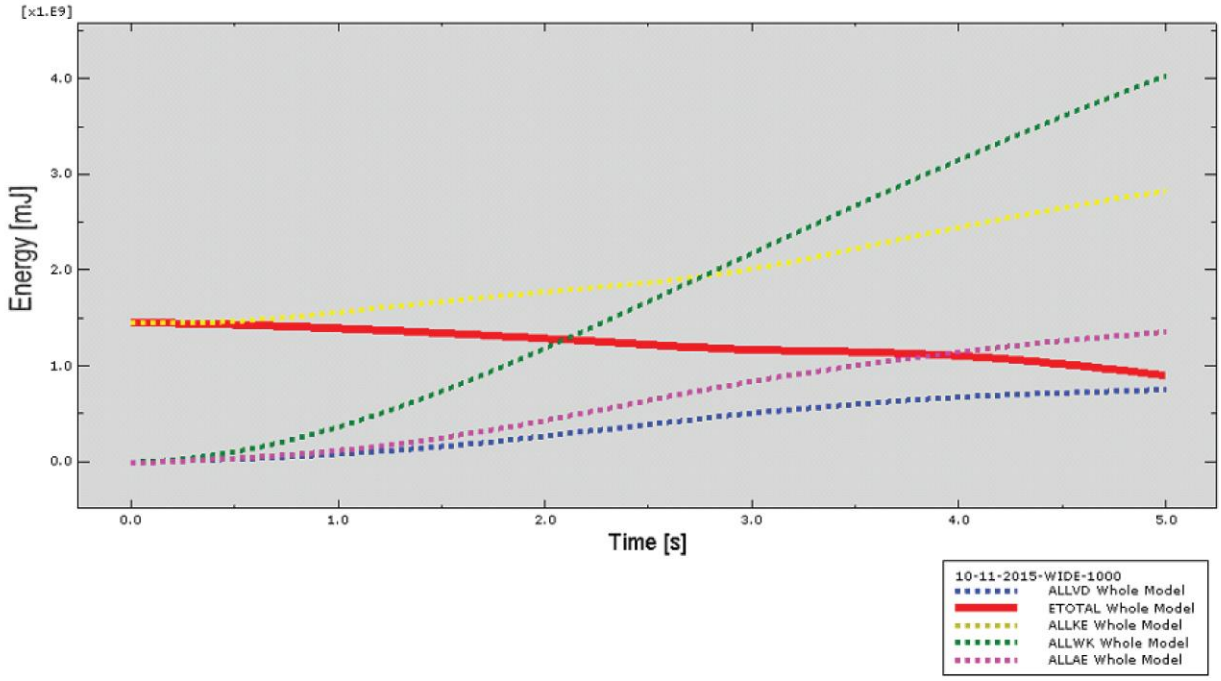

Figure 34 Plot of the different energy contributors together with the total energy for the wide model with a predefined keel velocity of 1000 mm/s.

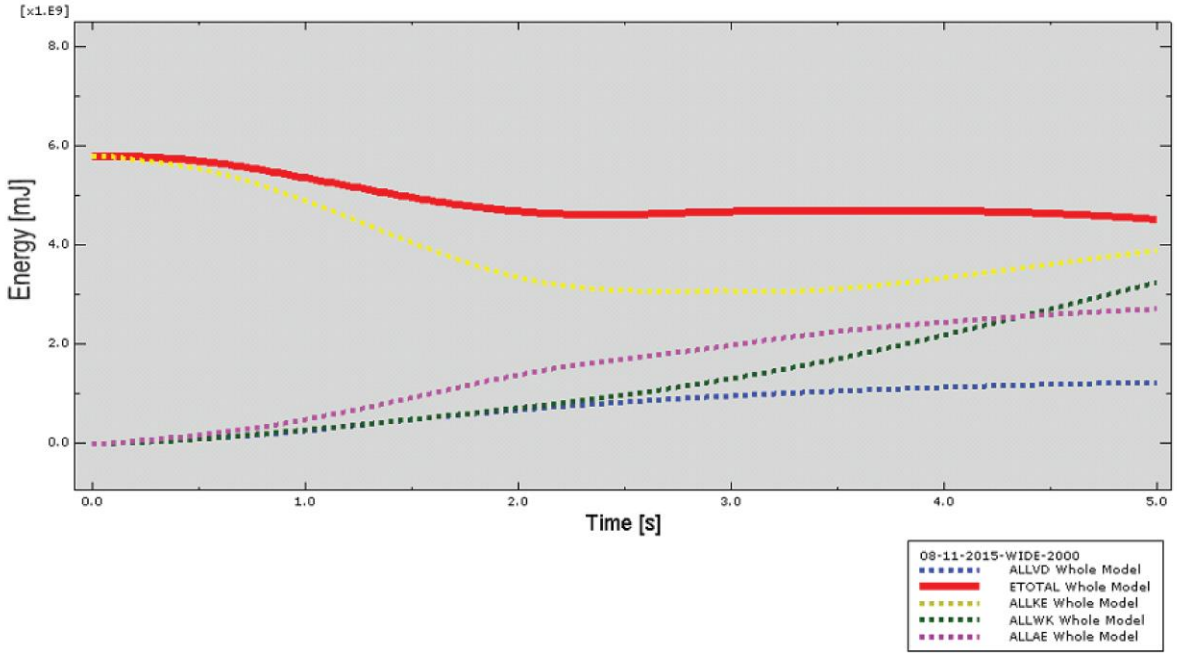

Figure 35 Plot of the different energy components together with the total energy for the wide model with a predefined keel velocity of 2000 mm/s.

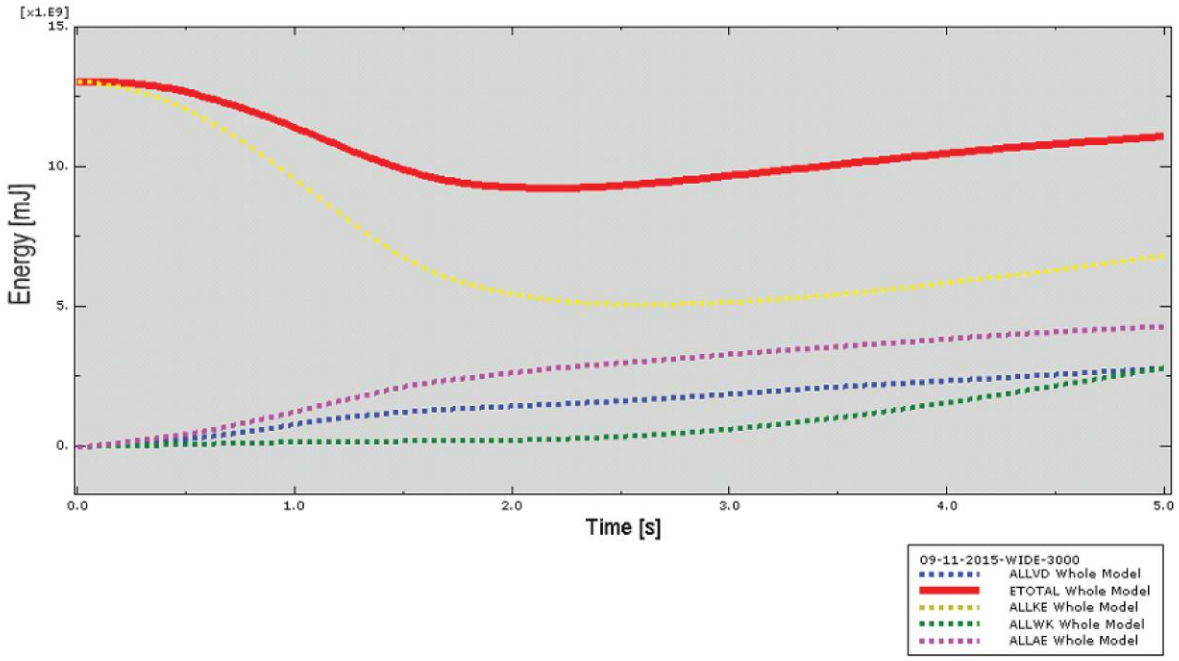

Figure 36 Plot of the different energy components together with the total energy for the wide model with a predefined keel velocity of 3000 mm/s.

The energy from external work and the internal energy both increase through the model, which is essential for a constant energy. On the other hand, the viscous dissipation seems to have an unreasonable increase for increased keel velocity. It is clearly seen in figure 36, and it should ideally be a small fraction of the real energies. The internal energy is also small for this model, compared to the models with lower velocity fields.

4.3.2 Intermediate model

Figure 37 shows plots of the total energy for the intermediate model for a predefined keel velocity of 1000, 2000 and 3000 mm/s. The plots are remarkable equal to the plots for the wide structure. The drop in energy for the highest velocity of 3000 mm/s, and a better accuracy for the 1000 and 2000 mm/s models seems to hold for the intermediate model as well.

Figure 38, 39 and 40 summarize the energy contributors for the model with a predefined velocity field of 1000, 2000 and 3000 mm/s respectively. Again, the artificial energies seems to be in a reasonable range, the energy from viscous dissipation shows lower values compared to the wide model.

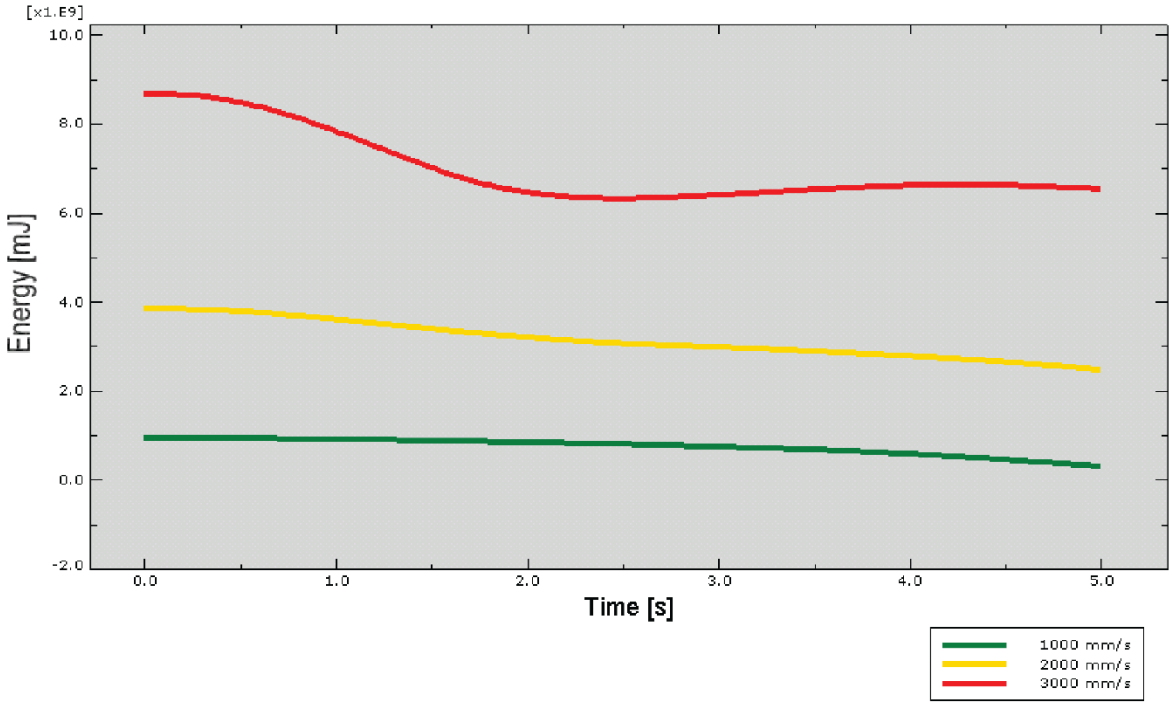

Figure 37 the total energy for the intermediate model plotted for three different velocity fields.

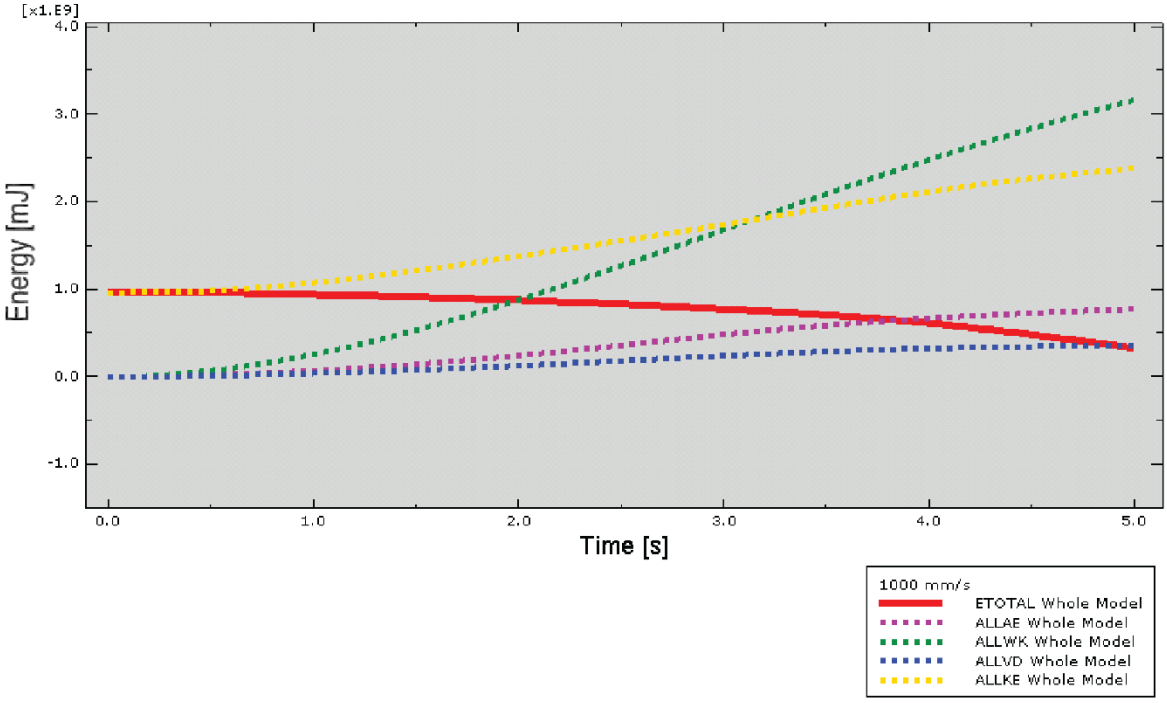

Figure 38 Plot of the energy contributors for the intermediate model with a predefined keel velocity equal 1000 mm/s

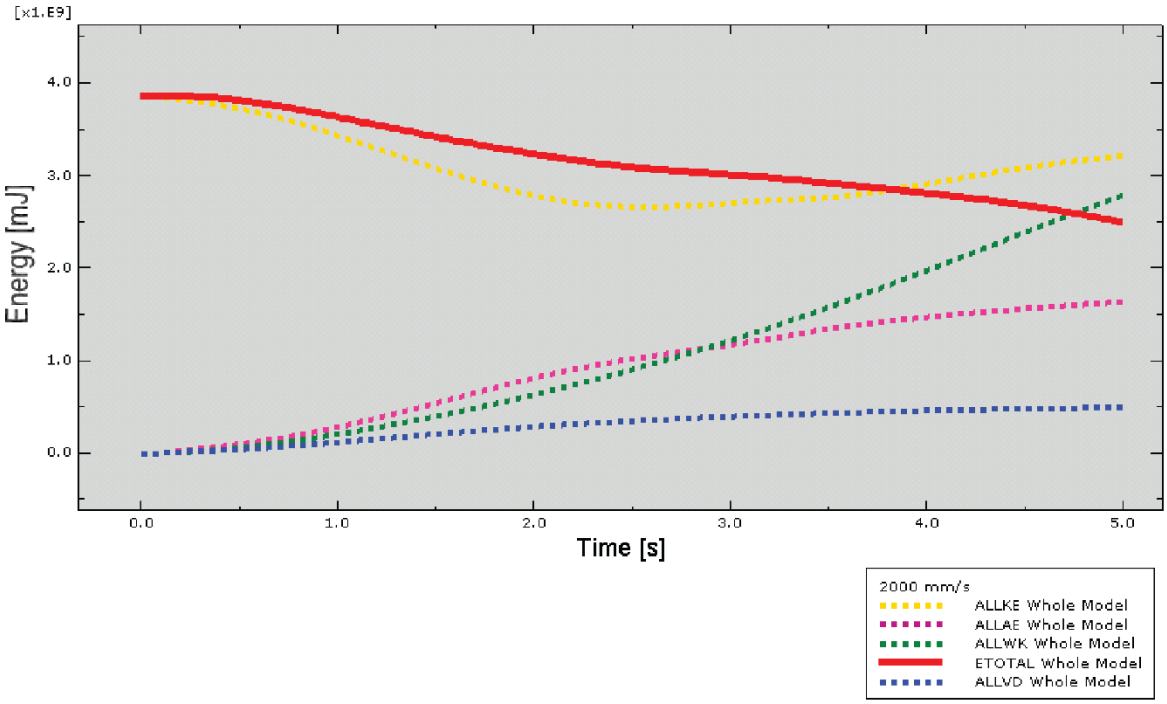

Figure 39 Plot of the energy contributors for the intermediate model with a predefined keel velocity equal 2000 mm/s

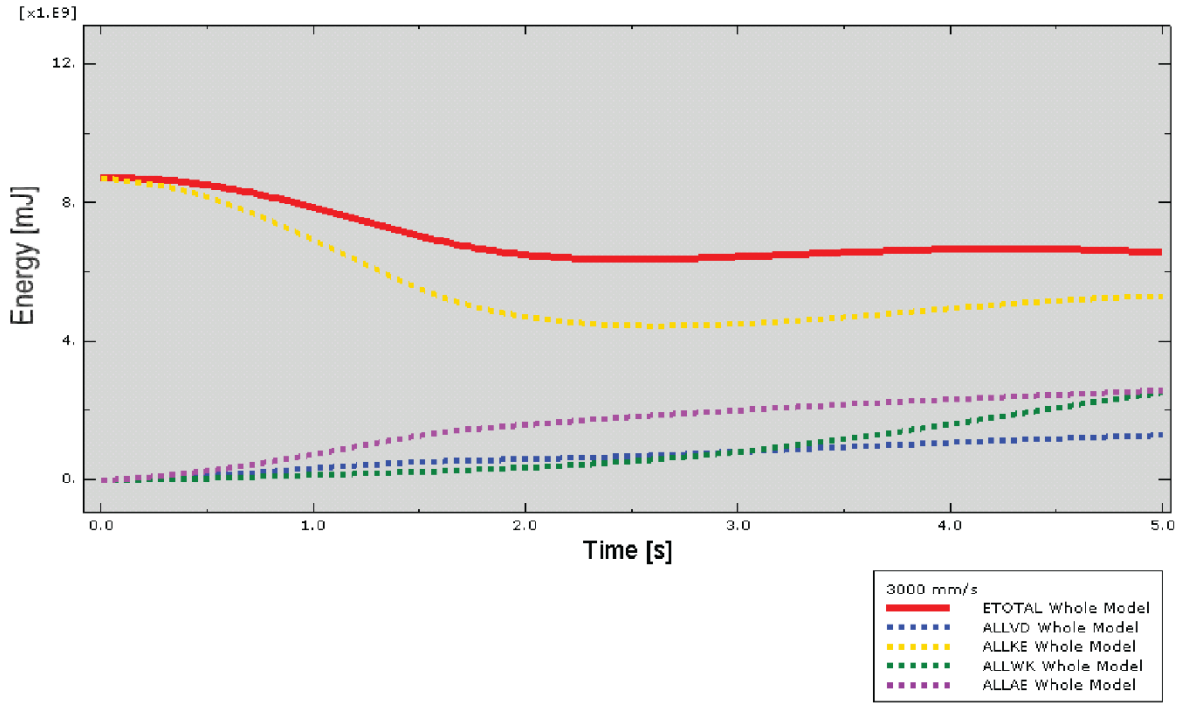

Figure 40 Plot of the energy contributors for the intermediate model with a predefined keel velocity equal 3000 mm/s

4.3.3 Narrow model

As previously described, the effect of introducing a finer mesh has been studied for the narrow model. The narrow model I is a refined model, while the narrow model II is identical with the mesh for the wide and the intermediate model (see table 5 for descriptions). The reason for an additional investigation of the narrow model is partly self-explained by figure 41, 42 and 43. The models show a pronounced drop in energy after some seconds of simulation. Note that the scale of the graphs are smaller, which makes the drop look more dramatic compared to the wide and the intermediate model.

On the other hand, the artificial energies are negligible and both the internal energy and the external work increases, which is good in terms of less numerical errors in the model.

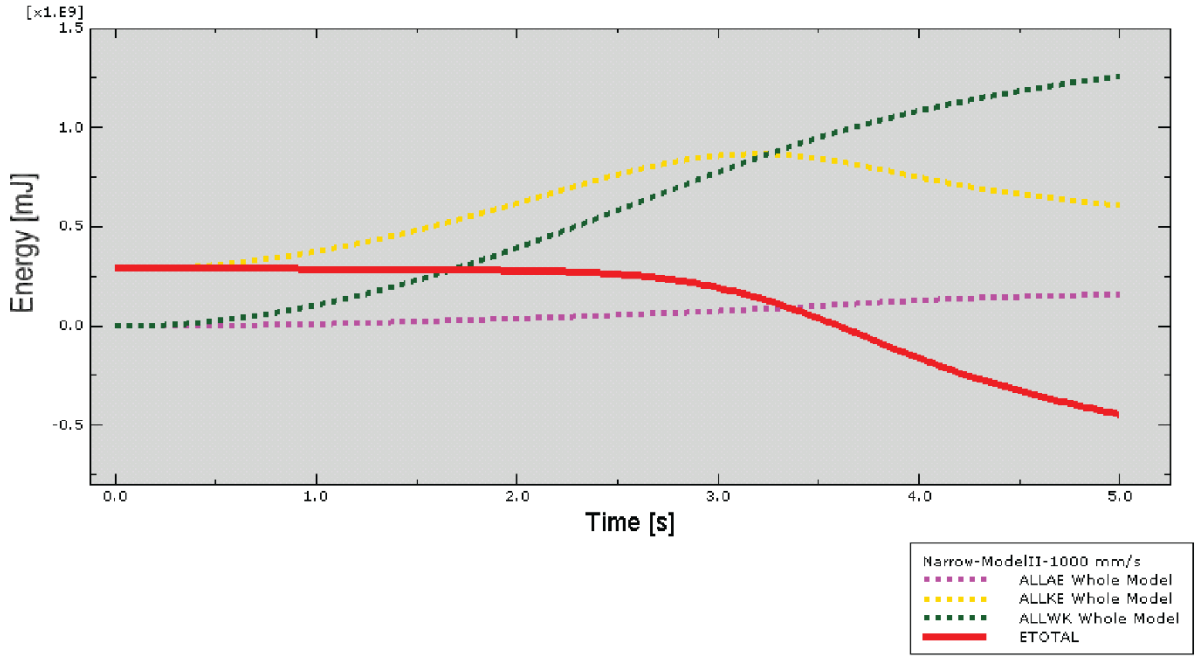

Figure 41 Plot of the energy contributors for the narrow model II with a predefined keel velocity equal to 1000 mm/s.

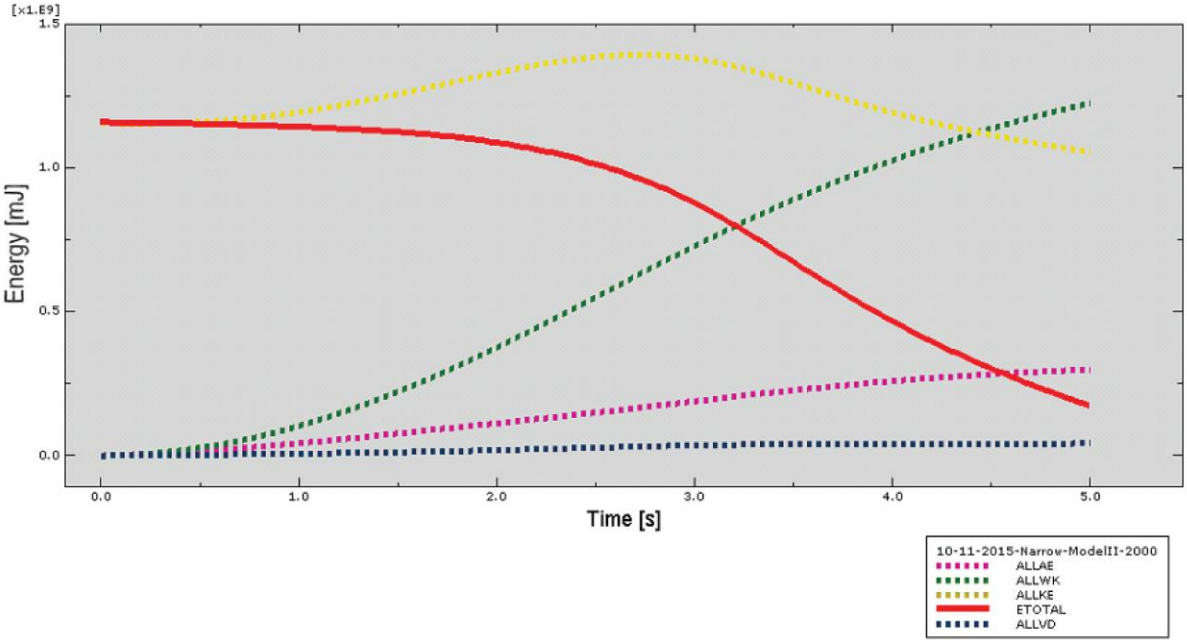

Figure 42 Plot of the energy contributors for the narrow model II with a predefined keel velocity equal 2000 mm/s

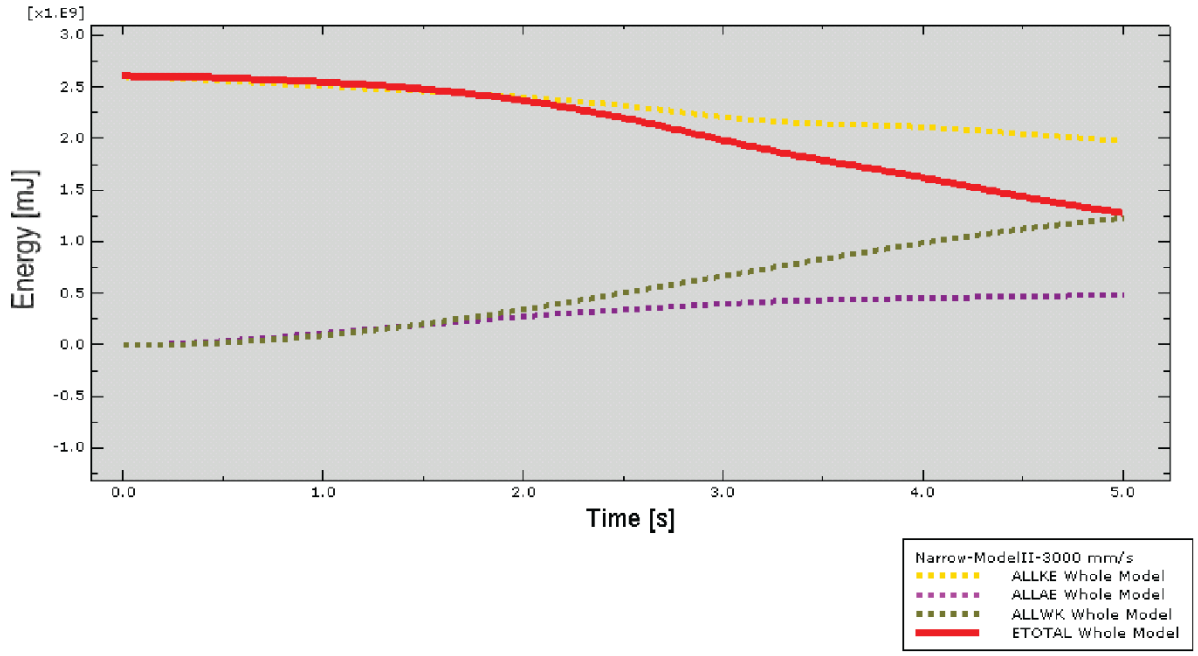

Figure 43 Plot of the energy contributors for the narrow model II with a predefined keel velocity equal 3000 mm/s

Figure 44 shows a comparison of the total energy for the two narrow models I and II. The variance in the initial total energies (for equal keel velocity) is primarily caused by different keel lengths for the two models. Thus, model II gets a higher kinetic energy, but the relatively deacrease in total energy seems to be in the same scale or close to equal. That fact is the most important observation from the figure. It draws the conclusion that the decrease in energy has another explanation than too coarse mesh. A small improvemtent in the accuracy is seen for all the velocities, but there is still a decrease that matters.

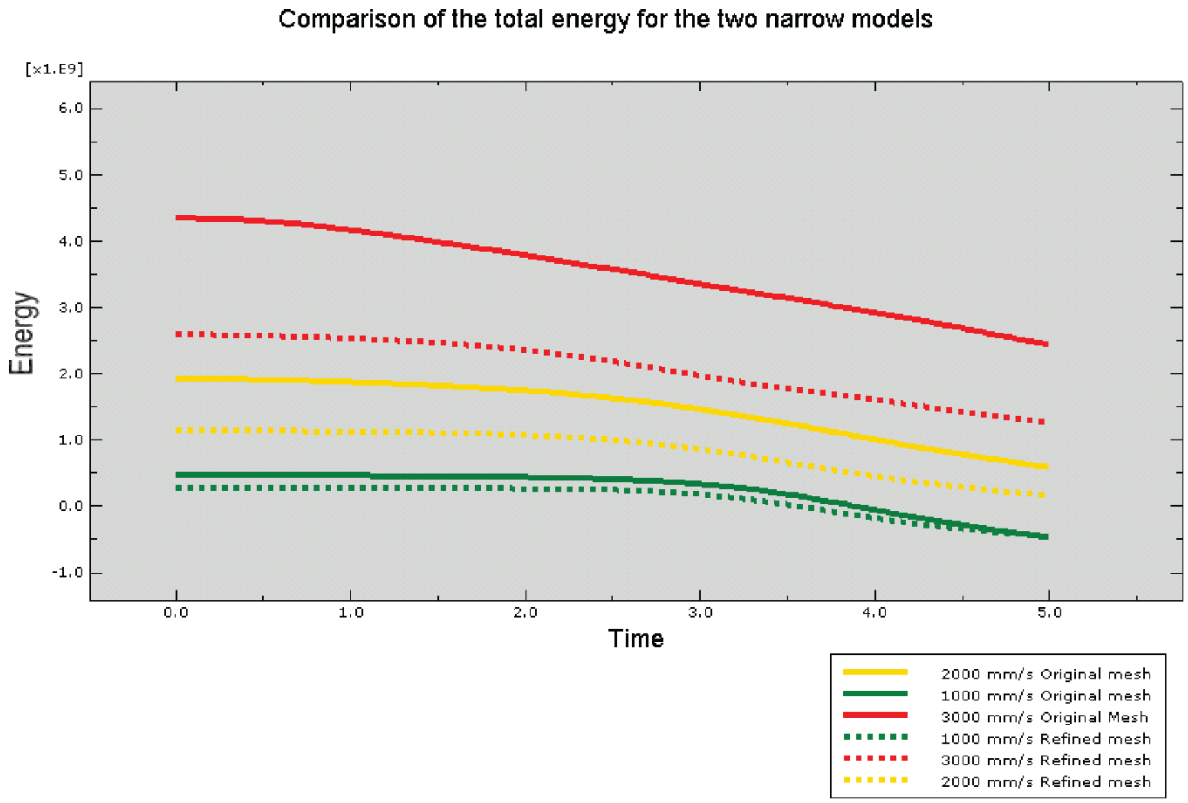

Figure 44 A comparison of the total energy for the two narrow models I and II. "Original mesh" in the legend box corresponds to narrow model II, while the "refined mesh" is narrow model I.

4.4 Reaction force

Below follows a summary of the most important results for the reaction forces for the three different models. The plots include investigations of the three different velocity fields of 1000, 2000 and 3000 mm/s.

The previous section showed a possible trend that increased keel drifts gives a worse accuracy for the energy balance. Considering those results, how should one proceed to analyse the results? For the further work, it seems logic to place greater emphasize on the reaction forces that comes from the higher accuracy models. The question comes back in the discussions chapter.

4.4.1 Wide model

Figure 45 gives the reaction force over time for the wide model (D=10 m) plotted for the three different predefined velocity fields. It appears that the maximum load has been reached for all the three cases. From three seconds and later, all the plots seems to approach a level of steady state. Five seconds of total interaction might be enough to track the maximum load, which is the main purpose of this thesis.

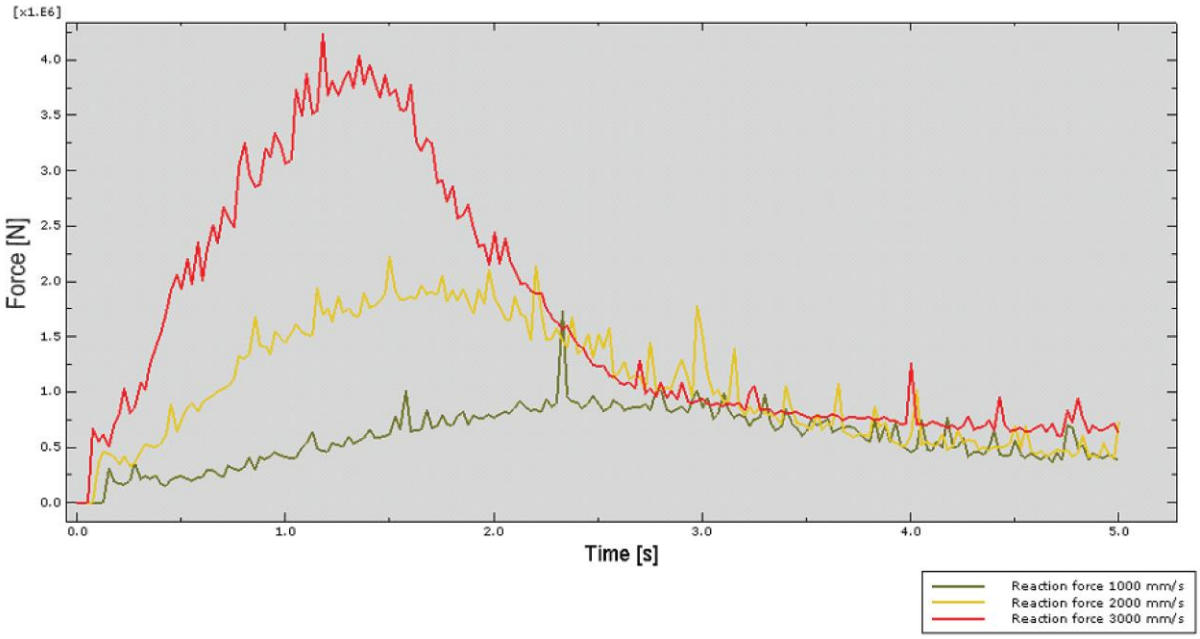

Figure 45 Plots of the reaction force for the wide model (D = 20 m) for the three different velocity fields of 1000, 2000 and 3000 mm/s

4.4.2 Intermediate model

Figure 46 gives the reaction forces analogous to figure 45, but for the intermediate model (D=10 m). Compared to figure 45, it is an astonishing similarity for the two models in terms of shape and interaction properties. At first sight, the two figures might seem identical, but the scale of the maximum forces are obviously different. It is still interesting to see the development in actions over time. The models reach maximum load more or less at the same time, just over a second for the 3000 mm/s models, in just under two seconds for the 2000 mm/s models and about 2.5-3 seconds for the 1000 mm/s models. Whether this is a coincidence or not is pure speculations.

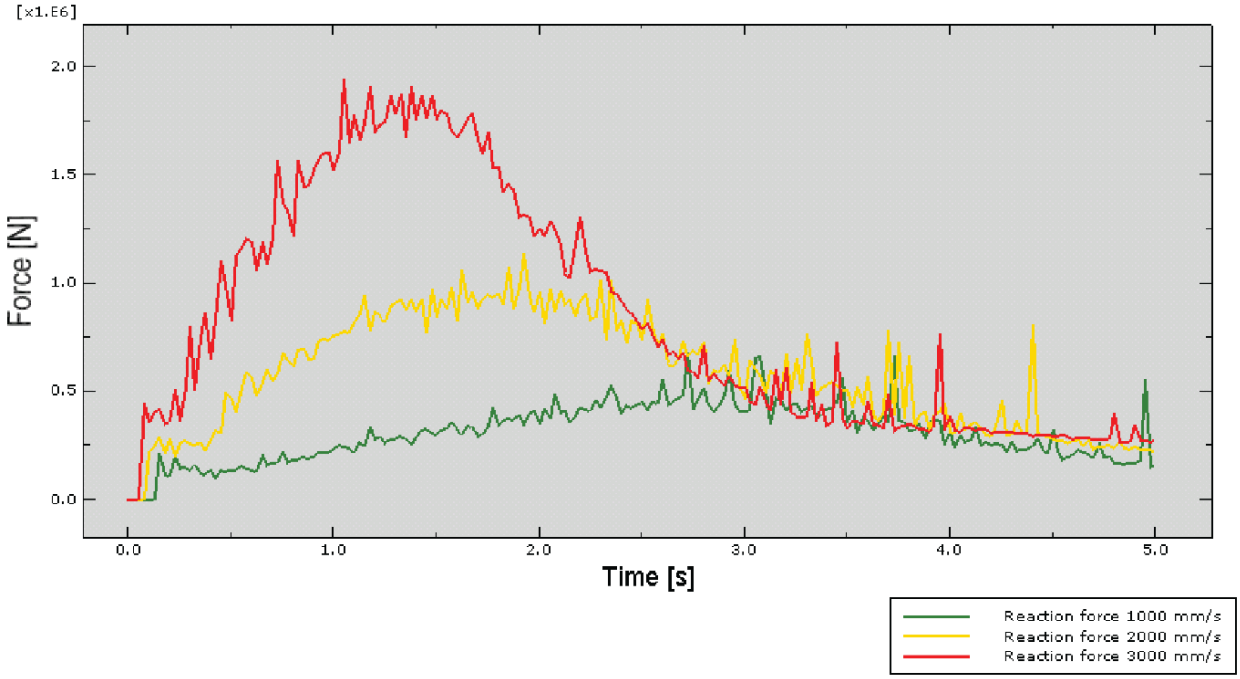

Figure 46 Plots of the reaction force for the intermediate model (D = 10 m) for the three different velocity fields of 1000, 2000 and 3000 mm/s

4.4.3 Narrow model

The narrow model is more distinct from the other two, and has a more unique interaction plot. Figure 47 shows this plot for reaction force over time, again for three different predefined velocity fields. It is seen quite some large spikes for the reaction force, especially for the 3000 mm/s model. This might coincide with where the biggest drop in the total energy occurs for the narrow model (see figure 49 in the next chapter for further discussions). The time when maximum force is reached is also different for the narrow model compared to the two others. Generally, one can say that the narrow model differs surprisingly much in a number of ways. However, also for this model it seems that the maximum load is reached, and the force approaches a steady state (goes to zero).

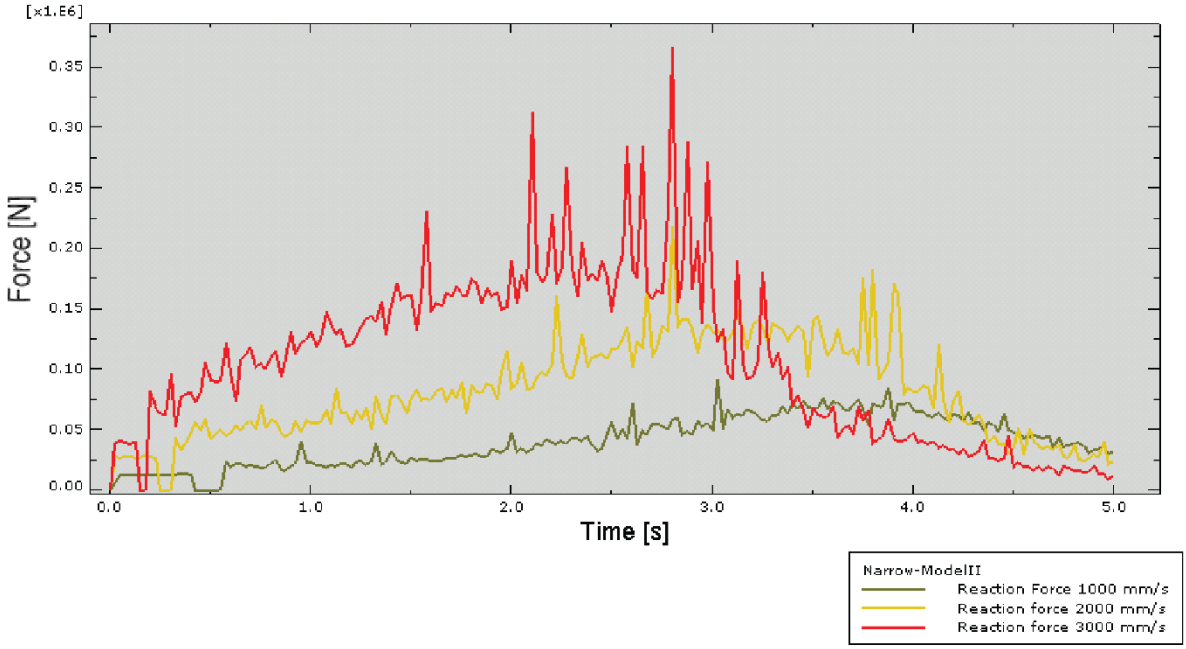

Figure 47 Plots of the reaction force for the intermediate model (D = 1.25 m) for the three different velocity fields of 1000, 2000 and 3000 mm/s

5 Discussion and Analysis

5.1 Introduction

The “Discussion and Analysis” chapter addresses the two issues regarding the energy balance and the keel actions, similar as seen in the “Results” chapter. The significant focus on the energy balance is because it directly relates to the numerical error and the accuracy. The aim is to discuss reasons for the decrease in the total energy, rather than to present the data once again. This applies particularly to the narrow model, as seen in the results chapter. In addition, there will be a brief discussion regarding the different modelling techniques. It is mentioned the effect of rounded contra sharp edges, and the use of a gradually increased buoyancy force compared to a constant force.

After the discussions related to the energy balance, it comes a comparison of the keel actions for the FE model and the ISO standard. This section tries to draw some bigger lines between the reaction forces and the width effect.

5.2 The energy balance

5.2.1 Rounded contra sharp edges

The reader might notice the lack of a presentation of the effect of rounded contra sharp edges. They were not included in the results chapter, but a brief discussion follows here. It proved to be one of the factors that improved the energy results significantly. It coincides with Nilsen (2015) who had similar observations in her thesis. Figure 48 illustrates the effect by a comparison of the wide model for a predefined keel velocity of 2000 mm/s. The dashed, red line has sharp edges, while the solid line is with fillets of radius 500 mm/s (equal to the model showed in the results chapter). The other parameters are identical for both models, which means the almost vertical drop in total energy around 2 seconds is solely because of this geometrical property. In general, it is a good practice always to avoid sharp edges. It is known to be a potential source of singularities, which yields numerical errors in the model.

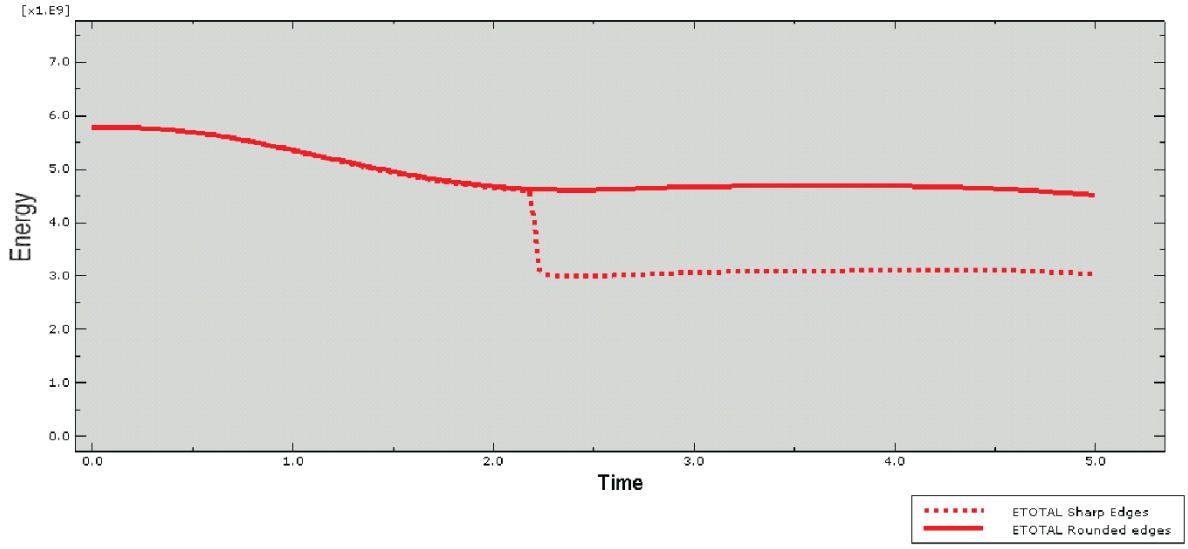

Figure 48 shows plots of the total energy for the model with sharp edges and the one with rounded edges. The pronounced drop in the total energy (dashed line) is solely because of the sharp edges.

5.2.2 Gradually increased buoyancy force

When the body force applies with its full magnitude all at once, the numerical model feels a state of "shock", which potentially increases the numerical errors. The model does not manage to adapt to the sudden applied load. The idea of a gradually increased buoyancy force is to avoid this effect. Firstly, an initial amplitude (for instance 10 percentage of the total buoyancy force) is defined. Secondly, the buoyancy force was ramped up to its full magnitude during the time of interaction.

The use of rounded edges proved a significant positive effect for the energy balance. The same does not apply for the use of a gradually increased buoyancy force. It showed neither any clear improvements nor worsening for the overall energy balance. From a force point of view, the models with a ramped up buoyancy are likely to show marginally higher values. The reason is that the vertical force component decreases, hence a relative increase in the horizontal component. In a larger picture, this fact is considered less important, and it does not follow any further discussions

5.2.3 Reasons for the decrease in total energy

Figure 49 shows the total energy and the reaction force for the narrow model. It seems to be a correlation between the maximum force and the decrease in the total energy. After the model reaches maximum load, it seems that the total energy declines linearly. The largest share of the energy loss also occurs in this region

It is chosen to focus on the narrow model, since it is here the most marked decline occurs. The percentage loss in energy is greater when the predefined velocity field increases. An increase in the velocity field for the keel, yields more plastic volumetric strains. As

previously mentioned, ABAQUS does not distinguish between the elastic and the plastic strain contributions for the given subroutine. It struggles to reproduce the given interaction, and the output data (especially for the internal energies) is affected. It seems reasonable that the increased energy losses comes from increased plastic volumetric strains, especially since the losses increase with increased keel drift.

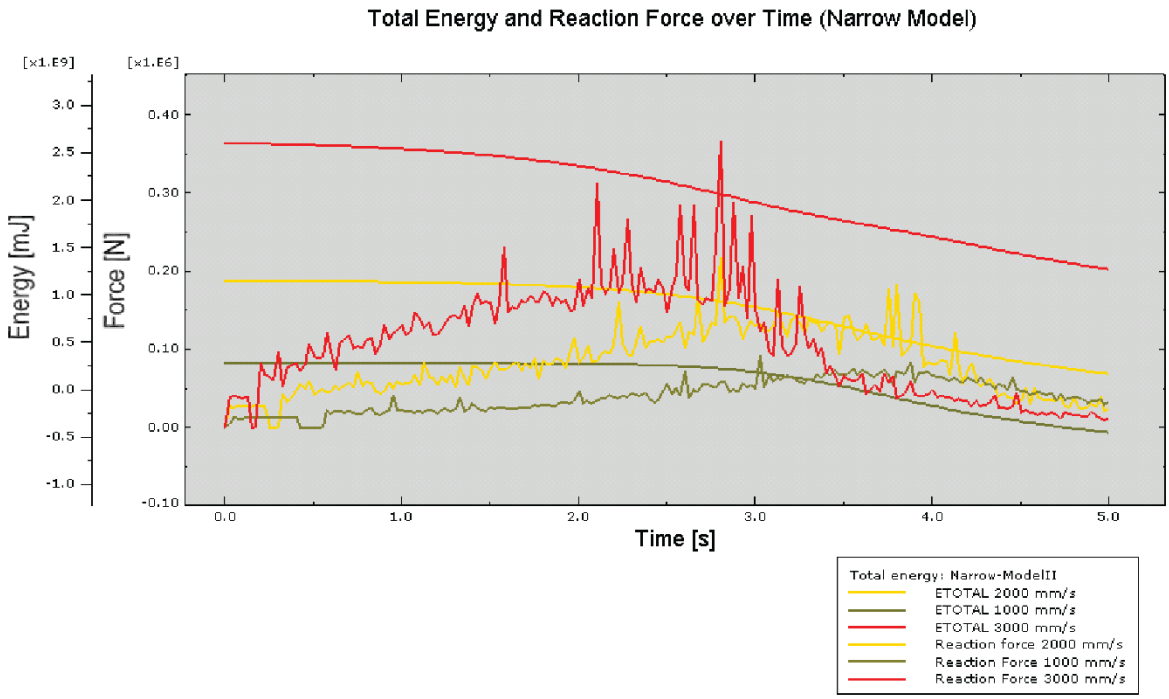

Figure 49 the total energy and the reaction force plotted over time for the narrow model (D=1.25 m)

5.3 Keel actions from ISO 19906:2010 compared to the FE model

5.3.1 Comparison

The results chapter showed us the keel actions from the FE models. Table 6 summarizes these results with the maximum force from each setup. Thereafter, figure 50 plots these values together with the corresponding ISO suggestion for a keel depth of 10 metres.

Table 6 sums up the FE results for the maximum forces for a given combination of predefined keel velocity and structural width.

Model	***Structural width [m]***	***Peak Values: Reaction forces [kN]***		
		1000 mm/s	**2000 mm/s**	**3000 mm/s**
Narrow model II	1.25	92	217	366
Intermediate model	10	679	1130	1940
Wide model	20	1730	2220	4235

Initially, the velocity field had no function other than to ensure that the keel achieved full contact with the structure. In retrospect, it appears that the needed rate is much greater than anticipated. Even a prescribed velocity field of 1000 mm/s is a high value. In cases where it was used lower values than 1000 mm /s, the structure interaction pushed the keel back. It means the keel did not have enough momentum to withstand the interaction.

Despite the use of high velocity values, the results for the keel actions are just as surprising. Figure 50 shows this. None of the numerical models are even close to the suggested values from ISO 19906:2010 (2010). For instance for a structural width of 1.25 m, the FE model (3000 mm/s) suggests approximately fifty-four per cent lower keel actions, but the percentage values decreases (too some extent) for the two other models. For the intermediate and the wide models, the FE suggestions are about thirty-nine and twenty-nine percent lower than ISO. These values comes from the 3000 mm/s model. The suggested keel actions are naturally even lower for the two other models. It brings up an issue regarding the accuracy of the different models. It is in principle a trade-off between reasonable keel actions and a stable energy balance. From an energy point of view, lower keel velocities gives better results and it yields a higher accuracy. At the same time, it seems that the reaction forces becomes unreasonable low when the keel velocity decreases.

In general, the energy balance should always play an important role, which means the 1000 mm/s and 2000 mm/s models are regarded a higher trustworthiness compared to the 3000 models. It also means that the intermediate and the wide model weigh heavier due to their better energy balance compared to the narrow model. With this in mind, it leads to the following new observations from figure 50: The 1000 mm/s and 2000 mm/s models have almost parallel lines in the region 10-20 meters. The slope differs markedly from the ISO suggestions; it has a less steep curve. If the given slope scales up to the ISO values, it yields that the keel actions should increase less for increased structural width compared to ISO suggestions. To summarize the most important observations so far:

- The FE model yields significantly lower keel actions
- The FE model predicts a gentler slope of the curve (given a linear fit). An increased width should according to this play a smaller role for the action forces.

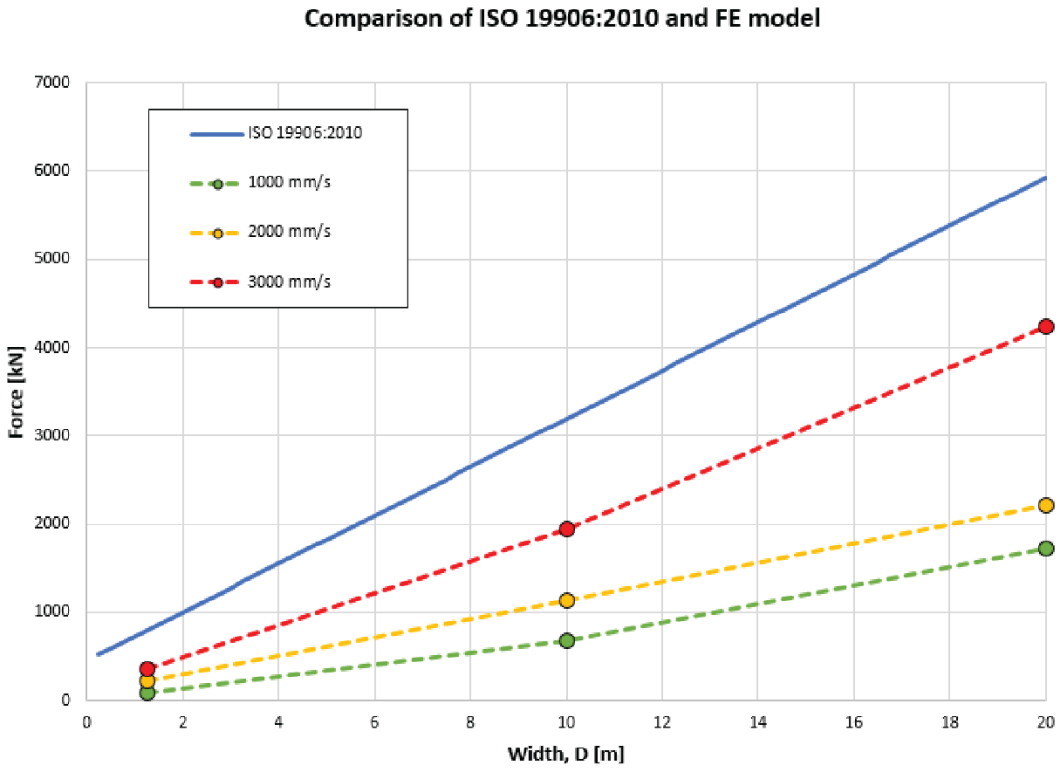

Figure 50 shows the ISO 19906:2010 suggestions for the keel action (h_k=10 m) compared to the numerical results.

Figure 51 attempts to fit the FE results to ISO 19906:2010 (2010) by an upper and lower bound in an conservative way. The results fits to a an upper bound corresponding to a keel depth of approximately 7.9 metres, while the lower bound fits to a keel depth of 3.9 metres. With other words, the FE results corresponds to keel depths that are twenty-one percentage shallower than the initial approximation (10 metres). This is for the upper bound value. For the lower bound is the value dramatically smaller. The upper bound line has a slope that naturally approaches the ISO 10 metre line, but it is still considerably lower. The next section treats what implications this has for the width effect on the structures.

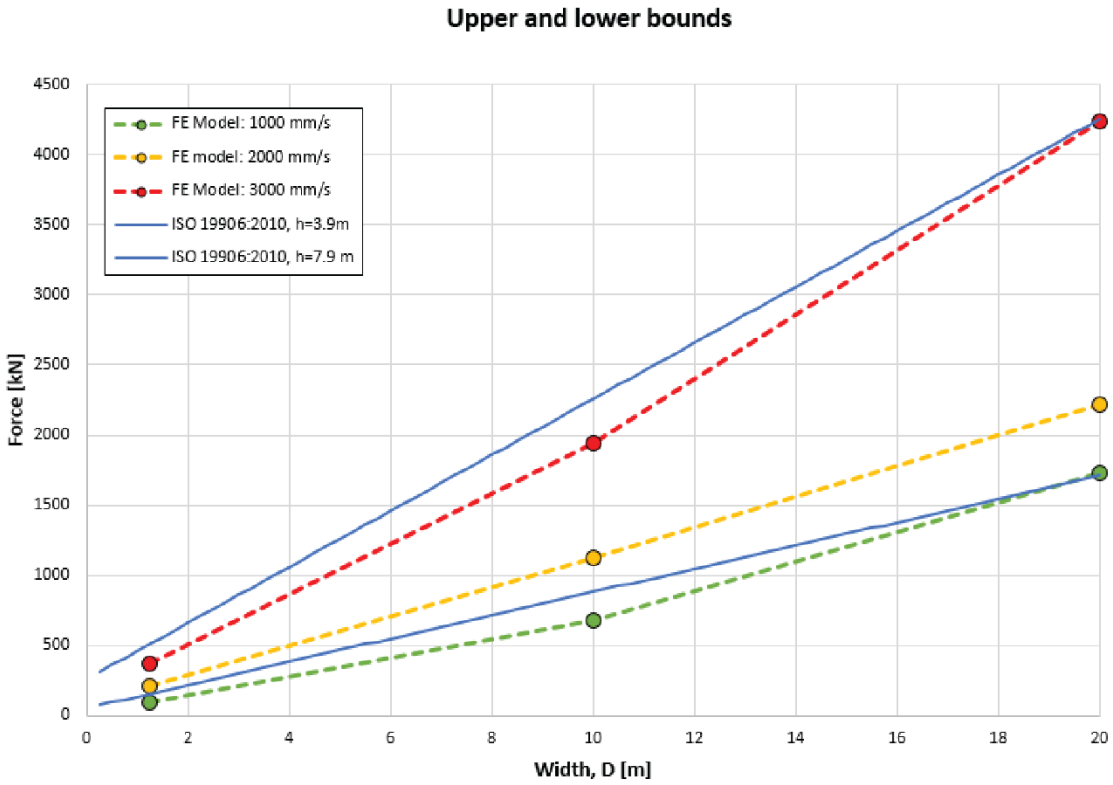

Figure 51 Plots of the FE results together with the nearest fits according to ISO 19906:2010

5.3.2 Regression

One of the key issues that remain for discussion; does the structure width have any other effects than the suggested linear fit from ISO? In order to draw any conclusion about the width effect, one have to look into regression lines for the FE results. It is tempting to say that it clearly also is a linear fit for the FE models, with reference to figure 52. It shows the linear regression line for the 2000 mm/s model, and it shows an almost perfect linear fit with the corresponding ISO line for a keel depth of 4.8 meters. The trend line and equations are identical for both cases, as seen in figure 52.

Similar lines can be drawn for the two other velocity fields, but by inspection of figure 51, they expect to give a poorer linear fit. They almost seem to fit an exponential regression. It is not under any circumstances tried to do this exponential fitting, for one important reason. It is a highly limited set of data provided from the FE analyses. Even to do a linear regression fit for such a small data set might mislead and draw false conclusions. The ideal is dozens of simulations for different structural widths to confirm or reject the relations found in figure 52. Here, the data bases on a three different structural widths.

That said the data from the 2000 mm/s model clearly seem to be the better in terms of energy balance and reaction forces. Thus, these data are naturally a subject for a more extensive comparison with the ISO values.

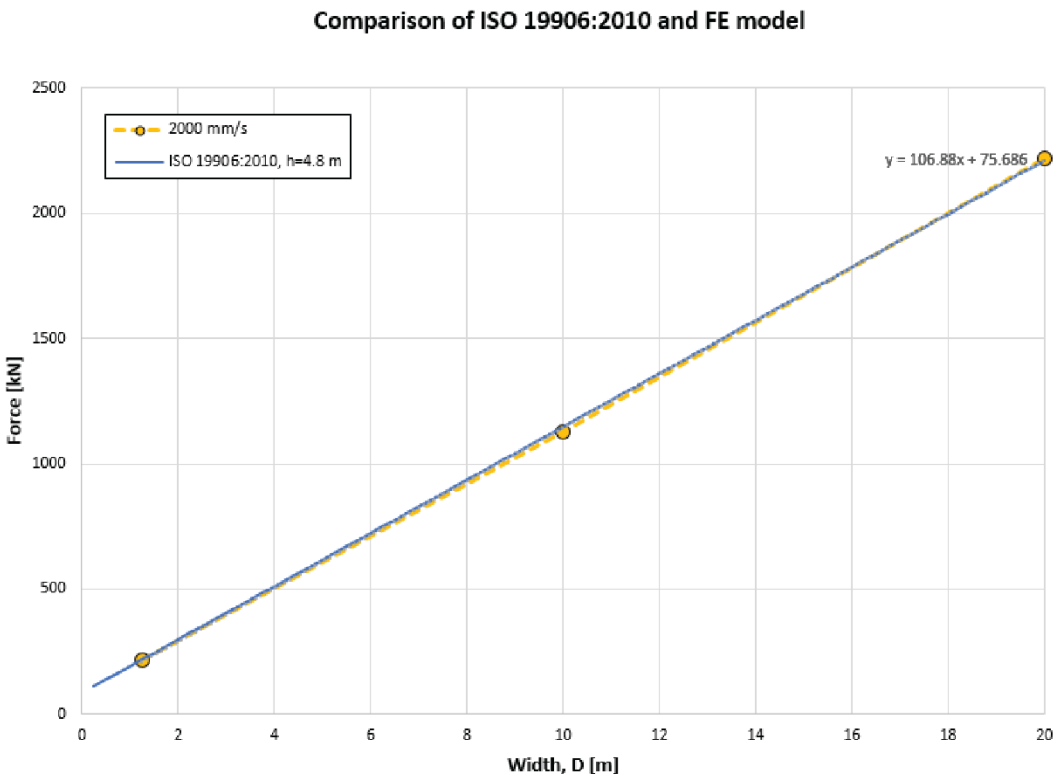

Figure 52 shows a linear regression line for the FE model with a keel velocity of 2000 mm/s.

Figure 53 shows linear regression lines for the initial investigation (ISO 19906:2010) with a keel depth equal to 10 metres. It also shows a regression line for the most reliable FE model (2000 mm/s). There are several reasons to substantiate this particular model, and figure 53 and 54 illustrate this quite well. Firstly, the linear fit seems to hold well for the whole region for the 2000 mm/s, as seen in figure 51. The plot in figure 54 disregards the results for the narrow model, in such a way that the linear regression lines relies only on the wide and the intermediate model. Still, the regression line (the slope) correlates very well with the line in figure 51.

Secondly, figure 54 also shows that for the intermediate to wide region, the slope for the 1000 mm/s and the 2000 mm/s models are almost identical. This shows a consistent trend regardless of the predefined velocity field. One knows that the energy balance shows good results for both models in this region. It makes the given findings more reliable.

These results are essential to describe the difference between the FE model and the analytical suggestions from Dolgopolov et al. (1975) and ISO 19906:2010 (2010). The FE model has proved to give a linear fit just as the ISO standards, but it is a gentle slope compared to the analytical suggestions. The slope angle for the 2000 mm/s model is approximately 6.1°, while the ISO gives a slope angle of 15.3°. For every unit length increase in structural width, the ISO predicts more than twice (approximately 2.5 times) the keel action from the 2000 mm/s FE model. Figure 55 tries to illustrate this fact. The figure does not take into account that there is also a large gap in the initial values for the two models. Considering this, there are two factors that contribute to the markedly lower FE predictions. Note that this study only investigates a keel depth equal to 10 meters.

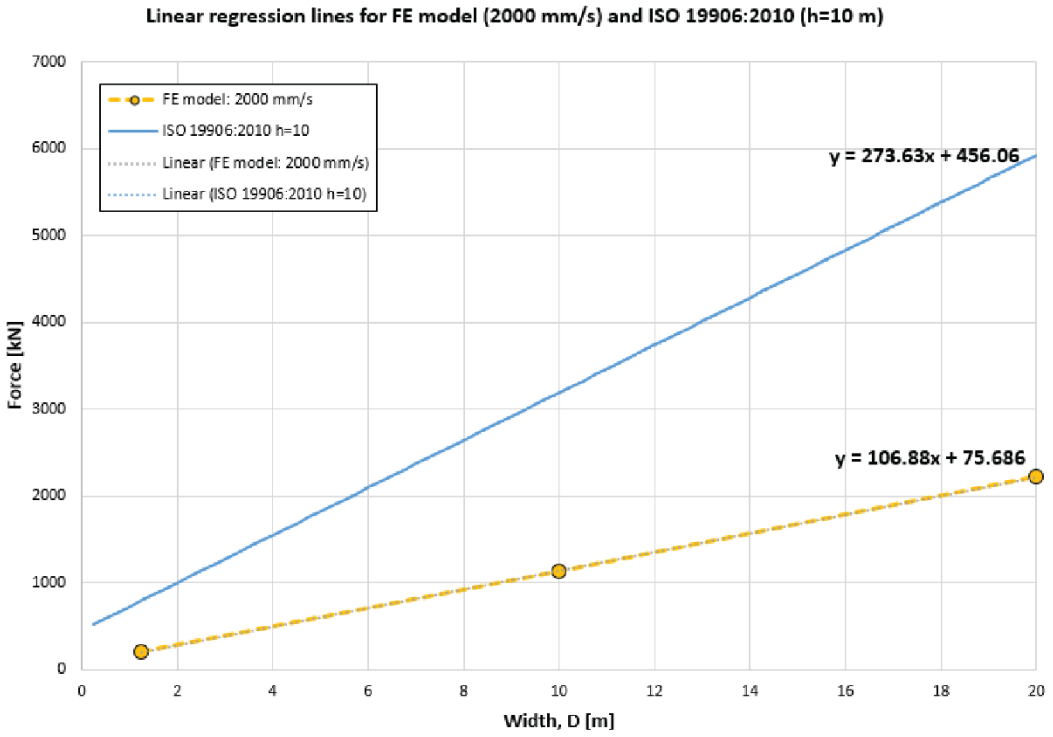

Figure 53 Regression lines for the FE model (2000 mm/s) and the ISO 19906:2010 for h =10 m.

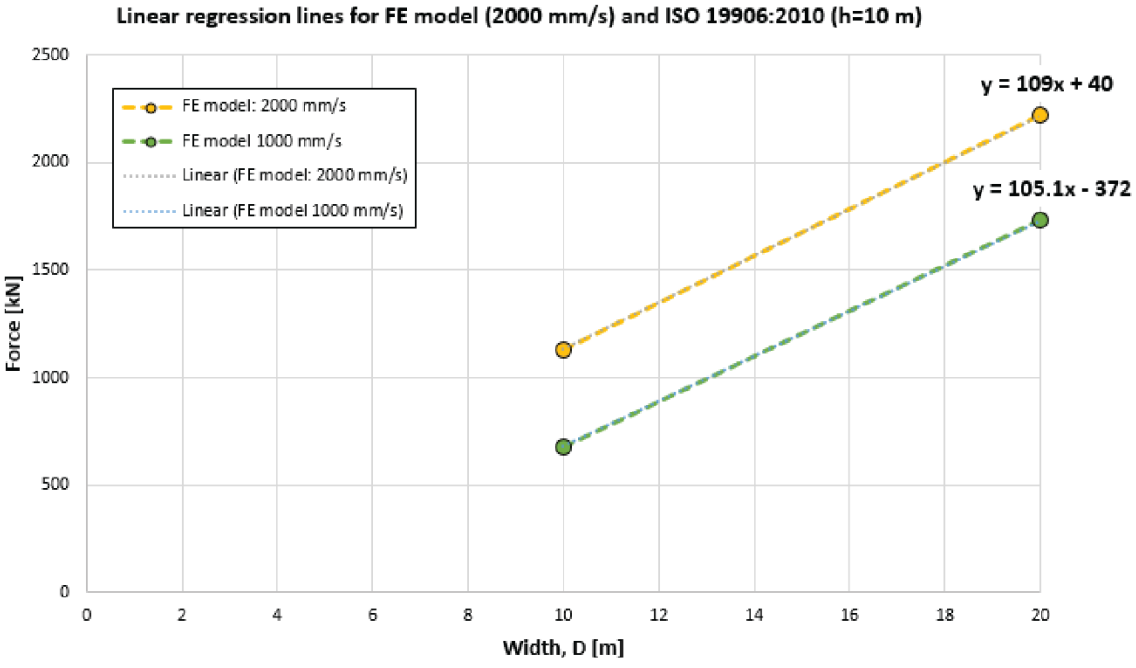

Figure 54 Linear regression lines for the 2000 mm/s and 3000 mm/s FE models. Note the slope of the curves, which are almost parallel.

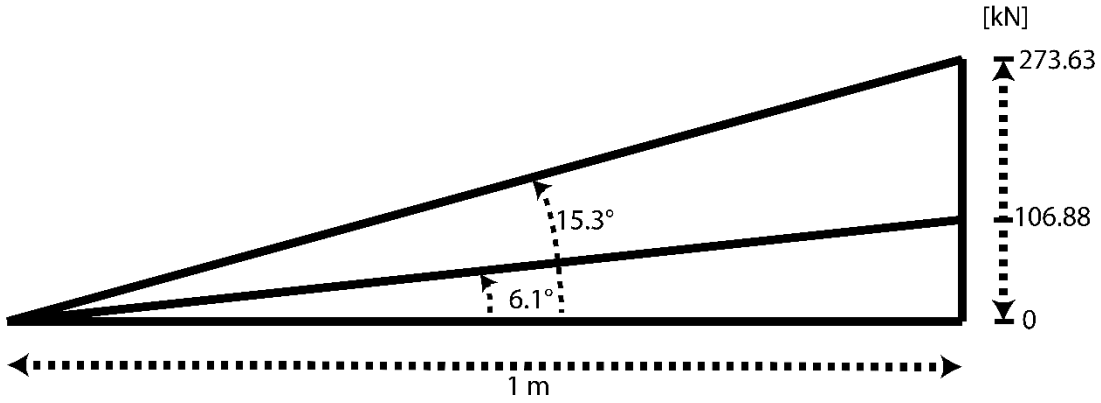

Figure 55 the linear difference between the ISO and the FE predictions for the first-year ice ridge actions. The figure does not take into account the difference in initial values, just the fact that the ISO suggestion is markedly steeper than the FE model.

6 Conclusions

In order to predict reliable results for the reaction forces, it proved necessary with extensive investigations and checks of the energy balance. The wide (20 m) and the intermediate (10 m) models showed accurate results already at an early stage (in terms of a total energy ≈ constant). On the other hand, the narrow model (1.25 m) showed energy losses that are still not in an acceptable range. Different attempts to improve the results for the narrow model also proved to give better results for the two other models. From an energy perspective, it draws the following conclusions:

- The use of rounded edges prove a significant positive effect for the energy balance. Sharp edges gave sudden drops or generally a higher energy decrease. The sharp edges lead to singularities in the numerical model that spoils the results.
- A gradually increased buoyancy force does not seem to give any particular effects on the energy. It showed neither any clear improvements nor worsening for the overall results.
- The initial mesh proved dense enough to give accurate results for both the intermediate and the wide model, but resulted in a poor accuracy for the narrow structure. A finer mesh worked partly as a remedy, but the computational time increased.
- The accuracy of the energy balance declines when the prescribed keel velocity increases. See further descriptions below.

The reaction forces from the numerical model are highly dependent on the prescribed keel velocities. An increased keel velocity yields reaction forces that approaches the analytical results from Dolgopolov et al. (1975), but it also seems to spoil the accuracy of the energy balance. These energy losses are expected to come from an increase in plastic, volumetric strains for increased velocities. The combination of ABAQUS and the user-defined subroutine for the CBM model struggle to reproduce this behaviour. From an energy point of view, it makes it more complicated to analyse the different contributions.

Initially prescribed forces of 1000-3000 mm/s are unrealistically high values compared to an actual ice drift. The attempt to apply the keel drift as a uniform boundary condition gave poor results in terms of energy losses and reaction forces. The best and most reliable results yields for the model where the keel drift applies as an initial velocity field. Especially in the lower range of prescribed velocities (1000 and 2000 mm/s).

The FE model has proved to give a linear fit just as the ISO standards, but it is a gentle slope compared to the analytical suggestions. The slope angle for the 2000 mm/s model is approximately 6.1°, while the ISO gives a slope angle of 15.3°. For every unit length increase in structural width, the ISO predicts more than twice (approximately 2.5 times) the keel action from the 2000 mm/s FE model.

In addition, the order of magnitude of the maximum forces are significantly lower than the ISO predictions. It means that the FE predictions of the keel actions shows a two-way effect compared to the ISO. The two effects are listed below:

1. The order of magnitude for the maximum forces are significantly lower.
2. The linear slope is significantly gentler.

The two statements above imply that the ISO standard suggest too high keel actions from the unconsolidated part. Additionally, the width has less to say for the total force than stated in the standards (by a factor of 2.5). These findings are quite surprising. Two metres per second is a high initial velocity, and the CBM model considers plastic effects in such a way that the yielding criterion increases when the breakage proceeds. It can be interpreted as the breakage energy is small and the yielding criterion unaltered, since the model predicts lower actions. Otherwise, an increased yielding criterion calls for a higher maximum force, which is not the case.

The linear fit seems to hold well for the whole region for the 1000 mm/s models. For the intermediate to wide region, the slope for the 1000 mm/s and the 2000 mm/s models are almost identical. This shows a consistent trend regardless of the predefined velocity field. One knows that the energy balance shows good results for both models in this region. It makes the given findings more reliable. The best fit for the linear regression is according to this equation 32. Equation 33 are the equivalent linear fit for the ISO actions (included for comparison).

$$y(x) = 107x + A \tag{32}$$

$$y(x) = 273x + B \tag{33}$$

, where

A and B	are constants
x	is the structural depth [m]
y	is the keel actions [kN]

Further Work

Below is a list of suggestions for further work. Some of these points are a natural successor from where this thesis ends (for instance a comparison with measured data), while others require a more extensive investigation. The listed order is arbitrary, and most of them have arisen during the work. Hopefully, the list can serve as clues for similar, future work.

- To try a different approach for the CEL model, and make a comparison of the two models, in terms of reaction forces and energy equations. A suggestion is to include the entire rigid body structure inside the Eulerian domain, instead of the top section sticking out. The drawback is that the top surface constraints must be defined inside the Eulerian domain.

- Make an axisymmetric model in order to save computational time. The mesh in this thesis proved to be sufficiently dense, but the computational time was high. The main problem was the server capacity and the storage of large output files. An axisymmetric model is much more efficient and it would address this problem.

- Apply the keel velocity as a boundary condition, but exclude the region closest to the structure. It could solve the contact problems that occurred for this type of loading. It seems that the loading closest to the structure "traps" the ice from an escape; instead it occurs an extensive crushing process.

- Varied the structural depths extensively more to have a better data set for analyses of the regression lines. It could substantiate or reject if a linear or an exponential fit seems to hold best. On the other hand, the 2000 mm/s model proved an almost perfect linear fit and correlation with the ISO 19906:2010 (2010).

- Varied the keel depth in the model, to see if the same relationship holds for both shallower and deeper keels.

- A comparison of the numerical results with keel action data from actual structures, for instance Moliqpaq, lighthouses etc.

References

DASSAULT SYSTÈMES 2012a. Abaqus Analysis User's Manual ABAQUS 6.12 Documentation.

DASSAULT SYSTÈMES 2012b. Abaqus/CAE User's Manual ABAQUS 6.12 Documentation.

DASSAULT SYSTÈMES 2012c. Conversion Tables, Constants, and Material Properties. ABAQUS 6.12 Documentation.

DOLGOPOLOV, Y., AFANASIEV, V., KOREN'KOV, V. & PANFILOV, D. Effect of hummocked ice on the piers of marine hydraulic structures. International Symposium on Ice Problems, 3rd, Proceedings, Dartmouth College, Hanover, NH. Aug., 18-21. 1975., 1975.

EINAV, I. 2007a. Breakage mechanics—Part I: Theory. *Journal of the Mechanics and Physics of Solids,* 55**,** 1274-1297.

EINAV, I. 2007b. Breakage mechanics—Part II: Modelling granular materials. *Journal of the Mechanics and Physics of Solids,* 55**,** 1298-1320.

EINAV, I. & PUZRIN, A. M. 2004. Pressure-dependent elasticity and energy conservation in elastoplastic models for soils. *Journal of Geotechnical and Geoenvironmental Engineering,* 130**,** 81-92.

EMDAL, A. 2012. *Introduksjon til Geoteknikk,* NTNU, Insitutt for bygg, anlegg og transport. .

HØYLAND, K. V. 2002. Consolidation of first-year sea ice ridges. *Journal of Geophysical Research: Oceans,* 107**,** 15-1-15-16.

HØYLAND, K. V. 2007. Morphology and small-scale strength of ridges in the North-western Barents Sea. *Cold Regions Science and Technology,* 48**,** 169-187.

HØYLAND, K. V. 2014. Ice mechanics, a brief introduction. Norwegian University of Science and Technology

ISO 19906:2010 2010. ISO 19906:2010 (E) Petroleum and natural gas industries - Arctic offshore structures International Organization for Standardization.

KÄRNA, T. & NYKÄNEN, E. 2004. An approach for ridge load determination in probabilistic design. *17th International Symposium on Ice. International Association of Hydraulic Engineering and Research,* 2**,** pp. 42-50.

KNOPP-SCHWYN, C. & FLAME, T. 2009. *Northern Sea Route vs Southern Sea Route* [Online]. Available: https://commons.wikimedia.org/wiki/File:Northern_Sea_Route_vs_Southern_Sea_Route.svg#/media/File:Northern_Sea_Route_vs_Southern_Sea_Route.svg [Accessed 01.12 2014].

MOSLET, P. O. 2006. *Field testing of uniaxial compression strength of columnar sea ice,* Cold Regions Science and Technology 48 1-14.

NILSEN, H. L. 2015. *Finite Element Simulations of Punch Test on Ice Rubble with the Modified Cam Clay Model.* Master's thesis, Norwegian University of Science and Technology.

NORDAL, S. 2014. *TBA4116 Geotechnical Engineering Adcanced Course - Lecture notes and background material,* Trondheim, Norwegian University of Science and Technology (Geotechnical Division).

STRUB-KLEIN, L. & SUDOM, D. 2012. A comprehensive analysis of the morphology of first-year sea ice ridges. *Cold Regions Science and Technology,* 82**,** 94-109.

THE ENGINEERING TOOLBOX. 2015. *Friction and Coefficients of Friction* [Online]. Available: http://www.engineeringtoolbox.com/friction-coefficients-d_778.html [Accessed 01.10.2015 2015].

TIMCO, G., FREDERKING, R., KAMESAKI, K. & TADA, H. Comparison of ice load calculation algorithms for first-year ridges. Proceedings International Workshop on Rational Evaluation of Ice Forces on Structures, REIFS'99, 1999. 88-102.

TIMCO, G. W. & BURDEN, R. P. 1997. An analysis of the shapes of sea ice ridges. *Cold Regions Science and Technology*, 25**,** 65-77.

WIKIVERSITY. 2010. *Nonlinear finite elements/Lagrangian and Eulerian descriptions* [Online]. Wikiversity. Available: https://en.wikiversity.org/w/index.php?title=Nonlinear_finite_elements/Lagrangian_and_Eulerian_descriptions&oldid=605415 [Accessed 19.11.2015 19.11.2015].

Appendix

A Energy balance

Equation 34 shows the general expression for the total energy for explicit dynamic analyses:

$$E_{Tot} = E_{KE} + E_{IE} + E_{VD} + E_{FD} + E_{IHE} - E_{WK} - E_{PW} - E_{CW} - E_{MW} - E_{HF} \approx Constant \quad (34)$$

, where:

E_{Tot}	the total energy
E_{KE}	the kinetic energy
E_{VD}	viscous dissipation
E_{FD}	frictional dissipation
E_{IHE}	internal heat
E_{WK}	external work
E_{PW}	work done by contact penalties, including general contact and penalty/kinematic contact pairs
E_{CW}	work done by constraint penalties
E_{MW}	work done in propelling mass added in mass scaling
E_{HF}	external heat energy through external fluxes
E_{IE}	internal energy, given by equation 35:

$$E_{IE} = E_{SE} + E_{PD} + E_{CD} + E_{AE} + E_{DMD} + E_{DC} + E_{FC} \quad (35)$$

, where

E_{SE}	strain energy
E_{PD}	plastic dissipation
E_{CD}	creep dissipation energy
E_{AE}	artificial strain energy

E_{DMD} damage dissipation energy

E_{DC} distortion control dissipation energy

E_{FC} fluid cavity energy

For our model, the following energy contributions are not relevant or negligible: E_{IHE}, E_{HF}, E_{PD}, E_{CD}, E_{DMD}, E_{DC}, E_{MW}, $E_{CW,}$ E_{FD} and E_{FC}. Equation 34 and 35 then become as shown in equation 36 and 37 respectively:

$$E_{Tot} = E_{KE} + E_{IE} + E_{VD} - E_{WK} - E_{PW} \approx Constant \tag{36}$$

$$E_{IE} = E_{SE} + E_{AE} \tag{37}$$

B MATLAB script of the keel actions from ISO 19906:2010

```
clc
clear all
close all

phi = 30;                           %[degrees]
u = tan(degtorad(45+phi/2));
c = 5*10^3;                         %[Pa]
e = 0.35;                           %keel porosity
rho = 920;                          %ice density [kg/m^3]
rho_w = 1025;                       %water density [kg/m^3]
g = 9.81;                           %gravity [m/s^2]
%W_s = 12;                          %sail depth
y = (1-e)*(rho_w-rho)*g;            %effectiv buoyancy
F = [];

x_0=0.1;
dx = 1/64;
x_1 = 25;
D = [x_0:dx:x_1];


for j=1:2:25
    h = j;


    for i=1:length(D)
        F(i)= u*h*D(i)*(0.5*h*u*y + 2*c)*(1+(h/(6*D(i))));
        P(i) = F(i)/(h*D(i));
    end

    G(j,:) = P*10^-3;              % Table of global pressure [kPa] for
h=1+n, n=0,2,4...
    K(j,:) = F*10^-3;              % Table of maximum force [kN] for h=1+n,
n=0,2,4..

end

G( all(~G,2), : ) = [];
K( all(~K,2), : ) = [];

figure()
plot(D,G)
xlabel('Width [m]','FontSize',17)
ylabel('Global pressure [kPa]','FontSize',17)
title('Structure width vs global pressure','FontSize',18)
h_legend = legend('h=1 m','h=3 m','h=5 m','h=7 m','h=9 m','h=11 m','h=13
m','h=15 m','h=17 m','h=19 m','h=21 m','h=23 m','h=25 m');
```

```
set(h_legend,'FontSize',13);
set(gca,'fontsize',14)

figure()
plot(D,K)
title('Structure width vs. keel rubble action','FontSize',17)
xlabel('Width [m]','FontSize',17)
ylabel('Force [kN]','FontSize',17)
h_legend = legend('h=1 m','h=3 m','h=5 m','h=7 m','h=9 m','h=11 m','h=13
m','h=15 m','h=17 m','h=19 m','h=21 m','h=23 m','h=25 m');
set(h_legend,'FontSize',13);
set(gca,'fontsize',14)

s = size(G);

%Rate of change in global pressure as a function of structural width.
for k=1:(s(1))
    for l=1:(s(2)-1)
        e(k,l) = ((G(k,l+1))-(G(k,l)))/dx;
        if e(k,l)>= -50
            R(k,l)=e(k,l);
            d(k,l)= D(l+1);
        end

    end
end

figure()
plot(D(1:end-1),e)
xlabel('Width, D [m]','FontSize',17)
ylabel('\DeltaP/\DeltaD','FontSize',17)
title('Average rate of change of P with respect to D','FontSize',18)
h_legend = legend('h=1 m','h=3 m','h=5 m','h=7 m','h=9 m','h=11 m','h=13
m','h=15 m','h=17 m','h=19 m','h=21 m','h=23 m','h=25 m');
set(h_legend,'FontSize',13);
set(gca,'fontsize',14)

%%%%NB! Values below are read out from the graphs/ Found by observation for
dx = 1/64 %%%

%Given DP/DD <= -50
X1 = [0.24 0.44 0.6 0.75 0.88 1.01 1.14 1.26 1.38 1.51 1.63 1.75 1.87];
%Given DP/DD <= -25
X2 = [0.34 0.63 0.85 1.05 1.25 1.43 1.62 1.79 1.96 2.14 2.31 2.48 2.65];
Y = [1 3 5 7 9 11 13 15 17 19 21 23 25];
figure()
plot(X1,Y,X2,Y)
legend('\DeltaP/\DeltaD <= -50','\DeltaP/\DeltaD <= -25')
xlabel('Structure width, D [m]')
ylabel('Keel depth, h_{k}')
```